SPATIO-TEMPORAL DEPENDENCY ANALYSIS OF EPILEPTIC INTRACRANIAL ELECTROENCEPHALOGRAPH

By

ANANT HEGDE

A DISSERTATION PRESENTED TO THE GRADUATE SCHOOL
OF THE UNIVERSITY OF FLORIDA IN PARTIAL FULFILLMENT
OF THE REQUIREMENTS FOR THE DEGREE OF
DOCTOR OF PHILOSOPHY

UNIVERSITY OF FLORIDA

2006

This dissertation is dedicated to my family, teachers and friends for their enduring love, support and friendship.

ACKNOWLEDGMENTS

It has been a privilege being Dr. Jose Principe's student. His constant guidance, encouragement and technical directions helped me tremendously in approaching research challenges. The fact that he has infinite time for his students makes him very special in my eyes. No wonder his enthusiasm, his quest for excellence and his abilities to inspire and motivate have taken him a long way. My experience as a researcher under his supervision has been very rich and fulfilling and I would like to thank him for teaching me how to research, for giving me enough freedom to explore problems independently and also for his valuable advice whenever I needed it most.

I would like to thank Dr. Chris Sackellares for being on my committee and offering me plentiful guidance in research. It is always a privilege to know someone like Dr. John Harris. I thank him for his support, both moral and technical, and also for serving in my committee. I also thank Dr. Mingzhou Ding for being on my committee and his valuable feedback in my research.

It is seldom that someone working in CNEL would not know or have heard of Dr. Deniz Erdogmus. I consider myself lucky having been around when Deniz was here. Besides being a great friend, he offered relentless guidance all along my research and his contributions in this accomplishment are as precious as anyone else's. I would also like thank Dr. Deng Shiau and Dr. Yadunandana Rao for their technical feedback.

I also wish to extend my acknowledgements to all the members of CNEL who have been primarily responsible for my fruitful stay in the lab. In particular, I would like to

cherish those productive discussions with Mustafa Can, Rui Yan , Jianwu Xu, Puskal, Sudhir, Han, Kyu-hwa and Jack. Overall, my stay in CNEL has been very rewarding and if I look back a few years from now, I am sure I'll say 'No doubt, those were my formative years.' I would like to extend my gratitude to the always cheerful Ellie Goodwin for her golden words of wisdom. Her ability to get things done was truly remarkable. I would also like to acknowledge Linda Kahila and Shannon for their extensive support and assistance during my stay at UF. Kartikeya Tripati has been very inspiring all along and I am very grateful to his constant support.

I would like to thank my family and friends for their constant love and encouragement. They have allowed me to pursue whatever I wanted in life. Without their guidance and affection, it would have been impossible for me to be where I am today.

Lastly, I would like to thank my life partner Madhoo for making my life so colorful and for being on my side whenever I need her. Her everlasting love has made me a better individual.

TABLE OF CONTENTS

page

LIST OF TABLES

LIST OF FIGURES

Abstract of Dissertation Presented to the Graduate School
of the University of Florida in Partial Fulfillment of the
Requirements for the Degree of Doctor of Philosophy

SPATIO-TEMPORAL DEPENDENCY ANALYSIS OF EPILEPTIC INTRACRANIAL ELECTROENCEPHALOGRAPH

By

Anant Hegde

May 2006

Chair: Jose C. Principe
Major Department: Electrical and Computer Engineering

There is evidence that the mechanisms leading to epileptic seizures can be understood by continuously tracking the ongoing spatio-temporal mappings in the brain. However, the exact spatio-temporal changes leading to epileptic seizures, although widely studied, are not yet well understood. Previous studies have mostly focused on individually tracking the dynamical changes along time. However, approaches to simultaneously explain a system's temporal changes in its overall spatial configuration can be much more effective in efforts to characterize epileptic events.

In this dissertation, we propose a simple statistical approach to quantify the temporal changes in spatial patterns of an intracranial EEG. Previously, we developed a non-linear synchronization measure, called the SOM-Similarity Index, to quantify mutual associations between various brain regions. We propose to apply the Mantel test statistics on the SOM-similarity indices to track the temporal changes of the spatial patterns.

Statistical comparisons between inter-ictal and pre-ictal states suggest significant changes in the spatial connectivity prior to a seizure.

Another aspect of this study investigates the regional groupings in the intracranial EEG spatial networks at different ictal-states. We develop a model that will allow us to study the various cluster patterns in an epileptic brain. Studies on 10 seizures from 2 patients reveal strong connections between the left-sub-temporal and the left-temporal depth areas. In addition, strong homologous connectivity is found in the orbito-frontal regions.

In the third aspect of this study, we investigate the differences in the synchronization levels between the focal and the non-focal hemispheres at pre-ictal and post-ictal states. Statistical tests confirm the existence of significant differences at pre-ictal states followed by a strong entrainment, 20 minute post-ictal period.

CHAPTER 1
SPATIO-TEMPORAL INTERACTIONS

1.1 Introduction

The word “interaction” in a system can possibly be referred to as an exchange of information between its components. A system can be understood to be made up of a large number of independent components, each acting as an individual sub-system. These sub-systems generally possess an independent environment of their own. However, in a synergetic environment, they also communicate or share information with their counterparts in such a way that the cumulative effect is responsible for the overall functioning of the system.

Even though the notion of a system is the same in any discipline, the specific interpretation or representation of the same differs and is usually tailored to suit our understanding. In physics or engineering, a system is usually considered to be made up of a set of well connected oscillators that are assumed to have independent rhythms specified over periods of time and expressed as time-sequences. Harmonics induced by the oscillator rhythms encode the state of the oscillator and perhaps the system as well. As a result of coupling with other oscillators in an interactive environment, a signal recorded from a transducer can be expressed in a number of ways: a) as a superposition of oscillations generated individually with oscillations shared from other oscillators or b) as a complex interactive process induced by phase, frequency or amplitude variations between oscillators in the spatial neighborhood. Thus the process where oscillators share

complex dynamics with their counterparts can be characterized as a state of mutual-harmony or synchronization. Referring to the degree of interaction, it is possible that it be weak or strong, but is nevertheless capable of triggering an event. While a lot of enthusiasm is placed on understanding the exact nature of synchronization, equal importance has been devoted to relate the event manifestations caused due to synchronization changes. Finally, synchronization analysis of the time-recordings of a physical system allows us to probe the underlying hidden dynamics involved in creating the system.

Synchronization changes in a system can be across both space and time. Particularly, in a multi-variate system, understanding the interactions among its various nodes, whose behavior can be represented along time as time-sequences, presents numerous challenges. One of the key aspects of tightly coupled systems with spatial extent is their ability to interact both across space and time, which complicates the analysis greatly. In biological systems such as the central nervous system, this difficulty is compounded by the fact that the components of interest have nonlinear complicated dynamics that can dictate overall changes in the system behavior [22]. In summary, it is important to realize that the spatial structures also undergo functional changes that can dictate the overall behavior of a system.

With the advent of sophisticated tools, multivariate time-signal analysis has become the forefront of research in discrete time signal processing [66-72, 85-87]. Time-sequences recorded from real-world systems encode huge amounts of information that are both temporally and spatially extended. Especially in neural systems, synchronization between cortical structures or local-field potentials recorded at the tissue level is believed

to be one of the prominent indicators of physiological and pathological events [21-22]. In the next section therefore, we provide a brief literature overview of the efforts in this area and then in the last part of this chapter, we try to address the fundamental question related to epileptic seizures that eventually served as a motivation for us to pursue this study.

1.2 Different Kinds of Synchronization

In the previous section, we introduced the notion of coupling and abstractly described it as a process of information exchange between components of a system. Exactly how information is shared is a question that remains ambiguous. Previous studies on multi-variate time series analyses have resulted in development of a wide array of signal-processing tools for quantification of coupling in systems. However, the general consensus on the best approach to quantify this phenomenon is largely uncertain.

Synchronization can be conveniently classified as linear or non linear [13]. Linear synchronization assumes that the processes are Gaussian distributed, stationary, ergodic and therefore the couplings can be expressed using just the first and second order moments. While some of the tools quantify the correlations by exploiting the time parameters such as amplitude or phase of the data, the others operate in the frequency domain to achieve the same [11, 60-63]. Recently, multi-resolution techniques have facilitated significant progress in exploiting the time and frequency parameters jointly [90].

One of the major advantages of assuming linearity is the fact that the system interactions can be quantitatively analyzed in great depth. However, assuming a linear model can be arguably very weak and in practice, it is very restrictive to assume that the functional mapping between two coupled systems is sensitive to the differences in first and second order moments. Nonlinear coupling can produce changes in the higher order

moments of stochastic signals without affecting appreciably the lower order moments, which raises concerns on the general applicability of these methods.

Most real world systems are evidently non-linear processes and their functional interactions are known to be dynamical in nature. Unlike in the linear case, it is hard to determine the exact functional mapping and therefore without any apriori assumptions, only the degree to which the two systems interact can be quantified [43]. This is exactly how most of non linear tools operate. These tools, in general, assume that if two systems are related, states of one system should be described by the states of another. Even though these techniques have a wider sense of applicability, they still suffer from the lack of analytical transparency, i.e. their inability to analyze the systems in depth. Another major setback is the huge demand in the computational complexity involved.

In the literature, synchronization between systems has also been distinguished as identical synchronization, phase synchronization and generalized synchronization. As far as the tools are concerned, they can be classified into two categories, 1) bi-variate and 2) multi-variate. As stated earlier, these classifications are made to suit the hypothetical definition of what synchronization is. In the next section, we provide a brief literature overview of the various signal processing tools designed to quantify the degree of synchronization between systems.

1.3 Second Order Synchronization Measures

The literature on quantification of the spatio-temporal couplings in multi-dimensional dynamical systems is rich and abundant, and for simplicity, it can be grossly divided into linear and non linear. This section reviews some of the widely used second order linear tools in this effort. We will discuss the common goals among these measures, their approaches and the advantages and trade-offs along the way.

1.3.1 Cross-Correlation

Cross-correlation analysis is one of the earliest and most relied-on linear techniques [6]. It measures the linear coupling between two signals and by design, is symmetric.

Consider an identically distributed stationary stochastic process X. Assuming ergodicity, represent a single time recording of the process as the discrete time-signal *x(n)*, *n = 1,2,….M*, where *M* is the number of total number of samples in the signal. Cross-correlation between two discrete time signals *x(n)* and *y(n)* can be estimated as a function of lags, τ , as follows:

$$\hat{R}_{xy}(\tau) = \frac{1}{(N-\tau)} \sum_{i=1}^{N-\tau} x_i y_{i+\tau}, \quad \tau = -N-1,...,-1,0,1,.....N-1 \tag{1.1}$$

Due to the symmetric property, $\hat{R}_{xy}(\tau) = \hat{R}_{xy}(-\tau)$. If μ_x, μ_y are the mean-estimates of x(n) and y(n) respectively, the cross-covariance between *x(n)* and *y(n)* can be estimated as:

$$\hat{C}_{xy}(\tau) = \hat{R}_{xy}(\tau) - \mu_x \mu_y \tag{1.2}$$

Again, it is obvious that $\hat{C}_{xy}(\tau)$ is symmetric. Cross-correlation coefficient between x(n) and y(n) can now be defined as the cross-covariance normalized by the product of the square root of the variances of the two signals. Mathematically,

$$\hat{\rho}_{xy}(\tau) = \frac{\hat{C}_{xy}(\tau)}{\hat{\sigma}_x \hat{\sigma}_y} \tag{1.3}$$

where $\hat{\sigma}_x$, $\hat{\sigma}_y$ are the standard-deviations of *x(n)* and *y(n)* respectively. $\hat{\rho}_{xy}$ is normalized between -1 and +1. The bounds represent strongest correlation (positive and negative) while 0 represents independence.

Similarly, define $X(\omega) = F(x(n))$ and $Y(\omega) = F(y(n))$ as the Fourier transform equivalents of *x(n)* and *y(n)* respectively. If the cross-spectrum $\hat{C}_{xy}(\omega)$ and the auto-spectrums $\hat{C}_{xx}(\omega)$ and $\hat{C}_{yy}(\omega)$ are defined accordingly, normalized cross-coherence can be mathematically represented as

$$\hat{\sigma}_{xy}(\omega) = \frac{\hat{C}_{xy}(w)}{\sqrt{\hat{C}_{xx}(w).\hat{C}_{yy}(w)}} \tag{1.4}$$

The cross-coherence quantifies the degree of coupling between X and Y at each frequency. Again, the bounds are the same as in cross-correlation coefficient.

One of the problems with cross-correlation and the cross-coherence measures is that they are symmetric. Symmetry fails to quantify the directional information and therefore allows us to know only the average amount of information exchanged between X and Y. Also, as with most other techniques, pair-wise computation is a limitation with correlation/coherence analysis as well.

1.3.2 Partial Directed Coherence (PDC)

Efforts to improve on the correlation technique resulted in development of multivariate auto-regressive modeling techniques such as directed coherence, directed transfer functions (DTF) [19-20], and partial directed coherence (PDC) [2-3, 91]. It is a frequency domain technique based on the concept of Granger-causality [27] which says that *an observed time series $x_j(n)$ causes another series $x_i(n)$, if knowledge of $x_j(n)$'s past significantly improves prediction of $x_i(n)$*. Along the same lines, the reverse case may or may not be true. One way to make a quantitative assessment of the amount of linear interaction and the direction of interaction among multiple time-series would be by translating the concept of Granger-causality into a mathematical model such as a multi-

variable autoregressive model (MVAR). This will enable us to check the number of predictable variations arising from using the knowledge of the past samples of another time-series to predict the current sample of the time-series of interest.

The partial directed coherence (PDC) from *j* to *i* at a frequency *f* is given by

$$\pi_{ij}(f) = \frac{A_{ij}(f)}{\sqrt{a_j^H(f)a_j(f)}} \tag{1.5}$$

where

$$A_{ij}(f) = \begin{cases} 1 - \sum_{r=1}^{p} a_{ij}(r)e^{-j2\pi fr}, i = j \\ -\sum_{r=1}^{p} a_{ij}(r)e^{-j2\pi fr}, otherwise \end{cases} \tag{1.6}$$

$a_{ij}(r)$ are the multivariate auto-regressive (MAR) coefficients at lag *r*, obtained by finding the least-squares solution of the MAR model

$$x = \sum_{r=0}^{p-1} A^r x(p-r) + n \tag{1.7}$$

Here, $A^r = \begin{bmatrix} a_{11}^r & a_{12}^r & . & a_{1N}^r \\ . & . & . & . \\ . & . & . & . \\ a_{N1}^r & a_{N2}^r & . & a_{NN}^r \end{bmatrix}$ and $x(p-r) = \begin{bmatrix} x_1(p-r) \\ x_2(p-r) \\ . \\ . \\ x_N(p-r) \end{bmatrix}$

p represents the depth of the AR model, *r* represents the delay and *n* represents the prediction error or the noise. Note that $\pi_{ij}(f)$ represents the relative coupling strength of the interaction of a given signal source *j* with regard to signal *i* as compared to all of *j'*s interactions to other signals. It turns out that the PDC is normalized between 0 & 1 at all frequencies. When *i=j*, the PDC represents the influence of a signal's past on its current state. The PDC also differentiates between direct and indirect interactions among

multiple time series. Evidently, the MVAR models are better than most bivariate measures because they use information simultaneously from all the channels, and thus are able to unambiguously distinguish between direct and indirect causal connectivity between nodes [41].

1.3.3 Synthetic simulation

Suppose that three simultaneously observed time-series are generated as follows

$$\begin{aligned} x_1(n) &= 0.1\sin(2\pi f_1 n) + \sin(2\pi f_2 n) + \sin(2\pi f_3 n) + w_1(n) \\ x_2(n) &= 0.75x_1(n-2) - 0.1x_2(n-1) + w_2(n) \\ x_3(n) &= 0.36x_2(n-4) + Cx_1(n-1) + w_3(n) \end{aligned} \tag{1.8}$$

where $f_1=0.1f_s$, $f_2=0.2f_s$, $f_3=0.44f_s$, sampling frequency f_s=100Hz; Coefficient C denotes the coupling strength between x_1 and x_3. w_1, w_2 & w_3 are zero-mean uncorrelated white noise processes with identical variances equal to 0.5.

One can observe from (1-5) that x_2 is influenced by x_1 and x_3 is influenced by x_2 and can possibly be influenced by x_1 as well, depending on the coupling strength C. Therefore, x_3 can be influenced by x_1 directly or indirectly or both directly and indirectly. The coupling state diagram is plotted in fig. 1-1.

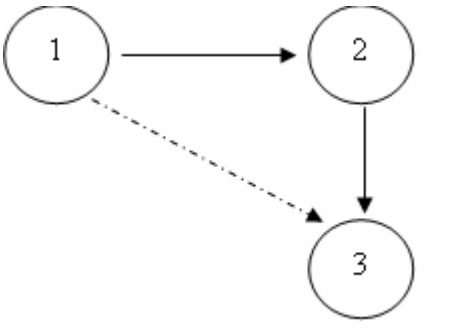

Figure 1-1. Coupling diagram showing the direction of interactions between nodes, x_1, x_2 and x_3.

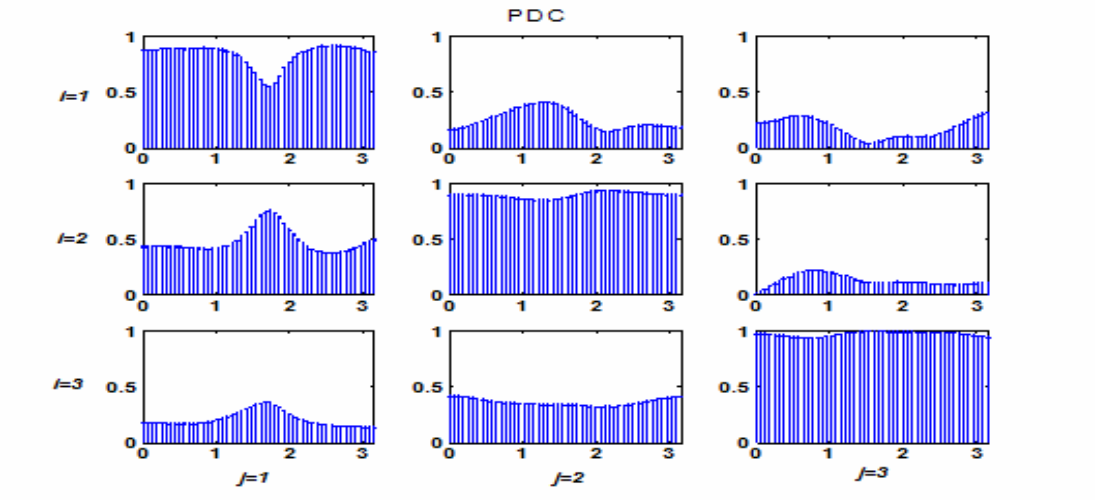

(a)

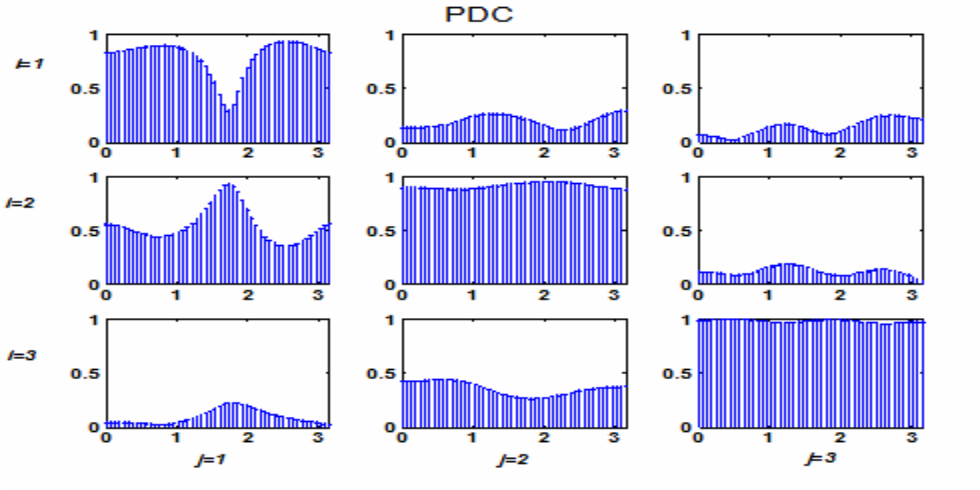

(b)

Figure 1-2. Matrix layout plots for PDC, describing the interactions in example simulation (1-8). πij indicates the influence of xj on xi at frequency f. The x-axis limits range from 0 to pi, and the y-axis limits range from 0 to 1. a) Case when C = 0.3 and b) C = 0.

Corresponding PDC matrix plots for the case when $C = 0.3$ are shown in fig 1-2a. The plots clearly suggest a dependency of x_2 and x_3 on x_1. Dependency of x_3 on x_2 is also prominent from the plot. All the other plots (excluding the diagonal plots) indicate some minor influences in the reverse direction, i.e, x_2 to x_1 etc. However, a suitable statistical threshold may clearly indicate an unambiguous influence among the nodes. The PDC

results seem to be in agreement, at least qualitatively, with the coupling diagram in Fig 1-1.

For the case when there is no direct coupling between x_1 and x_3, i.e, C=0, the plots are described in fig. 1-2b. In this case, PDC indicates a much lesser influence of x_1 on x_3, as expected from its design.

Qualitatively, the PDC plots are reasonably good indicators of directional dependence between multi-variate structures. However, it is difficult to exactly mark the directions without setting an appropriate threshold. Quantitatively, the information on the exact amount of coupling between two signals at a particular frequency f, as determined by PDC, is ambiguous. In the simulation example, we created x_2 and x_3 using direct and indirect influences from x_1. Since x_1 is the driver and also is composed of multiple sinusoids (f_1, f_2 & f_3), it is natural to expect the frequency-spectrum of x_2 and x_3 to mainly consist of these sinusoidal frequencies. This also implies that the coherence between these time-structures will be strong at these pole locations. However, the PDC plots fail to provide that information, as we can see from fig.1-2a and 1-2b. The coherence plots are either smeared across all the frequencies or exhibit high values at frequencies other than the expected frequency locations.

The MVAR approaches have been used to determine the propagation of epileptic intracranial EEG activity in temporal lobe and mesial seizures [2-3, 10, 19-20]. However, these models strictly require that the measurements be made from all the nodes, or the directional relationships could be ambiguous. In addition, there is no clear evidence of causality relationships among the cortical structures and as suggested in Rodriguez et al. [84], the nature of synchronization is mostly instantaneous or without any detectable

delay. The applicability of MVAR measures is constrained to the linear dependencies even though there are strong evidences pointing to non linear patterns of interactions [23].

1.4 Mutual Information

Linear measures are typically restricted to measure statistical dependencies up to the 2nd order. If signals are Gaussian distributed, the 2nd order statistics are sufficient to capture all the information in the data. However, in practice, most signals are either non-Gaussian or quassi-Gaussian rendering the linear statistical measures inadequate. As an alternative, information theory measures [11-12, 66-68, 94-95] have been widely claimed as acceptable choices to exploit the higher order statistical dependencies between signals. A useful quantity is the mutual information approach that measures the Kullback-Liebler (K-L) divergence between the joint probability and the product of the marginal probabilities [11].

Consider that the vector samples $\mathbf{x} = \{\mathbf{x}_1,\ldots,\mathbf{x}_N\}$ from an information source in a d-dimensional signal space. Suppose that these samples are drawn from the distribution f(x). Similarly, let the vector samples $\mathbf{y} = \{\mathbf{y}_1,\ldots,\mathbf{y}_N\}$ form another information source in a d-dimensional signal space belongs to distribution g(x). By definition, mutual-information between ***x*** and ***y*** can be computed as follows

$$\begin{aligned} I(x;y) &= \iint_{x,y} f_{xy}(x,y)\log\frac{f_{xy}(x,y)}{f_x(x)f_y(y)}dxdy \\ &= \iint_{x,y} f_{xy}(x,y)\log f_{xy}(x,y)dxdy - \int_x f_x(x)dx - \int_y f_y(y)dy \\ &= H(x)+H(y)-H(x,y) \end{aligned} \tag{1.9}$$

where $f_{xy}(x,y)$ is the joint probability event between x and y, and $f_x(x)$, $f_y(y)$ are the marginal probabilities, respectively. *H(x)* can be regarded as the average measure of

uncertainty and in the information theory literature is also called as Shannon's marginal entropy, in x. Similarly *H(y)* is Shannon's marginal entropy in y, while their joint entropy is denoted by *H(x,y)*.

MI has been successfully used to quantify statistical couplings in biological applications such as newborn cardio-respiratory systems [70-72], event related potentials (ERPs) [65] and epileptic seizures [66-68]. One of the problems with this approach, however, is that it requires large data sets for probability density estimation making it computationally unviable. Efficient algorithms such as generalized mutual information function (GMIF) have been recently proposed [70-72] to enable speedy computation using very small data sequences.

1.5 Phase Synchronization

Conceptually, if the rhythms of one signal are in harmony with that of the other, the two signals are known to be phase locked [99]. Phase synchronization can therefore be defined as the degree to which two signals are phase locked.

Most of real world signals have broad spectra. For example, EEG signal recordings are usually in the range of 0.1 to 1000 Hz even though they are usually band pass filtered between 0.1 and 80 Hz since a major portion of the energy is contained in that spectrum. The EEG can be classified roughly into five (5) different frequency bands, namely the delta (0-4 Hz), theta (4-8 Hz), alpha (8-12 Hz), Beta (12-16 Hz) and the Gamma (16-80 Hz) frequency bands. Freeman [21] demonstrated evidence of phase locking between EEG frequency bands across different regions of the brain, leading to certain clinical events such as evoked potentials. Similarly, it is also believed that phase synchronization across narrow frequency EEG bands, pre-seizure and at the onset of seizure [81-83] may provide useful hints of the spatio-temporal interactions in epileptic brain.

The procedure normally adopted to measure phase synchronization consists of initially tracking the instantaneous phases of the two signals of interest. This is followed by computing their differences called the relative phase. Quantifying the distribution of the relative phase will yield an index describing the degree to which the two signals are phase locked. Hilbert transform [33, 49, 75, 81-83] is a widely used signal-transformation trick to compute the instantaneous parameters of a time-signal. The following subsection briefly describes the steps involved.

1.5.1 Hilbert Transformation

Consider a real-valued narrow-band signal $\boldsymbol{x(t)}$ concentrated around frequency f_c. Define $\tilde{x}(t)$ as

$$\tilde{x}(t) = x(t) * \frac{1}{\pi t} \tag{1.10}$$

$\tilde{x}(t)$ can be viewed as the output of the filter with impulse response

$$h(t) = \frac{1}{\pi t}, \; -\infty < t < \infty \tag{1.11}$$

excited by an input signal $x(t)$. We call this filter a Hilbert transformer.

Next, we construct an analytical signal

$$z(t) = x(t) + j\tilde{x}(t) \tag{1.12}$$

which contains only positive frequencies. Our objective is to extract the instantaneous parameters of the signal such as instantaneous amplitude, instantaneous frequency and the instantaneous phase. *z(t)* can also be expressed in Cartesian co-ordinates as

$$z(t) = A(t)e^{j\theta(t)} \tag{1.13}$$

where A(t) is the instantaneous amplitude and $\theta(t)$ is the instantaneous angle of the signal x(t). $\theta(t)$ can be expressed as

$$\theta(t) = \cos(\omega_0(t) + \varphi(t)) \tag{1.14}$$

$\varphi(t)$ is the instantaneous phase of the signal and $\omega_0(t)$ is the instantaneous frequency of the signal x(t).

Hilbert transforms are accurate only when the signals have a narrow-band spectrum, which is unrealistic for most real-world signals. Pre-processing of the signal such as decomposing it into narrow frequency bands is needed before we apply Hilbert transformation to compute the instantaneous parameters. There are several ways of breaking a signal into its sub-band components. Previous work [48, 76-80] to achieve signal decomposition either points to a bank of digital FIR filters or the sub-band coding using wavelet transforms. In the former, a multitude of conventional FIR filters are designed to cater to the desired pass-bands using the Hamming or the Hann window. It is well known from the signal processing literature that the transient events of the signal, such as the spike activity and the sudden transitions that quite often exist in real signals, are not adequately captured using the conventional FIR filters. In other words, it is essential to capture the changing events in the signal locally at the time of their occurrence. If the signal is non-stationary, the requirement for locality is certainly not met with conventional FIR filters. The Wavelet filters [101] have shown better capability of representing a signal in both the time and frequency domain and also capture the transient details of the signal more effectively than the conventional digital FIR filters. However, in both the techniques the decomposition does not always lead to narrow-band signals. In other words, the decomposed signals do not conform to the definitions of a narrow-band signal, even though they exist in a very narrow band frequency range. Certain conditions need to be met to define a meaningful instantaneous frequency on a narrow-band signal. They are as follows:

- the signal needs to be symmetric with respect to the local zero mean, and
- the signal should have the same number of zero crossings and extrema.

1.5.2 Empirical Mode Decomposition (EMD)

EMD is another preprocessing technique [34] in which the data are decomposed into narrow band components called the intrinsic mode functions (IMF). Consider a broad-band real-valued signal *s(t)*. Using an iterative sifting process [34], the IMF components are extracted from the signal *s(t)*, iteratively. The first step in the sifting process involves identifying the local minima and the maxima of *s(t)*, and then using an interpolation filter to combine the extremas. The local mean of the signal m_1 is computed using the local extrema information and subtracted from *s(t)* i.e,

$$s(t) - m_1 = h_{11} \tag{1.15}$$

The new signal is checked for the above 2 conditions. If it did not satisfy them, the whole sifting process is repeated on h_{11} to obtain say h_{12}. This sifting process is iteratively repeated until an IMF component, say h_1, satisfying the two criteria is obtained. The whole sifting process is now repeated on the residue signal $s_1(t)$ obtained from subtracting the IMF component h_1 from the original signal *s(t)* i.e,

$$s_1(t) = s(t) - h_1 \tag{1.16}$$

Eventually, all the successive IMFs satisfy the narrow band constraints. The second condition is particularly essential in order to ensure that the instantaneous frequency does not have any undesired fluctuations, introduced by asymmetric wave forms. Contrary to previously discussed methods, the EMD derives IMFs or the basis functions directly and adaptively from the data. This characteristic makes it particularly useful to detect local

changes in the signal. The basis functions can be empirically shown to be orthonormal and complete.

We demonstrate the ability of the EMD to decompose a signal into its narrow-band components by presenting a simple synthetic simulation. Consider a non-stationary stochastic process $X(t)$ consisting of a combination of sinusoidal components and noise (constructed as shown in fig. 1-3). Components x_1 and x_3 consist of 100 Hz (f_1) and 450 Hz (f_3) sinusoid oscillations respectively and span over the entire duration of the signal $X(t)$. x_2 is a sinusoidal component of frequency 260 Hz (f_2) , spanning only for some period of the entire signal's duration. The signals were sampled at 1024 Hz (f_s) frequency. Decomposition of X(t) into its narrow band components using EMD is shown in fig 1-4.

The IMF components (fig 1-4a) and their corresponding frequency spectrum (fig 1-4b) reveal a few things and can be listed as follows

1. All three frequencies are well separated by the EMD and also the middle panel in fig 1-4a shows how the frequency component f2 exists only between the time-duration that it was created in.
2. There exists leakage of f2 and f3 into IMF1, but by looking at the power spectrum, it is easy to observe that the energy at these frequencies is very low compared to f1.
3. Peak to peak amplitude of the extracted IMFs is almost half of the peak to peak amplitudes in the original signal; however, this is just a scaling problem and can be easily resolved by scaling up each of the IMFs.
4. The Hilbert spectrum, computed using the information from the instantaneous parameters of the IMFs, reveals the joint time-frequency structure of the signal. The extraneous frequencies are either created during the first transient period or due to the presence of noise. Energy at these frequencies is below 0dB.

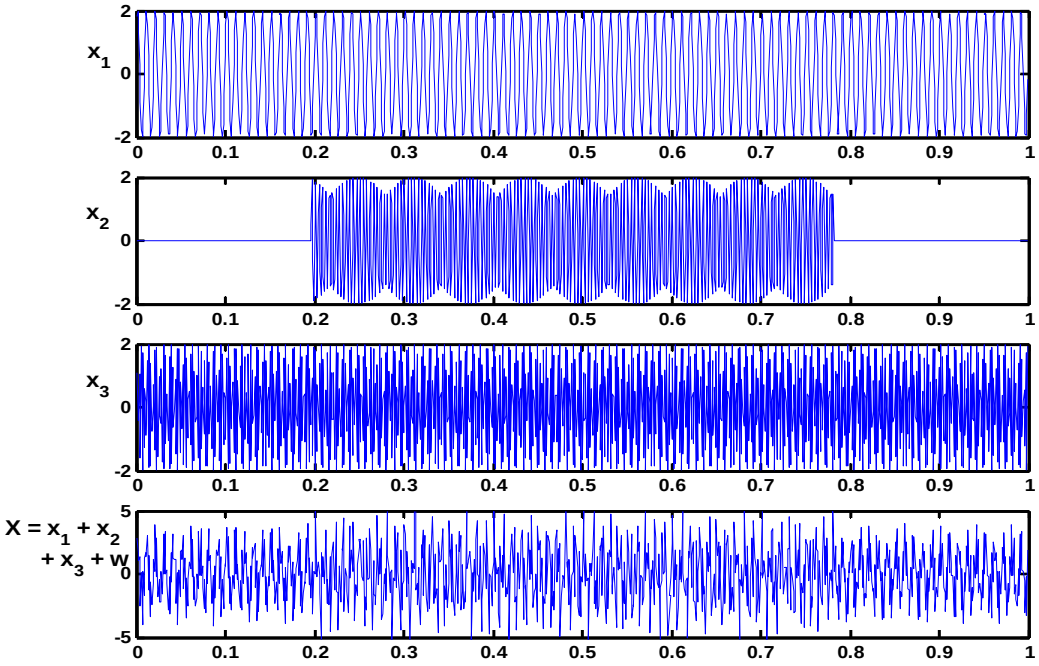

Figure 1-3. Synthetic Sinusoidal signal X(t) and its components x1, x2 and x3. X(t) also consists of noise w~N(0, 0.1)

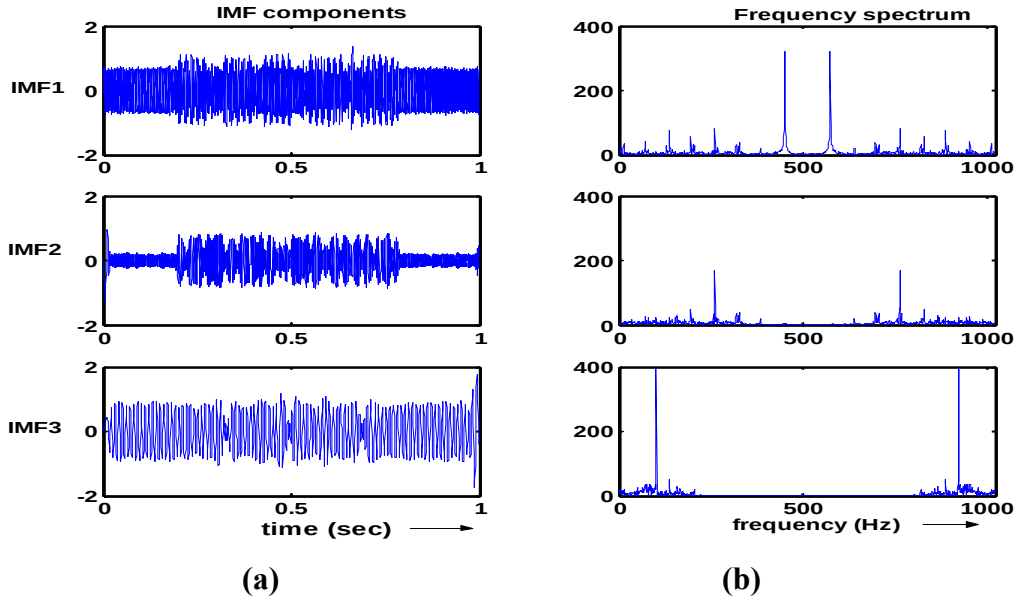

Figure 1-4. Decomposition of sinusoids using EMD. a) IMF components obtained from successive decomposition of x(t) using the EMD b) Corresponding frequency spectrum of the IMF components. IMF1 predominantly consists of 450 Hz, IMF2 consists of 260 Hz and IMF3 consists of 100 Hz, as desired.

1.5.3 Wavelet decomposition

As described in previous sections, one of the many ways to achieve narrow-band decomposition is by using ortho-normal wavelet filters [101]. For the same synthetic signal *X*(t), we apply the '7 length Daubechies' filter functions, at various scales, to achieve signal decomposition (fig 1-6).

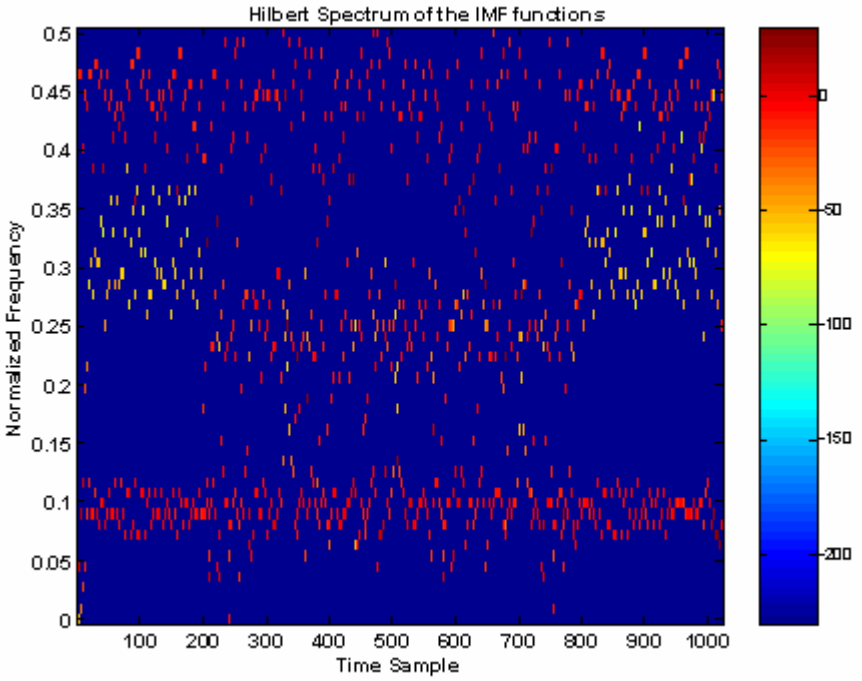

Figure 1-5. Hilbert spectrum constructed from the IMF functions. The spectrum reveals the presence of 100 Hz and 450 Hz along the entire signal duration. Presence of 260 Hz (corresponding to 0.26 on the Y-axis) component between the 200th and 800th sample (corresponding to approximately 0.2 and 0.8 second) is also clearly visible from the spectrum plot. The leakage frequencies are mainly due to the transient oscillations created in the first few samples of the IMFs and also due to noise.

The following observations indicate the superior ability of EMD compared to wavelets in a non-stationary scenario.

Two spurious frequency components of reasonably high energy, namely 150 Hz and 240 Hz are created by wavelet analysis and synthesis (reconstruction) filters.

5. Qualitative comparison of Hilbert spectrum plots (fig 1-7 and fig 1-5) suggest a larger smearing of the frequencies in wavelets compared to EMD.

6. The amount of energy leakage from the 260 Hz component into the first panel (fig. 1-4b) is considerably higher than the corresponding amount of energy leakage in IMF (first panel in fig. 1-4b).

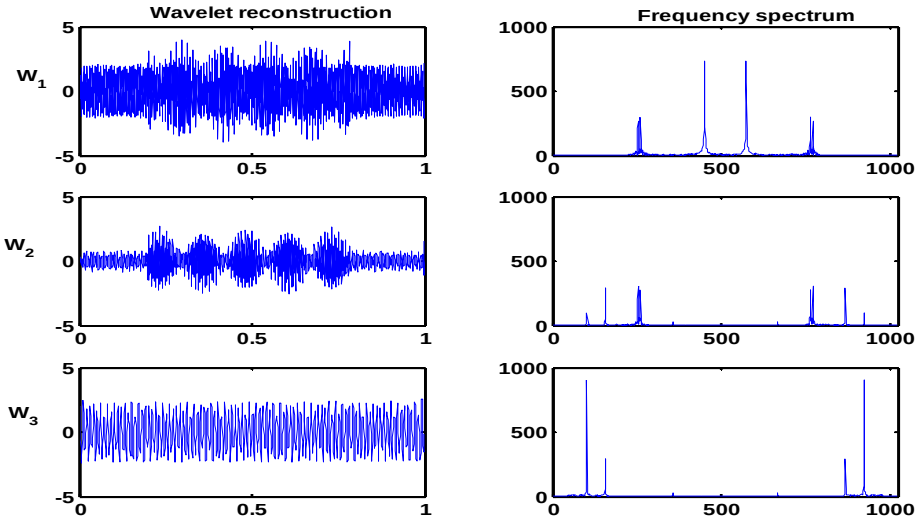

Figure 1-6. Decomposition of sinusoids using wavelets. Left) Wavelet reconstructed components obtained from using Daubechies 7-scaled filters. Right) Corresponding frequency spectrum of the wavelet reconstructed signals. W_1 predominantly consists of 450 Hz, but also has a major portion of 240 Hz. W_2 has more power concentrated in 260 Hz and 150 Hz frequencies and IMF3 consists of 100 Hz, as desired. Presence of spurious frequencies such as 240 Hz and 150 Hz are revealed using wavelet-decomposition.

1.5.4 Indexing Phase Synchronization

As we saw earlier, the Hilbert transformation is a useful time domain to a time-domain transformation technique to compute the instantaneous phase of a signal. Due to the narrow band constraints, any wide-band signal needs to be broken down into its narrow band components and we saw that EMD and wavelet filters can be used as potential pre-processors to achieve the same. Once a meaningful estimate of the instantaneous phases is obtained, we need to determine the degree of phase locking by quantifying them with a suitable metric.

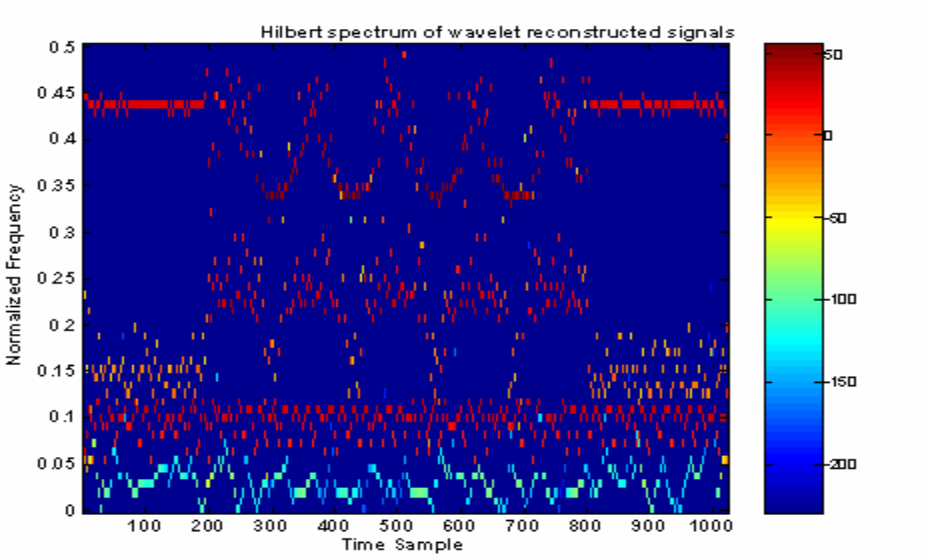

Figure 1-7. Hilbert spectrum constructed from the wavelet reconstructed narrow-band signals. The spectrum reveals the presence of 100 Hz and 450 Hz along the entire signal duration. Frequencies in the range of 200 Hz and 350 Hz (corresponding to 0.26 and 0.35 on the Y-axis) are smeared between the 200th and 800th sample (corresponding to approximately 0.2 and 0.8 second). Presence of 260 Hz is not very clear from the spectrum plot.

Let $\varphi_x(t)$ denote the instantaneous phase of one of the narrowband components of *x(t)*. Similarly, let $\varphi_y(t)$ be the instantaneous phase of the corresponding narrowband component of y(t). Relative phase *Φ(t)*can be computed as the difference between $\varphi_x(t)$ and $\varphi_y(t)$ i.e, $\phi(t) = \varphi_x(t) - \varphi_y(t)$, t = 1, 2,……, N. The relative phase or the phase-difference *Φ(t)* forms a distribution and a number of metrics can be used to compute an index of phase synchronization by using the distribution of *Φ(t)*. Two popular metrics exist in the literature [60-63, 81-83, 85, 99]. The first one expresses the phase synchronization index as a deviation in the distribution of *Φ(t)* from the uniform distribution Φ_{diff} [85, 99]. If we use the Shannon's definition for entropy, comparison of the entropy H of *Φ(t)* with entropy of a uniform phase distribution H_{unif} will result in,

$$\chi = \frac{H_{unif} - H}{H_{unif}} \tag{1.17}$$

Note that $\chi = 0$ for complete lack of synchronization and is 1 for perfect phase-locking. Another metric commonly used synchronization index is the phase locking value (PLV), also called as mean phase coherence [81-83]. It is given by,

$$\chi = \left| \left\langle e^{j\phi(t)} \right\rangle_t \right| \tag{1.18}$$

The bounds are the same as in previous index.

EMD is a useful pre-processing technique for decomposing a time-series into its narrow band components. However, it does not provide any design parameter using which a signal can be filtered into specific bands of interest. In phase synchrony analysis where instantaneous phase is used as the synchrony metric to evaluate phase-locking between two time-series, it is very important that the narrow band components of the time-series are in sufficiently narrow (such as 2 to 4 Hz pass band range) spectra. While it is possible to apriori design a conventional FIR filter catering to a desired pass band and stop band, the EMD does not provide the luxury of choosing the desired frequency bands. Due to the fact that EMD adaptively derives its basis functions based on the data, the IMFs of two different signals can easily lie in different bands. Hence, another limitation associated with using EMD is that, it is not possible to compare between the IMFs of two signals.

Unlike the MVAR model based approaches, the applicability of phase-synchrony measures is restricted to bi-variate time-series [10]. We also saw that both the synchronization indices are symmetric and are therefore incapable of providing the directionality of dependency. Also they are restricted to identifying only the phase locking between time-signals. Synchronization between two systems is a general phenomenon and can broadly be defined as the functional relationship governing the

oscillation of the two systems [88-92]. The function could be linear invertible, linear non-invertible, non linear invertible and non linear non-invertible. Phase synchronization, being only a subset of the general synchronization definition, fails to address the overall functional relationship between systems.

1.6 Non-Linear synchronization measures

A lot of studies in the last two decades, to quantify nonlinear dependencies [88-93] between two or more signals have met with reasonable success. As pointed out earlier, most real world systems can be characterized as non linear processes [52-54] with their samples dynamically evolving from interacting with past samples of the same process as well as from the samples in the spatial neighborhood. Functional non linear mappings are generally very hard to characterize and the fact that the recordings are embedded in noise makes it harder.

A common procedure in any non linear measure is to construct a system map (or the Poincare map) by embedding a scalar time series into a high dimensional Euclidean space and building a trajectory by connecting the time points in that space [98]. This is followed by computations that are generally directed towards determining the mean distances between the mutual neighbors in the phase space of the signals. The synchronization indices indicate the degree to which the state of one system is a function of another and vice-versa.

1.6.1 Signal Reconstruction

Taken's embedding theorem states that under certain conditions, it is possible to construct a finite dimensional dynamical system from a scalar time series $\{x_t\}_{t=1}^{N}$, where $x_t = g(u_t)$. u_t is the actual dynamical system, residing in dimension say 'd'. Taken [98]

postulated that, using time-delay embedding the exact dynamics of a system can be reconstructed, while also preserving its topological characteristics. The reconstruction of the attractor is done from a finite time series of the observation of a single variable $x(t)$. Thus a multi-dimensional embedding space is constructed from the time series data, and a point in it represents the state of the system at a given time.

$$x_n = \begin{Bmatrix} x(t_n) \\ x(t_n - \tau) \\ x(t_n - 2\tau) \\ . \\ . \\ x(t_n - (d-2)\tau) \\ x(t_n - (d-1)\tau) \end{Bmatrix} \tag{1.19}$$

Note that time-delay reconstruction relies heavily on the embedding parameters such as the embedding dimension (d) and the delay time (τ). Nevertheless, these parameters are important since they convey a lot of information about the dynamical properties of the underlying processes. The embedding dimension d can be selected by the false-nearest neighbor criteria [98] and the delay time τ can be estimated by the method of mutual-information [98], or by measuring zeros of autocorrelation.

1.6.2 Non-Linear Synchronization Measures

Eckmann *et al.* [17] proposed the method of recurrence plots (RPs) that represents the recurrence of states in the phase-space trajectory of a chaotic signal. Since chaotic systems are non linear in nature, this method has been fairly successful in detecting bifurcations and non-stationarities in time sequences. Cross-recurrence plot (CRP) is an extension of the RP idea to multi-dimensional time signals [24]. The CRP has found applicability in describing the time-dependency between multiple time-series recorded

from multiple locations. However, the lack of quantitative information and the computational complexity makes it tedious for analyzing large sets of data. One of the other drawbacks of this measure is that it fails to indicate the direction of information flow (or influence). Variants of recurrence plots [59] are used to measure recurrence of states in the phase-space between two chaotic signals. However, these plots are difficult to analyze due to the lack of quantitative measures, in addition to their computational complexity.

Several other non linear measures were proposed following the definition of generalized synchronization by Rulkov and co-workers [88-92] Mutual predictabilities were defined and studied extensively by Schiff *et al.* [92] and Le Van Quyen *et al.* [81]. Principally, if two systems are functionally related, observing the states of one system should help predict the states of the other. A statistic constructed on this idea will indicate the relative strength of coupling as well as the direction of coupling between any two systems.

Recently, Arnhold *et al.* [1, 76] introduced the similarity–index technique (SI) to measure such asymmetric dependencies between time-sequences. Conceptually, this method relies on the assumption that if there is a dependency between two signals, the neighboring points in time will also be neighboring points in state space. In other words, if there is a functional dependency between two signals, then the recurrence of dynamics of one signal will mean the recurrence of dynamics in the other signal.

Arnhold *et al.* [1, 76] propose to search for recurrence in the signals' state-space, which poses an enormous computational burden, especially for large data sets. In this dissertation, we propose a self-organizing map (SOM) based improvement to this method

to reduce computational complexity, while maintaining accuracy. This is achieved by mapping the embedded data from signals onto a quantized output space through a SOM specialized on these signals, and utilizing the activation of SOM neurons to infer about the influence directions between the signals, in a manner similar to the original SI technique. The approach not only facilitates real-time computation but it also enables us to derive long-range synchronization patterns.

1.7 Objectives and Author's Contribution

Mechanisms involved in the synchronization among neural populations have received a lot of attention in recent years [4-5, 8-9, 14-16, 42, 60-63, 97] It is agreed that even in the normal physiological states, the neuron ensembles at the cortical structures always interact and undergo a certain degree of synchronization. The Response to sensory stimulations in the form of cohesive firing of neurons is known to lead to certain transient changes. A larger question, however, that is still debated upon is whether elevated synchrony in firing in a spatial neighborhood and its subsequent propagation to other areas in the brain can lead to pathological situations such as seizures, stroke or Alzheimer's.

Epileptic studies on adults and neo-nates have been widely researched [26, 35-40, 60-62, 82]. Researchers from different disciplines have contributed immensely in understanding the various neurological aspects leading to seizures. Synchronization and de-synchronization between the cortical networks are believed to be one of the plausible reasons for this neurological disorder. It is soon becoming clear that epilepsy is a dynamical disease [56], i.e. the macroscopic spatio-temporal dynamical across different regions of the brain are consistent with rapid, sometimes gradual and often very subtle nonlinear dynamical interactions. It is believed that synchronization occurs due to both

local and global discharges of the neurons. From the epilepsy perspective, quantifying the changes in spatio-temporal interactions could potentially lead to the development of seizure-warning systems. This quantification would also help us identify the regions that actively participate during epileptic seizures.

In this dissertation, we apply the SOM-SI measure on epileptic seizure data to investigate i) the temporal evolution of dependencies at different stages of a seizure, ii) temporal changes in spatial connectivity of signals as a seizure is approached and iii) spatial-temporal clustering of channels at different stages of seizure.

In Chapter 2, we present the SOM-based SI measure to quantify spatio-temporal patterns. The SOM based SI approach to detect spatial interdependencies can be generalized to any multi-variate dynamical system. Initially we present this idea from a general perspective and then proceed to demonstrate the robustness brought about by the SOM-improvisation through synthetic simulations. In chapter 3, we propose a spatio-temporal clustering model that effectively utilizes similarity indices to achieve time-series clustering. From an application standpoint however, the goal of this thesis is to identify spatio-temporal connectivity's in epileptic seizures. In chapter 4 we present the application of our model to epileptic intracranial EEG data and analyze the clustering results on a large set of seizures. In chapter 5, we investigate the hypothesis that the spatial patterns in intracranial EEG undergo significant changes as the brain progresses towards a seizure state. This chapter also investigates if the dependencies in the focal hemisphere are significantly different from the non-focal hemisphere, at pre-seizure and post-seizure states. Chapter 6 presents a detailed discussion on conclusions and possible directions for future research.

CHAPTER 2
SELF-ORGANIZING-MAP BASED SIMILARITY INDEX MEASURE

2.1 Introduction

In this chapter, we will mainly discuss the Similarity Index (SI) measure proposed by Arnhold *et al*. [1] and the proposed SOM based improvement to the SI measure. Simulations with synthetic data are used to demonstrate the applicability and robustness of the proposed SOM based SI measure.

2.2 The Similarity Index Technique

Synchronization between two signals X and Y is understood, in principle, as a functional mapping between X and Y. In most neuro-biological systems especially, it is realistic to expect the functional mappings to be nonlinear. The attractors of functionally synchronous systems are related such that, the trajectory of one system partly describes the trajectory of another and vice-versa. In unilateral coupling, if the trajectory of Y is influenced by the trajectory of X, then Y is said to be functionally dependent on X. However, in instances where bi-directional relationships exist, the trajectory of Y can also partly influence the trajectory of X. In such a case, it is important to quantify two aspects of synchronization: direction and strength.

Using the principles of generalized synchronization defined by Rulkov [88] and, Arnold *et al.* [1] recently formulated a synchronization measure to characterize functional relationships between non linearly coupled systems. Assume that X and Y are two time series generated by a system, which are embedded into two vector signals in time using delays. $N(X|Y)$ is defined as the average dependency of X on Y and it can be written as,

$$N(X \mid Y) = \frac{1}{N} \sum_{n=0}^{N-1} \frac{R^n(X) - R^n(X \mid Y)}{R^n(X)} \tag{2.1}$$

where $R^n(X)$ is the average Euclidean distance between the state-vector of X_n and the remaining state-vectors in X. Y-conditioned Euclidean distance $R^n(X|Y)$ measures the average Euclidean distance between X_n and the vectors in X whose corresponding time-partners are the k-nearest neighbors of Y_n. This measure takes values in [0, 1], where 0 implies no coupling and 1 implies perfect synchronization. In other words, 1 suggests that recurrence of a state in Y implies a recurrence in X [1, 7, 8, 45, 78]. On the same principles, $N(X \mid Y) = 0$ implies complete independence between X and Y. By design, SI can quantify nonlinear dependencies.

Similarly, it is possible to quantify the average dependence of Y on X by

$$N(Y \mid X) = \frac{1}{N} \sum_{n=0}^{N-1} \frac{R^n(Y) - R^n(Y \mid X)}{R^n(Y)} \tag{2.2}$$

Comparing $N(X|Y)$ and $N(Y|X)$, we can determine which signal is more dependent on the other. The difficulty with this approach is that at every time instant, we must search for the k nearest neighbors of the current embedded signal vectors among all N sample vectors; this process requires $O(N^2)$ operations. This high complexity hinders real-time implementation and analysis. In addition, the measure depends heavily on the free parameters, namely, the number of nearest neighbors and the neighborhood size ε. The neighborhood size ε needs to be adjusted every time the dynamic range of the windowed data changes.

2.3 SOM-based Similarity Index (SOM-SI)

The SOM-based SI algorithm is aimed at reducing the computational complexity of the SI technique. The central idea is to create a statistically quantized representation of the dynamical system using a SOM [74, 89]. A SOM is a neural-network in which spatial

patterns from the input-space are mapped onto an ordered output space consisting of a set of neurons, called processing elements (PE). Thus each neuron in the SOM, based on its location on the map, compactly models different features/dynamics of the input.

For best generalization, the map needs to be trained to represent all possible states of the system (or at least with as much variation as possible). As an example, if we were to measure the dependencies between EEG signals recorded from different regions of the brain, it is necessary to create a SOM that represents the dynamics of signals collected from all channels. The SOM can then be used as a prototype to represent any signal recorded from any spatial location on the brain, assuming that the neurons of the SOM have specialized in the dynamics from different regions.

One of the salient features of the SOM is topology preservation [74, 89]; i.e., the neighboring neurons in the feature space correspond to neighboring states in the input data. In the application of SOM modeling to the similarity index concept, the topology preserving quality of the SOM feature of the SOM will be of added advantage, because of the fact that the neighboring neurons in the feature space will now correspond to neighboring states in the input data.

Assume that X and Y are two time series generated by a system, which are embedded into two vector signals in time using delays. Define the activation region of a neuron in the SOM as the set of all input vectors (the embedded signal vectors) for which the neuron is the winner based on some distance metric (Euclidean in most cases). Let X_n be the set of time indices of input vectors x_j that are in the activation region of the winner neuron corresponding to the input vector x_n at time n. Similarly define the set Y_n.
Then the procedure to estimate the directed SOM-SI between X and Y is as follows

7. Train a SOM using embedded vectors from both X and Y as the input.

8. At time n, find W_n^x, the winner neuron for vector x_n, and find W_n^y, the winner neuron for vector y_n.

9. To find $R^n(X)$, compute the average Euclidean distance between W_n^x and all the other winner neurons in the SOM. Similarly, compute $R^n(Y)$.

10. Determine the sets X_n and Y_n for W_n^x and W_n^y, respectively.

11. Determine the nearest neurons $W_{n,j}^y$ corresponding to vectors y_j, where $j \in X_n$.
Determine the nearest neurons $W_{n,j}^x$ corresponding to vectors y_j, where $j \in Y_n$.

12. Calculate $R^n(X \mid Y) = (1/q)\Sigma_{j=1}^{q} \| W_n^x - W_{n,j}^x \|$, where q is the number of elements in X_n.
Calculate $R^n(Y \mid X) = (1/q)\Sigma_{j=1}^{q} \| W_n^y - W_{n,j}^y \|$, where q is the number of elements of Y_n.

13. Compute the ratios,

$$N^n(X \mid Y) = \left(R^n(X) - R^n(X \mid Y)\right) / R^n(X) \tag{2.3}$$

$$N^n(Y \mid X) = \left(R^n(Y) - R^n(Y \mid X)\right) / R^n(Y) \tag{2.4}$$

14. Find *interdependencies* $N(X \mid Y)$ and $N(Y \mid X)$ as the average of $N^n(X \mid Y)$ and $N^n(Y \mid X)$ over all n.

15. Compute the SOM-SI as the difference,

$$\chi = N(Y \mid X) - N(X \mid Y).$$

Positive values of χ indicate that influence of X on Y is more than the influence of Y on X, while negative values indicate the opposite. Higher magnitude of χ indicates a stronger coupling of the signals [29].

The computational savings of the SOM approach is an immediate consequence of the quantization of the input (signal) vector space. The nearest neighbor search involves $O(NM)$ operations as opposed to $O(N^2)$ in the original SI, where M is the number of PEs.

Traditionally $M<<N$, hence, SOM-SI offers a significant reduction in computations compared to original SI.

2.4 Simulation Results

In this section, we demonstrate the viability of the SOM-based similarity index approach in determining couplings and influence directions between synthetic and real signals. One case study considers a coupled Rosseler-Lorenz system (as described in [7-8, 76, 78]), and the other considers real EEG signals.

2.4.1 Rosseler-Lorenz simulation

The same Rosseler-Lorenz example used by Quiroga *et al.* [76] is used here. A synthetic nonlinear dependency between a Rosseler (X) and a Lorenz (Y) system is created by having the second state of the Rosseler system drive the Lorenz system in the following manner

$$\begin{array}{ll} \text{Roessler} & \text{Lorenz} \\ \dot{x}_1 = -6\{x_2 + x_3\} & \dot{y}_1 = 10(-y_1 + y_2) \\ \dot{x}_2 = 6\{x_1 + 0.2x_2\} & \dot{y}_2 = 28y_1 - y_2 - y_1 y_3 + Cx_2^2 \\ \dot{x}_3 = 6\{0.2 + x_3(x_1 - 5.7)\} & \dot{y}_3 = y_1 y_2 - \frac{8}{3} y_3 \end{array} \tag{2.5}$$

where C is the coupling strength. To be realistic, measurement noise, up to 30dB SNR are added to both the systems. Two SOMs, one corresponding to x2 component of the Rosseler system and the other, corresponding to the y2 component of the Lorenz system (a new SOM for each value of C), were trained separately on embedded data, using an embedding delay of 0.3 time-units and embedding dimension of 4. Note that separate SOMs were trained because of the fact that the dynamics of the two systems were non-identical. However, in general, while working with signals generated from the same system, it suffices to train a SOM that represents all possible dynamics of that system. SOM neurons overlapped with the phase-space dynamics of the Rosseler system and the

Lorenz system (for different C values) are shown in Fig. 2-1. Each SOM is an 8x8 rectangular grid, and is trained on a set of 4000 samples using a Gaussian neighborhood function for about 400 iterations. The neighborhood radius (standard deviation of the Gaussian neighborhood function) is exponentially annealed starting from an initial value of 4 with a time constant of 100. The step size is also annealed exponentially from 0.08 using the same time constant.

Using the SOM-SI approach, the normalized indices χ are calculated for coupling strengths of C = 0, 0.5, 1, 2, 3 and 5. The robustness to varying SNR is demonstrated in the test data [31], as shown in Fig 2-2. Firstly, we observe that the asymmetric difference in the interdependencies between the Rosseler and the Lorenz system increases as the coupling (C) is increased (irrespective of the noise level). Despite the fact that the training was done with 30dB SNR level, the absolute values of the dependencies do not change much for SNR up to around 20dB, indicating noise-robustness. However, a drastic decrease in the absolute dependency values for 10dB and 0dB SNR situations suggest that the structural relationship between the two systems is being largely overwhelmed by the stochastic noise. In summary, we see that the idea of SOM modeling of system's dynamics not only reduces computational complexity but also preserves neighborhood mappings during noisy perturbations, thus providing enhanced noise robustness.

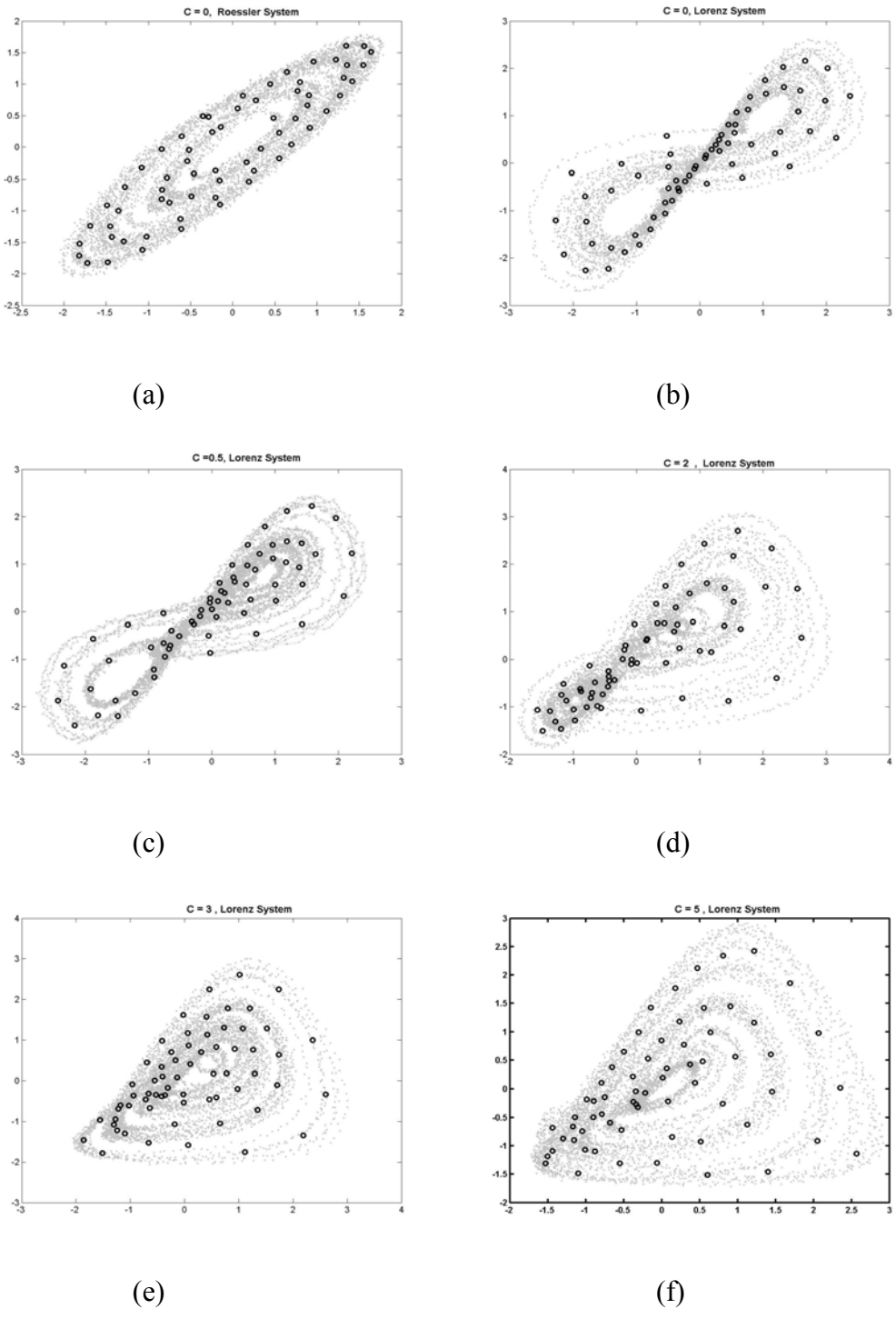

Figure 2-1. Phase-space trajectories of the Rosseler-Lorenz system for various coupling strengths a) Rosseler b) Lorenz (C=0) c) Lorenz (C=0.5) d) Lorenz (C=2) e) Lorenz (C=3) f) Lorenz (C=5). The SOM weights (circles) for each signal are superimposed on the trajectory.

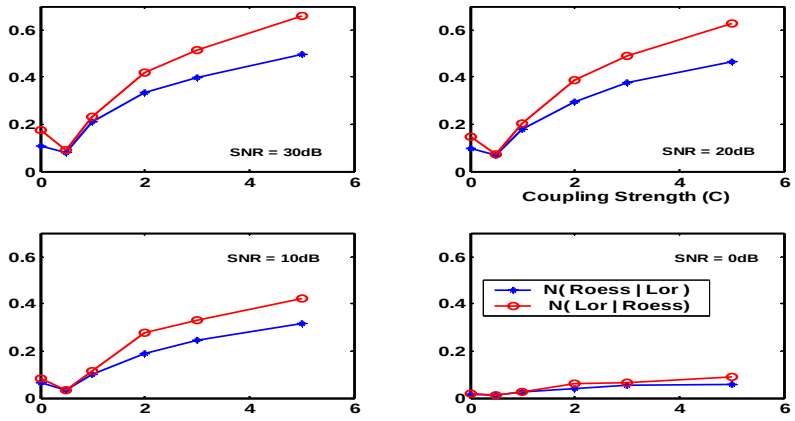

Figure 2-2. Illustrating the dependency relationships between the Rosseler (driver) and the Lorenz system (response) as a function of coupling strength.

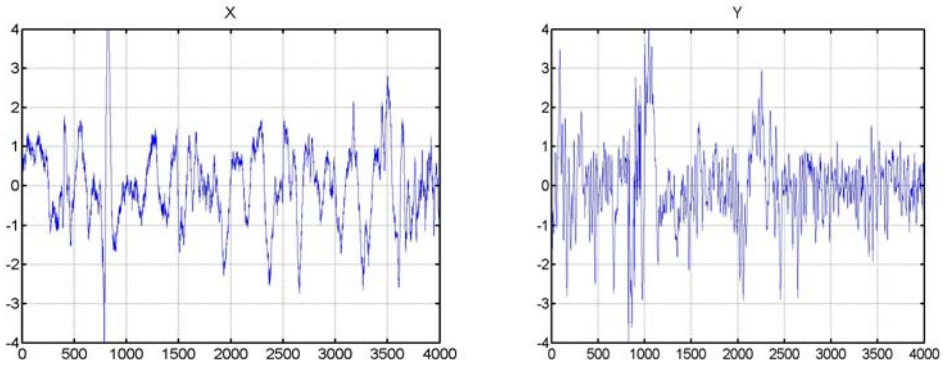

Figure 2-3. Original EEG signals X and Y. for the EEG simulation example

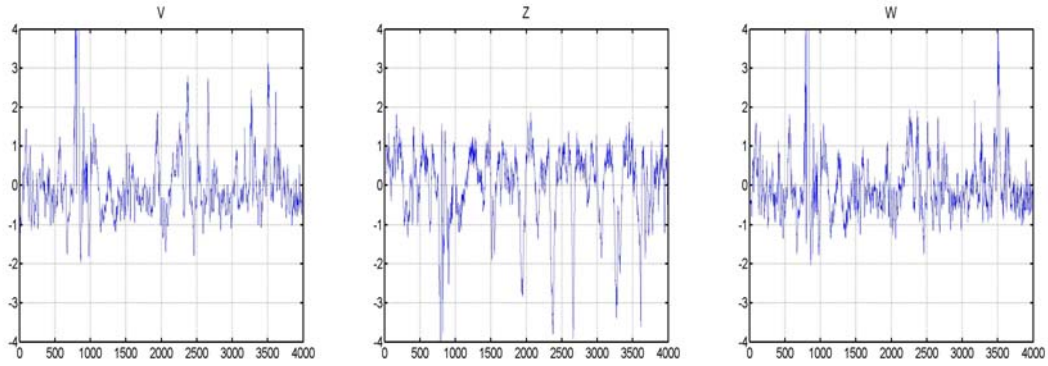

Figure 2-4. The nonlinearly mixed (synthetic) EEG signals V, Z, and W.

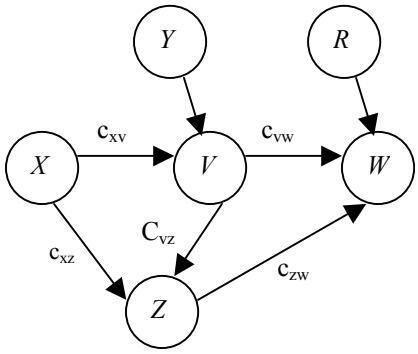

Figure 2-5. Schematic diagram of the coupling function between the signals.

2.4.2 Intracranial EEG Simulation

In this example [30], intracranial EEG signals recorded from epileptic patients are considered. Clinically, it is useful to know or find out the direction of information flow through intracranial EEG signals. This analysis may help locate the epileptic foci of the seizures as well as providing means of predicting them.

In this signal, since the intracranial EEG measurements are generated by a closed system (the brain), we assume that the dynamical statistics of the signals observed at different channels can be modeled using a single SOM, unlike the previous synthetic example, where a separate SOM was used for each signal. The SOM, however, must be trained using data that represents all possible psycho-physiological states that the intracranial EEG signals might exhibit. In the case of an epilepsy patient, these include pre-ictal, itcal and post-ictal states, in addition to the inter-ictal state.

In this example, intracranial EEG signals collected from two different patients at different locations (labeled *X* and *Y*) are used. A synthetic nonlinear functional relationship with influence direction from *X* to *V*, *W*, and *Z* is created according to (2.6). Care is taken in choosing these functions to make sure that the synthetic intracranial EEG

mixtures in (2.6) exhibit the characteristics of real EEG signals. The signals are shown in fig. 2-3. This is achieved by verifying that the time structure

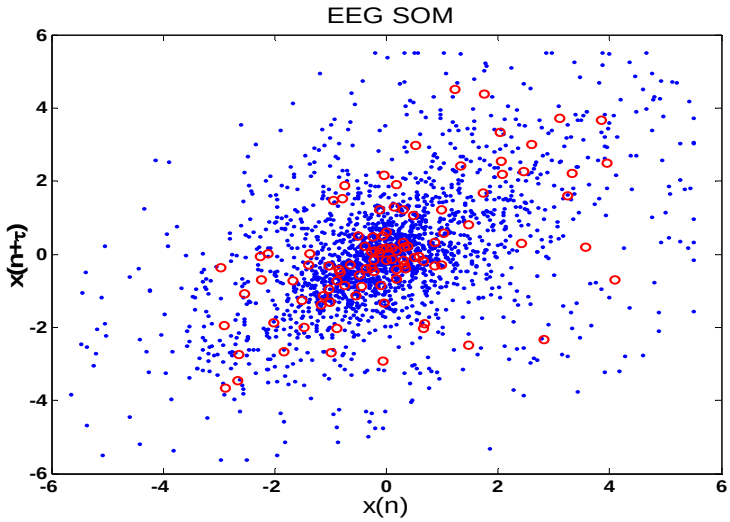

Figure 2-6. The phase-space trajectory of the training EEG signal (projected in two dimensions) and the weights of the trained EEG-SOM (circles).

and the power spectra of these signals are consistent with that of an EEG signal.

$$\begin{aligned} \boldsymbol{v}(\boldsymbol{n}) &= \boldsymbol{y}(\boldsymbol{n}) + \boldsymbol{c}_{\boldsymbol{xv}}\boldsymbol{x}(\boldsymbol{n}-2)\boldsymbol{x}(\boldsymbol{n}-3) \\ \boldsymbol{z}(\boldsymbol{n}) &= \boldsymbol{c}_{\boldsymbol{vz}}\boldsymbol{v}(\boldsymbol{n}-2) + \boldsymbol{c}_{\boldsymbol{xz}}\boldsymbol{x}(\boldsymbol{n}-2) \\ \boldsymbol{w}(\boldsymbol{n}) &= 0.05\boldsymbol{r}(\boldsymbol{n}) + \boldsymbol{c}_{\boldsymbol{zw}}\boldsymbol{z}(\boldsymbol{n}-2) + \boldsymbol{c}_{\boldsymbol{vw}}\boldsymbol{v}(\boldsymbol{n}) \end{aligned} \tag{2.6}$$

Here, $x(n)$ and $y(n)$ denote the original time sequences and $v(n)$, $w(n)$, and $z(n)$ denote the synthetic signals driven by the two original signals. In addition, $r(n)$ is a zero-mean unit-variance Gaussian noise term. The synthetic intracranial EEG signals are shown in Fig. 2-4 and the flow diagram representing the relationships in (2.6) is depicted in Fig. 2-5.

A 10x10 rectangular SOM (referred to as EEG-SOM) is trained using 3000 samples of embedded intracranial EEG data (with an embedding dimension of 10 and embedding delay of 30ms). The phase-space trajectory of the training data and the weights of the trained SOM are shown in Fig. 2-6. The normal EEG state is represented by the smaller amplitude activity (the dominant portion of the training data), whereas the

larger amplitudes correspond to the spiky, sharp, and slow wave activity formed during the ictal state of the brain, or to artifacts formed due to muscle movements, etc. After training the SOM, the normalized similarity index between the original signals *X* and *Y* is evaluated to verify whether these intracranial EEG signals are indeed independent or not.

The dependencies between *X*, *V*, *W*, and *Z* are also evaluated using the SOM to calculate the normalized similarity index. The results are summarized in Table 2-1, where both the coupling strength and the estimated similarity index between pairs of signals are presented.

Table 2-1. Coupling strength between pairs of signals, the normalized similarity index and the original similarity index between them.

Coupling Strength	χ		$S(X,Y) = S(X \mid Y) - S(Y \mid X)$	
$c_{xv} = 1$	-0.1668	$X->V$	-0.1112	$X->V$
$c_{xz} = 2$	-0.0756	$X->Z$	-0.0612	$X->Z$
$c_{vz} = -0.8$	0.0901	$Z->V$	0.0772	$Z->V$
$c_{vw} = 1$	-0.213	$V->W$	-0.336	$V->W$
$c_{zw} = 0.3$	-0.1225	$Z->W$	-0.1044	$Z->W$

The results obtained from the SOM-based SI measure and the original SI measure (in Table 2-1) is in perfect agreement. We conclude that X influences V and Z, V influences Z and W, and W influences Z. Comparing these with the flow diagram in Fig. 2-5, it is seen that all directional couplings are consistent with the true construction except for the relationship between V and Z. Possibly, this discrepancy is due to some cancellations between the couplings from X and from V. Also, we can see that V is exclusively constructed from the X and the Y components and does not have any

independent oscillations of its own, unlike W. These results indicate that the similarity index approach might not produce results that are consistent with what one would expect from the equations (if these are known) when the coupling diagram has closed loops.

2.5 Epileptic Intracranial EEG Data Description

Intracranial EEG signals were recorded from hippocampus, sub-temporal and frontal-cortex structures of epileptic patients having a history of complex-partial, partial-secondary and sub-clinical seizures of temporal-lobe focus, using bilaterally and surgically implanted electrodes (Fig 2-7). Using amplifiers with an input range of $\pm 0.6\boldsymbol{mv}$, the recorded signals were converted to narrow-band using an anti-aliasing filter with a cut-off range between 0.1Hz and 70Hz. Using an analog-to-digital converter with 10-bit quantization precision, the narrow-band signals were sampled/digitized at 200 samples/sec. Measurements involved recording intracranial EEGs from multiple sensors (28 to 32, with common reference channels) and the recordings spanned over 6 continuous days. A total of 55 seizures, of temporal lobe onset, were recorded from 5 patients, in the range of 6 to 18 seizures for each patient.

2.6 Testing the application of SOM-SI on Epileptic Intracranial EEG

In this section, we demonstrate the utility of SOM-SI in epileptic intracranial EEG analysis and statistically verify accuracy of the results with the original SI. A 25x25 EEG-SOM is trained using 3000 input vectors constructed by embedding (dimension, m = 10, delay, τ = 30ms) intracranial EEG signals collected from various regions such as temporal, sub-temporal, and orbit frontal, of an epilepsy patient. The EEG-SOM needs to represent all possible EEG-dynamics, so the training data must include samples from the inter-ictal, ictal, and the pre-ictal states of the patient. Fig. 2-8 shows the phase-space trajectory of the data and the PEs of the EEG-SOM in two-dimensions. The normal

EEG state is represented by the smaller amplitude activity (the dominant portion of the training data), whereas the larger amplitudes correspond to the spiky, sharp and slow wave activity,

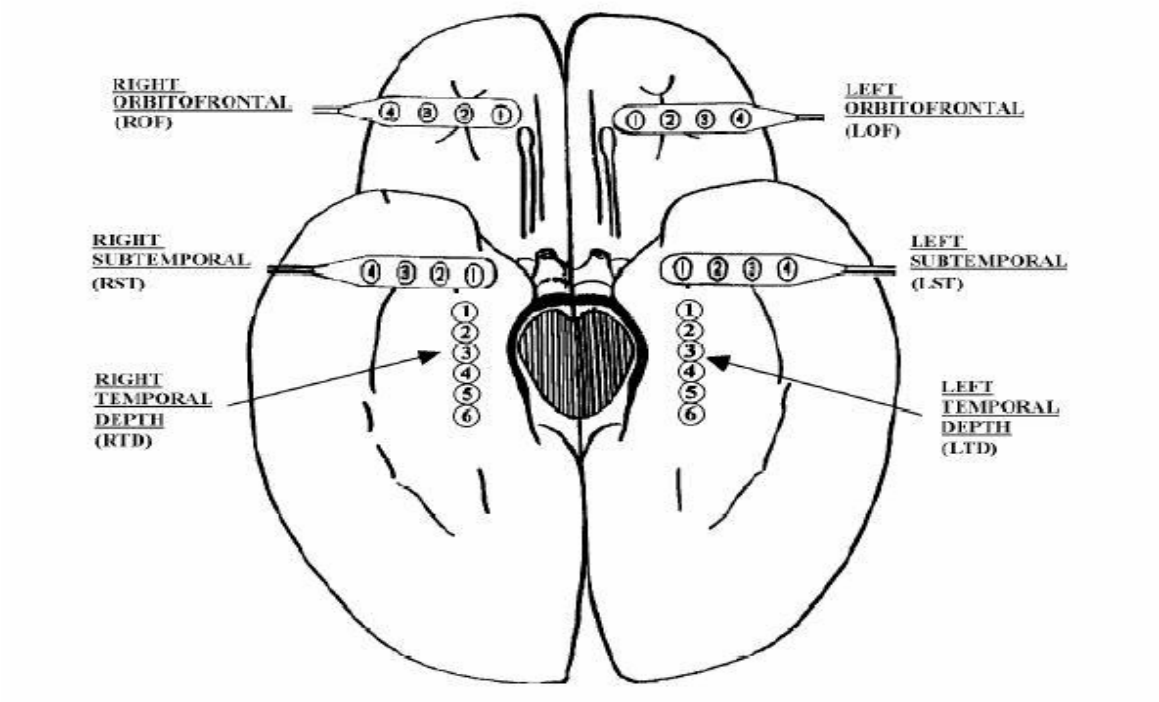

Figure 2-7. Diagram of the depth and subdural electrode montage in an epileptic brain. Electrode strips are placed over the left orbitofrontal (LOF), right orbitofrontal (ROF), left subtemporal (LST), right subtemporal cortex (RST). Depth electrodes are placed on the left temporal depth (LTD) and right temporal depth (RTD), to record hippocampus EEG activity.

mostly formed during the ictal state. We note that the distribution of the neurons is sparse in the higher amplitude region because of the density matching property of the SOM.

To ensure generalization of the SOM, a test set of intracranial EEG signals were quantized by the trained SOM. As seen from Fig. 2-9, the quantization results successfully approximate the dynamics of the test data set (projected in one-dimension). The correlation coefficient between the two signals was found to be 90.1%. For the most

part, the correlation coefficient was between 80% and 95%. Note that the amplitude errors are higher in the larger amplitude regions corresponding to spike and slow waves. This is expected because of the sparse distribution of the neurons in the higher amplitude regions. These errors can be compensated by using a larger SOM grid (> 25x25), but since the dynamics of the data are more important for the neighborhood information in the SI measure and computational complexity will be an issue, we chose not to increase the SOM grid size.

2.7 Statistical comparison between SI and SOM-SI

Next, we quantify the accuracy of the SOM-SI measure relative to the original SI measure by comparing their results. SI values were calculated on nearly 39 minutes of data corresponding to a pair of signals obtained from the right temporal (RTD4) and the right sub temporal depth (RST1) electrodes, corresponding to patient P093. The entire

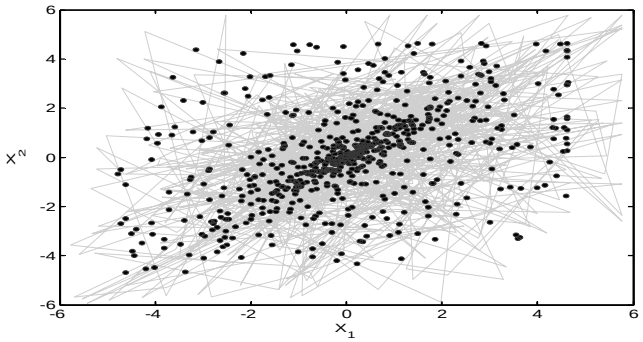

Figure 2-8. The phase-space trajectory of the training intracranial EEG signal (solid lines) superimposed on the weights (dots) of the trained 25x25 EEG-SOM grid.

interval of 39 minutes data was segmented into 230 non-overlapping windows of 10 seconds each. Fig.2-10 shows the interdependency values of both the measures. It is easy to see that the results from both the measures are in agreement to a large extent. There are also subtle differences, which need to be quantified using statistical tests.

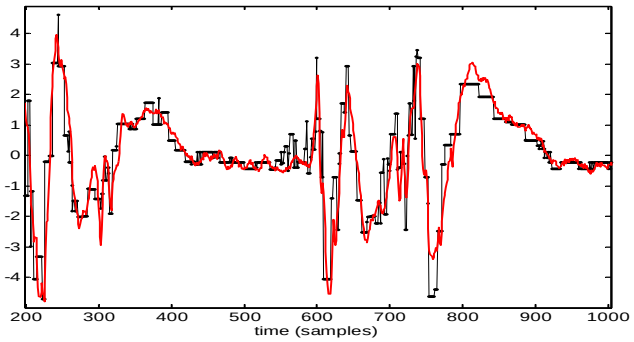

Figure 2-9. A qualitative illustration of the accuracy of the 25x25 EEG-SOM. Sample test signal (solid line) overlapped on the SOM-reconstructed output (dash and dot line). In this case, the correlation coefficient = 90.1%.

The comparison will be two-fold: (i) identify if the number of windows in which the predicted directions of influence differ is significant or not, (ii) given time instances where both measures agree on the direction, check if significant differences exist in predicted strengths of influence. Assuming that SOM-SI and SI measure values come from normal populations, we use the two-sided paired t-test to investigate the extent of disagreement between the two methods. The test was performed at a significance level of α=0.05, over a size of 138 randomly selected samples out of the 230 available samples.

Null hypothesis: H_0: $\mu_d = \mu_{(\chi_{som-SI} - \chi_{SI})} = 0$

Alternate hypothesis: $H_{1:}$ $\mu_d = \mu_{(\chi_{som-SI} - \chi_{SI})} \neq 0$

Paired t-test is chosen, because the observation in window 1 of original SI is obtained under similar conditions as the window 1 of SOM-based SI, and hence, the data may be said to occur in pairs. In this case, t_{exp} was found as -0.9441, whereas $t_{crit}=t_{(0.05),\ 137}=1.960$. Since $t_{exp}<t_{crit}$, we do not have enough evidence to reject the null hypothesis, H0. This was also the case in 20 other comparisons made using different electrode pairs from different patients. Therefore, we conclude that statistically the SOM-SI measure, computed with a 25x25 grid SOM, performs as well as the original SI measure.

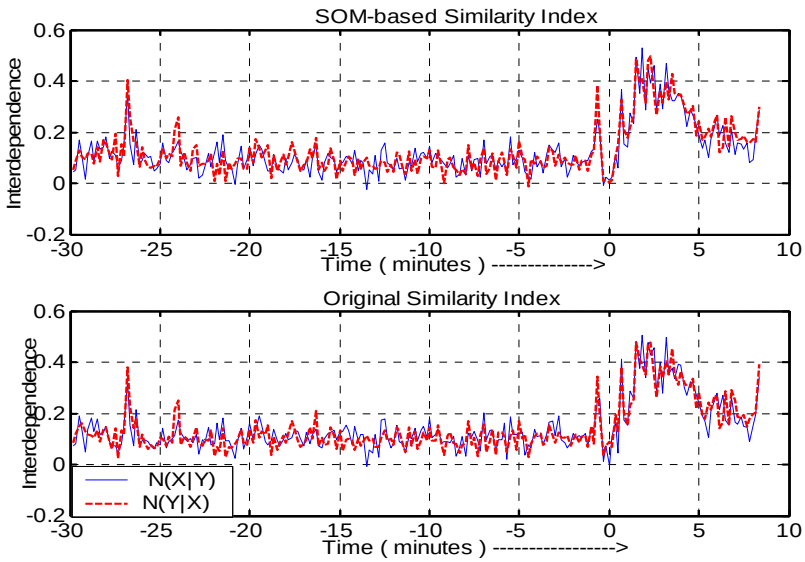

Figure 2-10. SOM-SI results showing the dependencies between two signals. X and Y correspond to channels RTD4 and RST1, respectively. The time instant '0' corresponds to the seizure onset (top). Results produced by the original SI (bottom).

2.8 Testing the Robustness of SOM-SI on Multiple SOMs

The previous simulations successfully demonstrated the accuracy of the SOM-based measure by statistically comparing its results with results from the original SI measure. For application on seizures especially, a 25 x 25 SOM grid was trained to embed all the dynamical states of the EEG attractor. SOM being one of the most important elements of this improvised measure, one of the pre-requisites of this approach is to ensure the following: a) that for data modeling purposes, the training set captures the essence of variance found in the dynamics of the ictal states from all the channels, for a given patient and b) the similarity indices computed using the SOM's processing elements (PEs) are independent of the SOM and the corresponding training data set. In other words, pair-wise similarity indices computed on two separate SOMs should be significantly close to each other, if not equal.

We performed a simple test to check the latter point before proceeding with extensive data analysis. From the multivariate intracranial EEG data samples of the patient P093, two separate training sets were constructed. One of the training sets consisted of portions of data sampled from the inter-ictal, ictal, pre and post-ictal states of seizures 1 & 2. The other training set consisted of data portions picked around seizure 4 & 5. Using the same normalization procedures on both the sets and with the same set of training parameters as before, two separate SOMs (called as SOM-1 and SOM-2 for convenience) were trained. Following that, the SOM-similarity indices were obtained from pair-wise analysis of interdependence among channels chosen from the ROF and LOF regions of the brain, as illustrated in Fig 2-11.

The test data from the ROF and the LOF regions were picked from intervals surrounding seizures 6 & 7, seizures 4 & 5 and seizure 11, respectively. Fig 2-12 shows the exact time-intervals of the test data. The similarity index profiles $\{N^1 (X|Y)_t$ and $\{N^2 (X|Y)_t$ obtained from computing the SOM-SI on large intervals (say time t = 1,…,T) of seizure data are quantitatively compared using the classical correlation coefficient and error-percentage as the comparison metrics. The error-percentage is computed as follows

$$\{e\} = 100 * \left\{ \frac{N^1(X \mid Y)_t - N^2(X \mid Y)_t}{N^1(X \mid Y)_t} \right\}_{t=1}^{T} \tag{2.7}$$

where N(X|Y) is the normalized interdependency of X on Y. Note that the notations X are Y are used to denote the two channels of interest. Normalized error *e* quantifies the percentage difference between the interdependency values from SOM-2 and SOM-1, keeping interdependency value from SOM-1 as the reference. From the error population, the fraction of the absolute error values less than 20% and the fraction less than 10% are

computed to determine the degree of dependence of the SOM-SI measure on the data used to train a SOM.

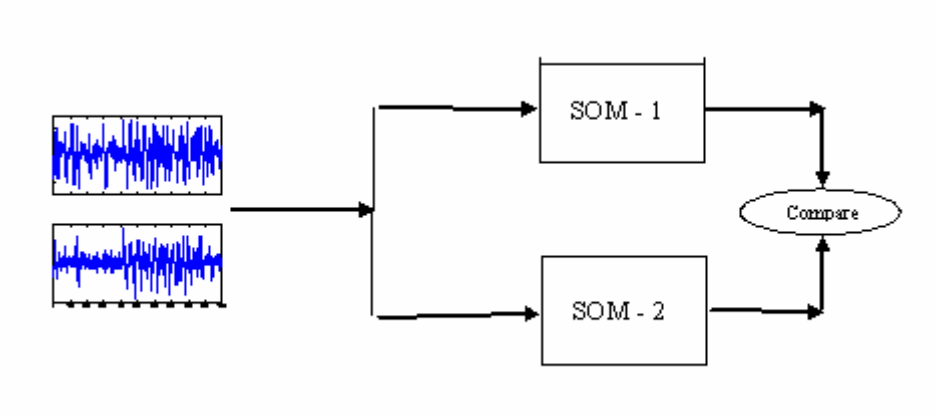

Figure 2-11. Experiment setup to compare SOM-Similarity Indices obtained from 2 separate maps.

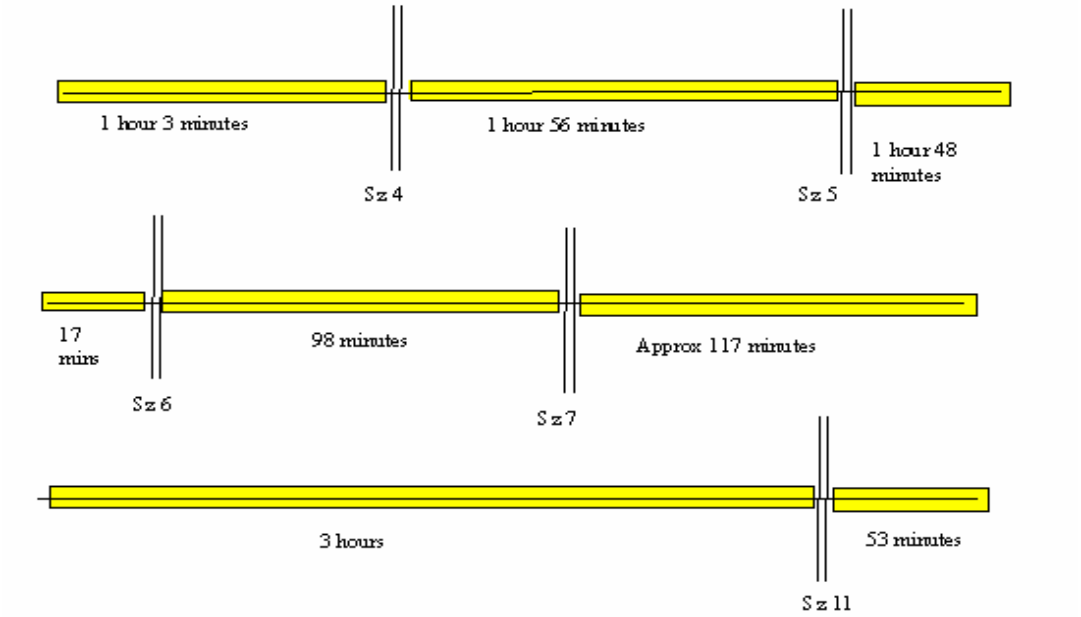

Figure 2-12. Time intervals from all the seizures used as test data (not drawn to scale)

For illustration, the results from analyzing the interdependency of LOF3 on LOF4 on various seizures are shown in fig 2-12. The histograms correspond to the error ensembles obtained from analyzing over long seizure intervals. Qualitatively, the superimposed traces in fig 2-13 indicate the extent of agreement or disagreement between the SOM-SI profiles. Table 2-2 compiles a summary of the agreement between the SOM-

SI profiles for about 13 hours of intracranial EEG data from 5 seizures. A large fraction of errors less than 20%, supported by a high correlation coefficient between the two SOM-SI profiles suggests that there was very little disparity between the SOM-SI profiles from SOM-1 and SOM-2. Besides, the high percentages also suggest the intracranial EEG data dynamics do not vary drastically from one seizure to another, and therefore the two SOM models produced the almost identical SI results. This finding will consequently support (or reinforce) our original belief that a well-trained SOM and a well picked training data set is sufficient to carry out independency analysis on all the seizures of a patient.

Overall, pair-wise analyses of the interdependency among 6 channels ($C_2^6 = 15$ combinations) on 5 seizures of P093 was performed on SOM-1 and SOM-2. The average correlation coefficient and the error results between the SOM-SI profiles are shown in Table 2-3.

Results from table 2-3 indicate that around 80% of the times, the differences between the SOM-SI results are less than 20%. This is not surprising considering that the differences are measured in percentages (2.7) and therefore even small discrepancies in the case of small dependency values can appear magnified. In addition, we also speculate that the discrepancies could be the outcome of the two SOMs being trained in an identical fashion instead of being fine-tuned to obtain the lowest reconstruction error in each. In

Table 2-2. Quantitative comparisons between the SOM-SI profiles obtained from SOM-1 and SOM-2. LOF3 & LOF4 data was projected on each of the SOMs and then the SOM-SI measure was applied to analyze the dependency of LOF3 on LOF4.

P093, Interdependency N(LOF3| LOF4)	**Correlation Coefficient (%)**	**Fraction of error less than 20%**	**Fraction of error less than 10%**
Seizure 6 & 7	95.74	0.8504	0.5597
Seizure 4 & 5	98.45	0.9234	0.7543
Seizure 11	91.59	0.6452	0.3614

general, if the SOMs can be designed to obtain the lowest reconstruction error, by iteratively choosing the best sets of parameters, a slight improvement in the performances can be easily achieved. But as it stands, a slight discrepancy can nevertheless be always expected although it may have very little impact in the overall scheme of analysis.

2.9 Summary

The similarity index measure determines directional dependencies between two signals using the basic assumption that two related signals will have similar recurrences of the embedded state vector. This method has high computational complexity in terms of the number of samples, since a search for nearest neighbors must be performed in the phase-space of the signal. In this dissertation, we proposed a SOM-based approach as an improvement over the original SI measure, for detecting functional dependencies among multivariate structures. This approach reduces the computational complexity drastically by exploiting the accurate quantization properties of the SOM in representing the dynamics of the signal in the phase space. Another advantage of the SOM-based

approach is that the difficulties that the original similarity index approach encounters in handling nonstationary data (such as the necessity to tweak parameters) are eliminated by training the SOM using samples from various regimes of the nonstationary system. On

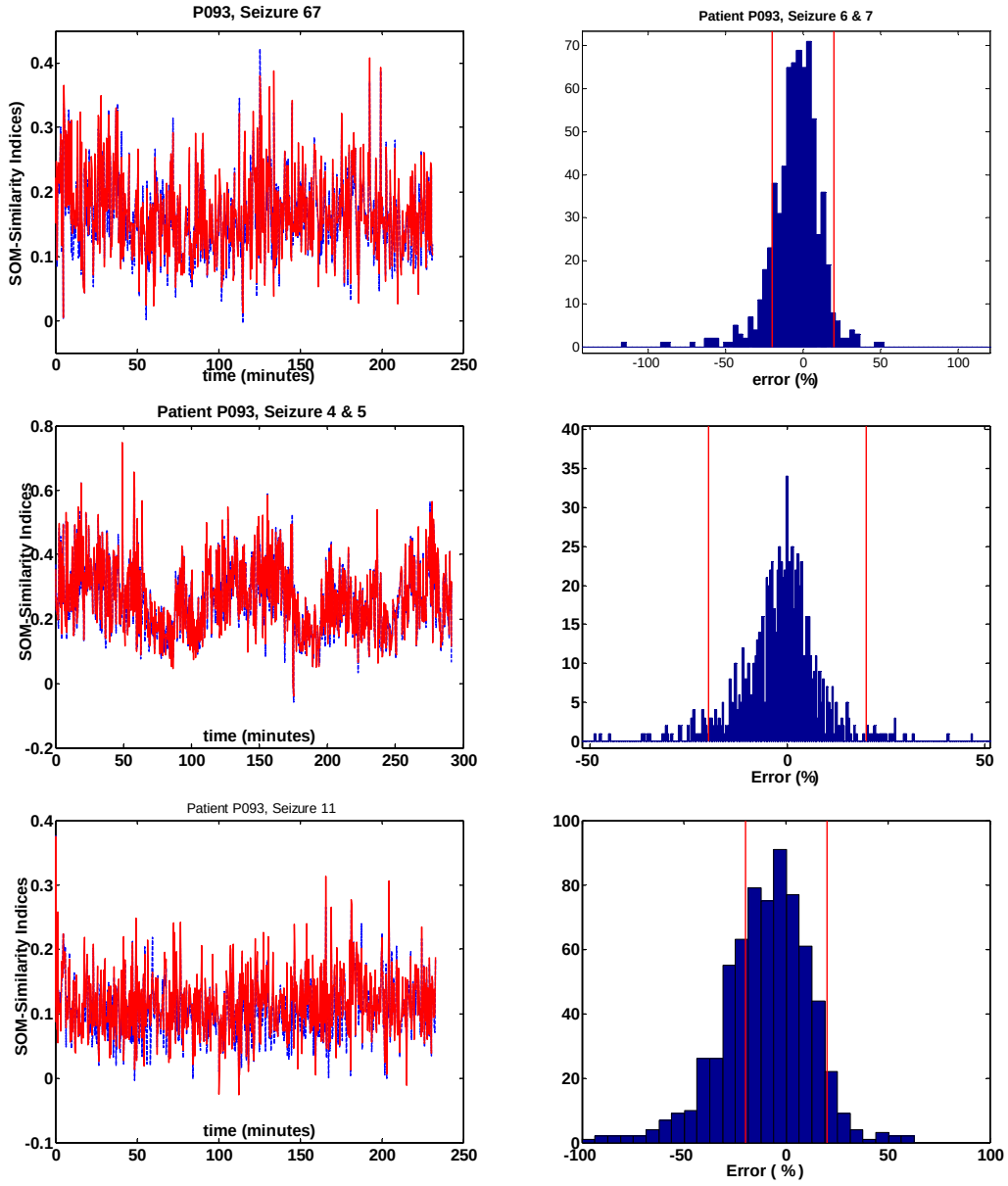

Figure 2-13. Comparing interdependencies between channels LOF3 and LOF4. Left : SOM-similarity profiles from the output of SOM-1 and SOM-2 are superimposed. Right: Histogram of the errors in %. Top: Seizure 4 & 5 Middle: Seizure 6 & 7. Bottom: Seizure 11.

Table 2-3. Summary of the comparisons between the SOM-SI profiles from SOM-1 and SOM-2. Each row represents the statistics (mean and variance) of pair-wise SOM-SI analyses of the epileptic intracranial EEG data from 6 channels (15 combinations).

P093	Correlation Coefficient (%)	Fraction of error less than 20%	Fraction of error less than 10%
Seizure 6 & 7	94.32 ± 2.85	0.79± 0.1	0.54 ± 0.12
Seizure 4 & 5	97.46 ± 1.08	0.91 ± 0.06	0.73 ± 0.12
Seizure 11	93.24 ± 2.06	0.71 ± 0.08	0.41 ± 0.07

the other hand, the SOM-based approach might suffer from inaccuracy if the quantization is severe. Therefore, the size of the SOM could be decided by a trade-off between representation accuracy and computational complexity. Through simulations, we also demonstrated the noise-robustness features of the measure.

CHAPTER 3
SPATIO-TEMPORAL CLUSTERING MODEL

3.1 Introduction

In Chapter 2, we proposed the SOM-SI measure [29-31] and demonstrated SOM's resourcefulness as a model infrastructure for computational purposes. Often, the time-sequences in a multi-variate system share similar information that is reflected in their interactive or synchronization abilities. By definition the word similar could mean that the information shared among a set of channels is stronger than the information they share with other channels. Such spatial similarities could possibly be momentary up to a few seconds or could even stretch to several minutes or hours. As we postulated earlier, spatio-temporal similarity changes could be one of the driving factors to trigger certain events in biological systems. From a seizure point of view, we suspect that analyzing the temporal changes in channel similarities could reveal some interesting aspects about the epileptic brain.

Similarity-based time-series clustering [25, 44] is a well researched topic in the area of dynamical graph theory. It is an extremely useful approach to characterize the spatial groupings in time-sequences. Similar time sequences are typically grouped based on their mutual interactions. In this study, using the SOM-SI as a computational tool to derive the distance/similarity/proximity matrix, we propose a clustering model to dynamically analyze the spatio-temporal groupings in muti-variate time sequences. Simple toy simulations are presented to validate the robustness of the model. Since our

goal is specific to intracranial EEG, we use this model in chapter 4 to track the seizure-related temporal changes in groupings.

3.2 Model for Spatio-temporal clustering

In this section, we propose a clustering approach to extract information on spatio-temporal distribution of multivariate time-measurements. A 3-fold approach consisting of spatial-discretization of the data using spectral-clustering technique [57, 64, 100], temporal quantification using hamming distance, followed by application of another clustering technique, is presented in Fig 3-1. The rational will become apparent during the explanation.

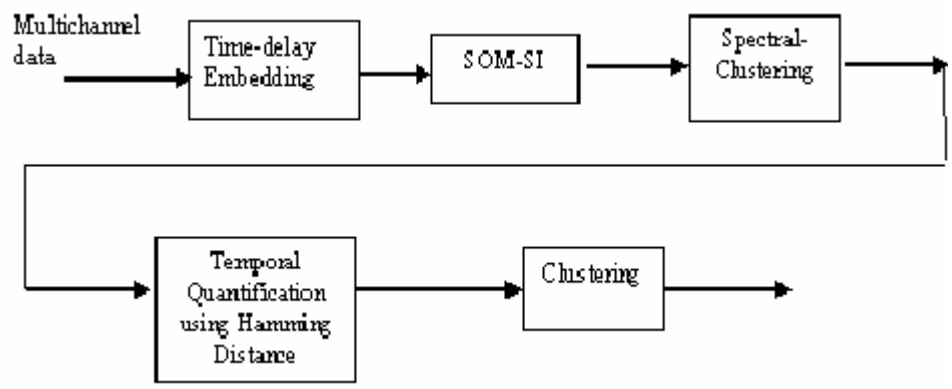

Figure 3-1. Block diagram to extract spatio-temporal groupings information in Multivariate EEG structures

Spectral clustering is one of the many clustering methods that use subspace decomposition on data-derived affinity matrix to achieve data-clustering. Using kernel methods, the data samples are projected onto a higher dimensional space where the discriminant analysis is much easier. Projecting the data onto a feature space results in tightly formed clusters such that the between cluster entropy is maximized and within cluster entropy is minimized. Spectral Clustering is inspired by the normalized cut theory in computer science where the distance between the nodes/data samples is interpreted as

an affinity matrix on which subspace decomposition yield membership labels of the nodes/data samples.

In our study, we use the standard spectral clustering algorithm by Ng *et al*. [64] to spatially cluster the similarity-indices obtained by the SOM-SI technique. The algorithm is outlined below,

1. Assuming N to be the number of nodes S = {s_1, s_2, …. s_N} and k as a priori specified cluster size, form a similarity matrix $A \in R^{NxN}$ using a distance metric.
2. Define D to be the diagonal matrix whose (i,i)th element is the sum of A's i_{th} row and construct the matrix $L = D^{-1/2} A D^{-1/2}$.
3. Find x_1, x_2, ….x_k , the k largest eigen-vectors of L and form the matrix E by stacking [x_1, x_2, ….x_k] $\in R^{NxK}$ the eigen-vectors in columns.
4. Form the matrix Y from X by renormalizing each of X's rows to have unit length.
5. Treating each row in Y as a point in R_k, cluster them into k clusters using k-means or any other distortion minimization algorithm.
6. Finally, assign original node (s_i) to cluster j if and only if row i of the matrix Y was assigned to cluster j.

Pair-wise evaluation of SOM-SI measure on all the possible combinations ($(C^N_2$, where N is assumed to be the number of channels) of a portion of a multi-variate time series leads to $k = 2*(C^N_2)$ similarity indices in the bounds of [0, 1]. *k* is multiplied by 2 because of the asymmetric nature of the SOM-SI measure. If we imagine the time-series as various inter-connected nodes in a multi-dimensional graph, the SOM-SI similarity indices represent the affinity or rather, the weights of the connection, between those nodes. Therefore, we can translate them into a square matrix of size *N* x *N*, where *N* is the # of channels. Since the weighting is normalized between 0 and 1, the diagonal elements representing the affinity of a channel with itself, are coded as 1.

However, to be able to perform spectral-decomposition on an affinity matrix, Ng's algorithm [64] requires that the affinity matrix be square and symmetric in nature. This is because the eigen decomposition yields orthogonal column vectors (also called eigenvectors) only if the projection matrix is square-symmetric. The asymmetric matrix can be transformed to a symmetric matrix by adding it to its transpose and dividing each entry by 2. Mathematically, if κ_1 represents the asymmetric affinity matrix, the transformation can be represented as,

$$\delta = \frac{(\kappa_1 + k_1^{\,T})}{2} \tag{3.1}$$

The transformed affinity matrix now represents the average information exchanged between all pairs of channels. This implies that we do not have the luxury of using the asymmetric nature of the dependencies to create a membership grouping among channels. In epileptic study however, we will see that the averaging of the dependency information will not affect channel dependencies because of the earlier observation that there is no major difference in the driving and receiving information of the channels.

On the transformed affinity matrix δ, eigen decomposition can be done, followed by *K*-means clustering. Consequently, we have a set of labeled clusters (number of clusters is set, based on significant eigen values) representing the membership of the channels.

If the above procedure is repeated over consecutive time windows (overlapped or non-overlapped), channel groupings obtained on each time-window can be arranged as in a matrix form as in (3.2).

$$\kappa_{spect} = \begin{bmatrix} 3 & 2 & 2 & . & . & . & . & . & 3 & 1 \\ 1 & 2 & 2 & . & . & . & . & . & 3 & 2 \\ . & . & . & . & . & . & . & . & . & . \\ . & . & . & . & . & . & . & . & . & . \\ 3 & 1 & 2 & . & . & . & . & . & 1 & 2 \end{bmatrix} \tag{3.2}$$

To characterize the average clustering of the channels over a longer period of time, we propose another, albeit simple, hierarchical clustering approach that uses hamming distance to derive the proximity matrix.

3.3 Temporal Quantification Using Hamming Distance

We showed in the previous section that the multivariate time-series can be grouped by using similarity-based clustering techniques such as spectral clustering. The spectrally clustered labels specify the groups of channels exhibiting high degree of within-cluster similarities and low between-cluster similarities. Often in applications such as epileptic EEG analyses, it is important to identify channel groupings over a longer period of time. The epileptic seizures, in particular, are characterized by dynamic states (inter-ictal, ictal, pre-ictal & post-ictal) that are known to possess both local and global spatio-temporal clusters. Channels associate and de-associate in time; however, depending on the psycho physiological state of the brain, certain groups of channels might have a higher likelihood of sharing same channel labels thus forging a long-term association. In epileptic intracranial EEG, identifying such state-dependent clusters may provide us with useful insights on the evolution of brain patterns during seizure states.

State dependent connections can be quantified by clustering rows of the κ_{spect} matrix that are similar with each other over a longer time interval, say *T*. Mutual Information is one of the widely used metrics to quantitatively evaluate the similarity between two discrete processes. However, in our study, using mutual information to

assess the degree of similarity between two channels/rows can have serious drawbacks. For any two channels, two pairs at different time-instances, having same elements (say 3 & 1) need not bear any semblance. This is because the cluster labels are arbitrarily labeled at each time-instance and do not have a fixed representation across time. Technically, it implies that the probability term $p_{(i=u,j=v),}\ \ i \neq j$, where i, j are the channels/rows in the κ_{spect} matrix and u, v are the channel labels/memberships, can be skewed unless $u = v$.

In this context, a very simple statistic to determine the degree of similarity would be to compute the relative frequency of any two channels sharing the same labels/groupings. In other words, in a time window of length T, we check the average number of times when the two channels of interest, share the same cluster label.

In an algebraic context, the above operation is equivalent to computing pair-wise hamming distance in a time window T. Of course, similarity would be obtained by subtracting the hamming distance from 1. That is,

If d_{ij}^{ham} is the hamming-distance between channels 'i' & 'j', similarity in probabilistic terms is obtained as,

$$p_{ij}^{sim} = 1 - d_{ij}^{ham} \tag{3.3}$$

Thus, computing the pair-wise similarity for all i & j combinations will result in a $\boldsymbol{P}$ matrix of size $N \times N$ (N is the number of channels). For convenience, we will call the matrix $\boldsymbol{P}$ the cluster-similarity matrix in all our future references.

Hierarchical clustering on the cluster-similarity matrix $\boldsymbol{P}$ will yield information on the cluster groupings over a time T. In the context of intracranial EEG data, clustering

will thus enable us to know the groups of channels that have similar behavioral structure in the brain, over a wider time interval.

3.4 Simulations with Synthetic Data

This section presents simple simulations to demonstrate the validity of hierarchical clustering approach to cluster a multivariate time-series data based on their mutual interactions.

3.4.1 Roessler – Lorenz System

Recall the Rosseler and the Lorenz system example from section 2.3.1. The idea is to first generate non linearly coupled dynamical signals in each system and identify mutual interactions using the SOM-SI measure. A hierarchical clustering algorithm such as spectral clustering is then applied to group the time-series into pre-determined number of clusters.

For the zero-coupling case (C = 0), 5000 data-samples from the non-transient portion of each of the 6 components are extracted as shown in Fig 3-2a. Observe that the time profiles of the first and the second components of each system have a strong phase-similarity between them. The dynamics of each system evolve as a result of non linear interactions within their components.

Ideally, only two SOMs suffice, each trained to represent the Rosseler and the Lorenz system individually. However, if non linear coupling is introduced between the two systems, the attractor dynamics change depending on the coupling strength. This situation will force us to have individually SOMs to represent each dimension of a system. Therefore, without any loss in generality, we train individual SOMs for each component of the Roessler and the Lorenz system. Specific to this simulation, each SOM was a 2-d grid of size 8 x 8 processing elements.

Affinity between the components is obtained by pair-wise computing the SOM-similarity indices. Further, groupings among the 6 time-profiles are obtained by applying spectral clustering algorithm. Spectral clustering, for a cluster-size $n = 2$, clear distinguishes between Rosseler and the Lorenz components. For visual purposes, we present the dendrogram (as in Fig 3-3a) generated in MATLAB 7.0. As expected, the Rosseler and the Lorenz components form separate individual groupings. The fusion levels also support the fact that the coupling strength C is very low (in this case = 0), by clearly suggesting weak between-component interaction.

The next case consists of establishing a coupling (C = 5) from the X_2, the 2^{nd} component of the Roessler to Y_2, the 2^{nd} component of the Lorenz system. Fig 3-2b shows the time-traces of the Roessler and the Lorenz components. It is clear that Y_2, (and therefore the Y_1, the1^{st} component as well) has an altered time-profile. In addition, since Y_2 and Y_3 of the Lorenz system also interact in a non linear fashion, we observe a clear change in the time-dynamics of Y_3. The procedure of applying SOM-SI to compute the affinity matrix followed by spectral clustering is repeated. Dendrogram is shown in Fig. 3-3b, to graphically illustrate the cluster organization. Firstly, we can observe that the topology of this dendrogram (for C = 5) is drastically different from the topology of dendrogram for C = 0. We no longer see two clearly separated Rosseler and Lorenz groupings. The fusion levels among the Lorenz components is still pretty much at the same level as they were for C = 0. However, the fusion levels between the combined Lorenz components and X_1, X_2 combined is reduced considerably, reflecting strong coupling introduced earlier. The topology-difference between the two dendrograms in fig.

3-3b suggests that due to the non linear coupling introduced in (2.5) through the coupling constant C, the dynamics of X_2 & X_1 are more closer to the dynamics to Y than to X_3.

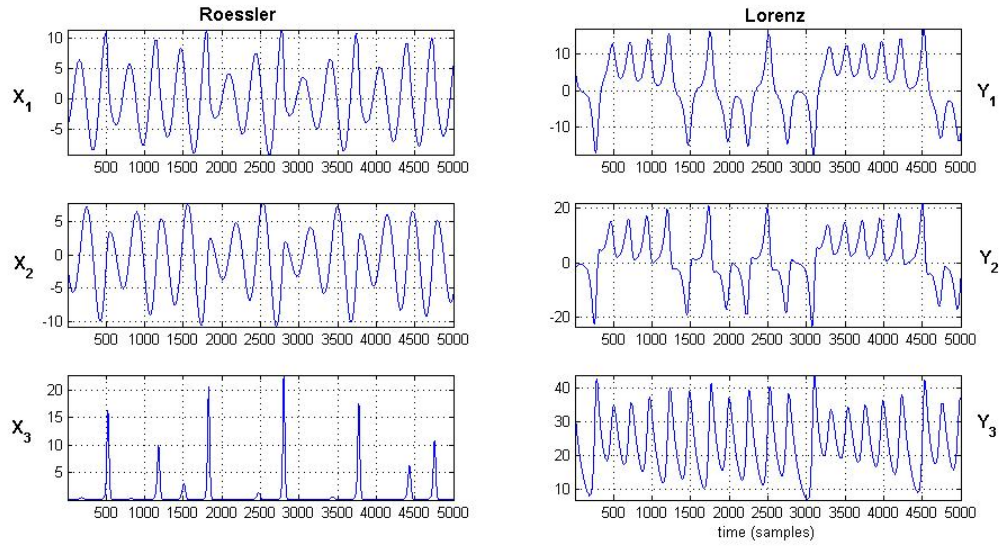

(a)

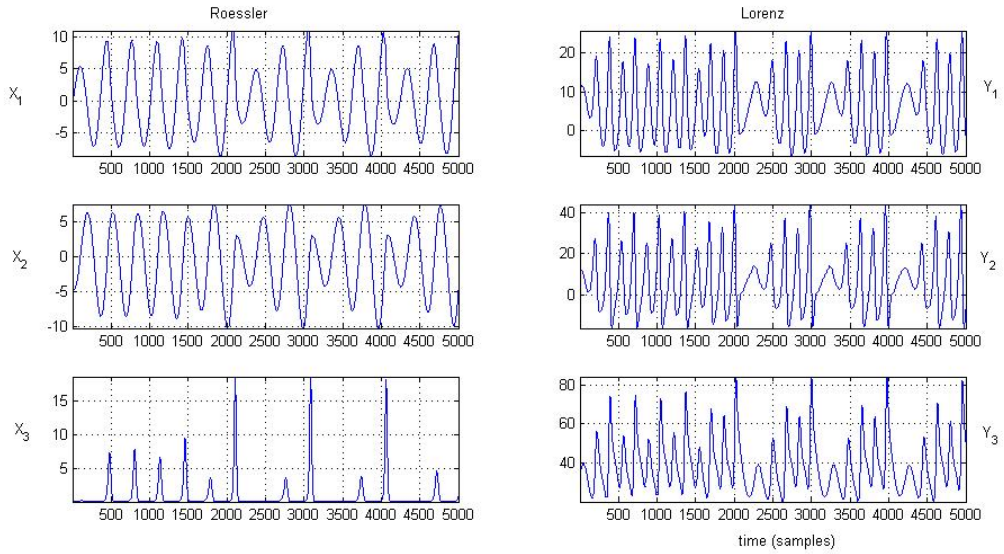

(b)

Figure 3-2. Time profiles of the Roessler and the Lorenz components. a) Coupling strength, C = 0 and b) C = 5

Table 3-1 shows the cluster groupings, obtained as a function of *n* for various coupling constants. While it is hard to obtain any distinction among the groupings, with *n* = 4, the difference is clear for *n* = 2. Spectral Clustering, consistent with the model construction and the observation in dendrogram, groups the X_1, X_2, Y_1, Y_2 & Y_3, components separately from X_3.

Table 3-1. Cluster groupings for the simulation example.

	C = 0	C = 5
# of clusters, n = 2	(X_1, X_2, X_3), (Y_1, Y_2 ,Y_3)	(X_1, X_2, Y_1, Y_2 ,Y_3), (X_3)
# of clusters, n = 3	(X_1, X_2, X_3), (Y_1, Y_2), (Y_3)	(X_1, X_2), (X_3), (Y_1, Y_2, Y_3)
# of clusters, n = 4	(X_1, X_2), (X_3), (Y_1, Y_2) , (Y_3)	(X_1, X_2), (X_3), (Y_1, Y_2) , (Y_3)

3.4.2 Linear Model

Consider a set of colored noise data obtained as the band-pass filtered output of an additive white-Gaussian stochastic process of zero mean and unit-variance (as shown in Fig. 3-2). Each of the outputs can be denoted by $s_i(t)$, $i = 1,2,.....,8$ & $t = 1,2,...,T$. We construe $x_i(t)$ as the observation measurements, sampled from eight (8) different channels of a spatio-temporal system, over an interval *T*. Observe that $x_i(t)$ is constructed by adding Gaussian white noise (of variance between 0.1 and 3) to $s_i(t)$.

$$\boldsymbol{x_i(t) = s_i(t) + n_i(t)} \tag{3.4}$$

Design of noise $n_i(t)$ is such that , a variance higher than 3 will destroy the structure of $x_i(t)$ to the extent that the signals become completely un-correlated with each other. Even though the two band-pass filters denoted by BPF_1 and BPF_2 respectively (as shown in fig. 3-3 and fig. 3-4) share different pass-bands, there is a significant amount of overlap as seen by the narrow separation of their pass-bands. It should also be noted from fig. 3-4 that some of the output measurements $x_i(t)$ can share the same band-pass filters. However the additive noise component $n_i(t)$ can introduce some stochastic differences in their linear structures. Measurements $x_i(t)$ that share the same band-pass filter can loosely be considered analogous to time-structures having reasonably strong linear-interactions. This is because information exchanged between two time-series can sometimes cause their phase dynamics to be similar.

We compute pair-wise cross-correlation indices (1) among all the channels to quantify the interactions or rather, the exact amount of information exchanged among the spatio-temporal measurements $x_i(t)$. Due to the fact that the signals are stochastic, linear and do not possess any complex or chaotic phase dynamics, we felt that the cross-correlation computation would suffice to indicate the amount of their pair-wise interactions. The cross-correlation indices as denoted by

$$\boldsymbol{R}^1 = \begin{bmatrix} \boldsymbol{R}^1_{1,1} & \boldsymbol{R}^1_{1,2} & . & . & \boldsymbol{R}^1_{1,8} \\ \boldsymbol{R}^1_{2,1} & \boldsymbol{R}^1_{2,2} & . & . & \boldsymbol{R}^1_{2,8} \\ . & . & . & . & . \\ . & . & . & . & . \\ \boldsymbol{R}^1_{8,1} & \boldsymbol{R}^1_{8,2} & . & . & \boldsymbol{R}^1_{8,8} \end{bmatrix}$$

denote the affinity matrix for the time series corresponding to say window 1. Repeating this process over a number of windows $\boldsymbol{W}$ will result in the spatio-temporal affinity

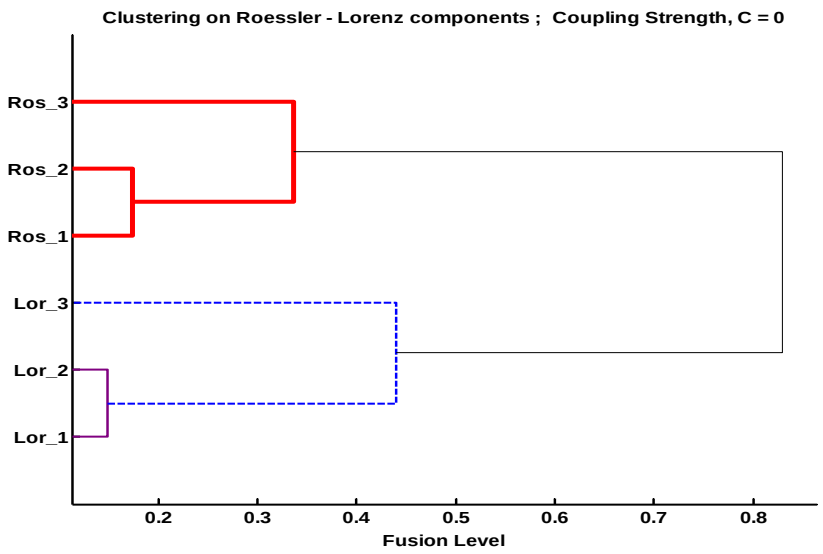

(a)

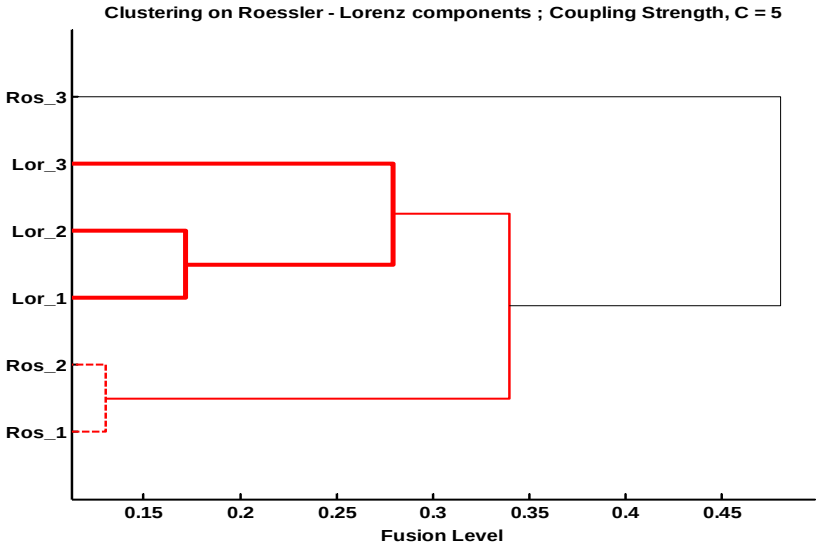

(b)

Figure 3-3. Dendrogram illustration of similarity-based time series clustering. a) Coupling strength, C = 0. The components of the two systems are clearly clustered separately. b) For C = 5, the 1st and 2nd components of the Roessler system form a stronger grouping with the components of the Lorenz system than the 3rd component of the Roessler system itself.

matrix $\boldsymbol{R} = \{\boldsymbol{R}^1 \quad \boldsymbol{R}^2 \quad . \quad . \quad \boldsymbol{R}^{\boldsymbol{W}}\}$, where $\boldsymbol{W}$ is the total number of windows. For each window, the spatial configuration/arrangement of the band pass filters is changed as follows

Configuration 1 (c_1): Channels 1, 2, 3 & 4 are passed through BPF_1 and Channels 5, 6, 7 & 8 are passed through BPF_2.

Configuration 2 (c_2): Channels 1 & 3 are passed through BPF_1 and Channels 2, 4, 5, 6, 7 & 8 are passed through BPF_2.

Configuration 3 (c_3): Channels 1, 2, 3, 4, 6 & 7 are passed through BPF_1 and Channels 5 & 8 are passed through BPF_2.

Configuration 4 (c_4): Channels 1, 3, 6 & 7 are passed through BPF_1 and Channels 2, 4, 5 & 8 are passed through BPF_2.

Total number of Windows $\boldsymbol{W}$ is fixed to 100 and the probability of random occurrence of channel configurations is as follows: $\{p(c_1) = 0.5,\ p(c_2) = 0.1, p(c_3) = 0.1, p(c_4) = 0.3\}$. Applying the spectral clustering algorithm on the spatial-correlation matrix of each window $\boldsymbol{R}^{\boldsymbol{i}}$ resulted in

$$\lambda_{\boldsymbol{spect}} = \begin{bmatrix} 1 & 2 & 1 & 2 & 1 & 1 & 2 & . & . & . & . & 1 \\ 1 & 2 & 2 & 1 & 2 & 2 & 2 & . & . & . & . & 1 \\ 1 & 2 & 1 & 2 & 1 & 1 & 2 & . & . & . & . & 1 \\ 1 & 2 & 2 & 1 & 2 & 2 & 2 & . & . & . & . & 1 \\ 2 & 1 & 2 & 1 & 2 & 2 & 1 & . & . & . & . & 2 \\ 2 & 2 & 2 & 2 & 1 & 2 & 1 & . & . & . & . & 1 \\ 2 & 2 & 2 & 2 & 1 & 2 & 1 & . & . & . & . & 1 \\ 2 & 1 & 2 & 1 & 2 & 2 & 1 & . & . & . & . & 2 \end{bmatrix}_{(8\boldsymbol{x}100)}$$

$$\begin{matrix} \uparrow & \uparrow & \uparrow & \uparrow & \uparrow & \uparrow & \uparrow & & & & & \uparrow \\ c_1 & c_3 & c_2 & c_4 & c_4 & c_2 & c_1 & . & . & . & . & c_3 \end{matrix}$$

This illustration shows how the cluster labels are assigned to the channels depending on their configuration, denoted by $\mathbf{c_i}$'s. Heuristically, it is evident that the channels can either be clustered in groups of four or in groups of two. For the case when the number of clusters equals four (4), the hamming-distance based clustering resulted in cluster assignment of the channels

C_1: {1, 3}, **C_2:** {2, 4}, **C_3:** {6, 7}, **C_4:** {5, 8}.

Specifying only 2 clusters resulted in

C_1: {1, 2, 3, 4}, **C_2:** {5, 6, 7, 8}.

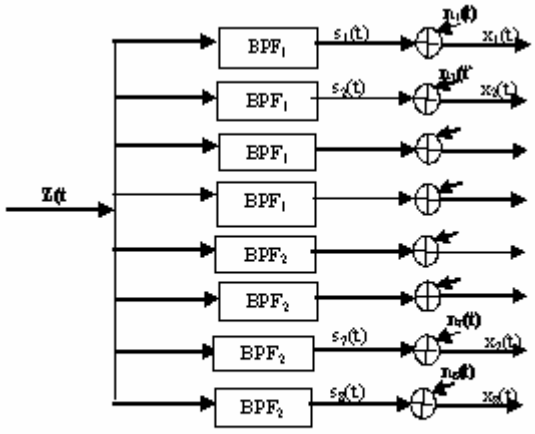

Figure 3-4. Model showing the generation of linearly dependent signals using configuration 1.

We can easily see that the results with 4 clusters and 2 clusters are in perfect agreement with the construction of the spatio-temporal configurations. Channel 1and 3 are always together and belong to the same cluster, regardless of the configuration. Likewise, channels 5 and 8 always belong to the same cluster; although different from the cluster to which 1 and 3 belong to. This is because the source data ***Z(t)*** is always passed

through BPF_2 to obtain channels 5 and 8, unlike channels 1 and 3 that are obtained by filtering $\boldsymbol{Z(t)}$ by BPF_1. The channels 2 and 4 and similarly 6 and 7 change their memberships often enough and therefore can be partitioned into separate clusters.

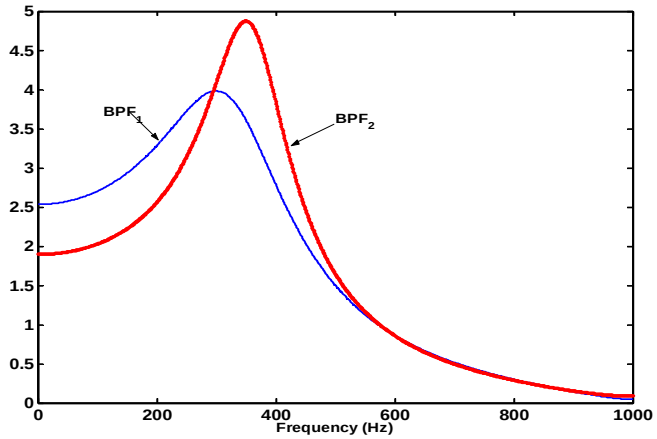

Figure 3-5. Plot showing the two band pass filters, separated by a narrow pass band

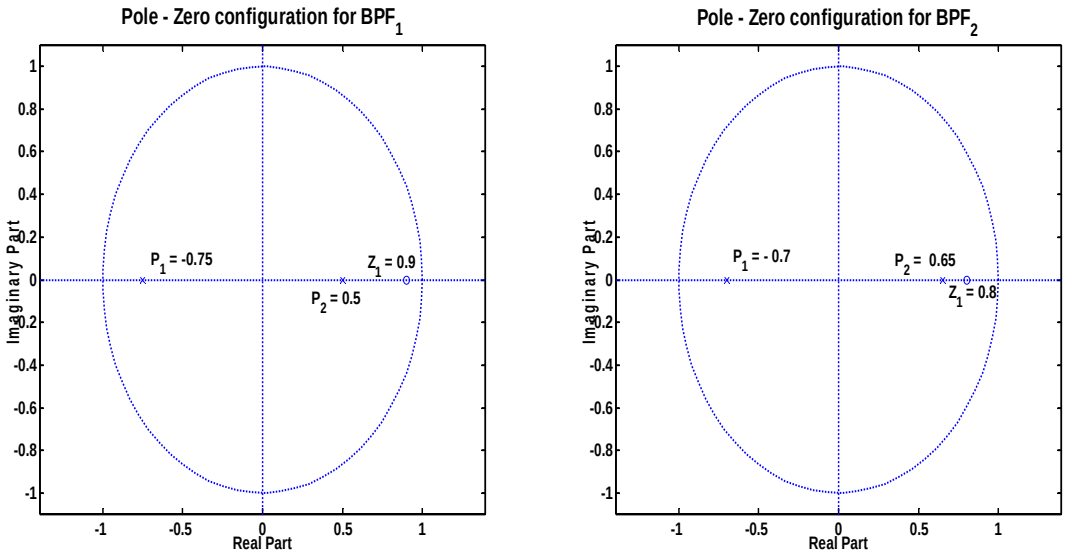

Figure 3-6. Z-planes showing the pole- zero configurations for the two band-pass filters in Fig 3-5.

3.5 Summary

Adopting a similarity-based time-series clustering approach, we proposed a spatio-temporal model to evaluate long term clusterings in multi-variate time series data. The earlier proposed SOM-SI measure is used as the distance measure to evaluate the affinity between various nodes in time-series. One of the major issues in any clustering problem is determining the appropriate number of clusters. In our model we use the spectral clustering algorithm in which it relatively easier to specify the cluster size. This is because the significant eigen values can directly provide a reasonable indication of the number of centroids in the data. Similarly, through simulations we showed that the dendrograms can also be used to get useful hints for choosing the number of clusters. Simulations on Roessler-Lorenz dyamical system and on a linear set up demonstrate the efficacy of our proposed approach to evaluate long term associability patterns among dynamically connected nodes.

CHAPTER 4
APPLICATION OF SPATIO-TEMPORAL MODEL TO EPILEPTIC INTRACRANIAL EEG

4.1 Introduction

In the last chapter, we proposed a spatio-temporal model to extract groupings from long term multivariate recordings. This chapter will focus on the application of that model on the epileptic intracranial EEG time series. The first part of the chapter will describe the details on the application of the model and the second part will discuss the results of analyses on 11 complex-partial seizures, from 2 epileptic patients.

4.2 Application of SOM-SI on Epileptic Intracranial EEG Data

The temporal changes in the spatial structure of an epileptic brain was analyzed on twenty four (24) representative channels recorded bilaterally from the orbito-frontal, temporal and sub-temporal regions on the brain. One of the fundamental requirements for analyzing the dynamics of a non linear system is to construct the state-space attractor from just a single recording of the time-series. From previous studies that estimated intracranial EEG attractor size using correlation-dimension techniques [38-39], we know that the EEG state space is bounded between 3 and 10. This is of course assuming that the data is entirely noise-free and infinite amount of measurement data is available. The large range in dimension is due to the fact that the properties of the EEG dynamical system undergo dimension changes with changes in brain's physiological states and pathological conditions. On our intracranial EEG data, the embedding dimension (m) and the delay

(τ), however, were chosen to be m = 10 and τ = 4. The parameters were compatible with other studies [38-39], performed on the same data.

The following steps describe the procedure to track the spatio-temporal connectivity patterns in intracranial EEG data.

1. Choosing suitable embedding parameters, intracranial EEG attractors in higher dimensional state space is constructed using Taken's time-delay embedding theorem [98]. On 10 second epochs, pair-wise analyses of interdependence among 24 channels are computed using the SOM-SI measure.

2. The similarity indices, from every window, are translated into an asymmetric similarity/affinity/proximity matrix. Since spectral clustering involves eigen-decomposition on a symmetric affinity matrix, the asymmetric matrix is transformed to a symmetric matrix by adding itself to its transpose and dividing by 2.

3. With the number of clusters (say n1) specified apriori, spectral clustering on the affinity matrix results in channels being labeled as one of the n1 clusters.

4. Steps 1 to 3 are repeated for all the successive windows, representing 10-second stationary segments. However, the overall ability of the channels to associate with each other over a longer time-duration needs to be quantified.

On 30 minute time segments (equal to 90, 10-second windows), pair-wise Hamming-distance based cluster-similarity matrix *P* is computed among all the channels. The matrix elements essentially index the probability of channels to group into the same cluster over a 30 minute time interval.

Spectral clustering or any other clustering algorithm on the cluster-similarity matrix *P* will result in final cluster memberships. The number of clusters is fixed to n_2.

For computing similarity indices in step 1, the epoch length of 10 seconds is chosen as a tradeoff between stationarity and sample-size requirements. Also note that the successive windows are 10 seconds apart (alternate 10 second windows), for reasons specific to computational feasibility.

For illustration, we present the results of SOM-SI mutual interactions on a seizure data in Fig 4-1. Pair-wise SOM-SI analysis of the interdependence between 24 channels resulted in some interesting observations. Firstly, the SOM-similarity indices are temporally averaged (over 3 windows) to smoothen out the fluctuations between windows. On the smoothened interdependence indices, for each window and for each channel, we find the maximum driving influence that the channel exerts on any other channel. Over windows (in time) these maximum driving indices give the maximum driving ability of the particular channel of interest. The maximum driving abilities are evaluated for every channel under consideration and for simplicity; we show the driving abilities for just 6 channels in fig 4-1. In the inter-ictal stage, low driving ability of all the channels indicate that the channels are de-synchronized, even though they exhibit an upward trend. Synchronization goes up momentarily a few minutes pre-seizure and at the onset of the seizure, there is a sudden drop followed by a gradual increase post-seizure. Higher degree of post-seizure global synchronization is followed by a gradual drop, leading to the inter-ictal state.

It is clear from fig.4-1 that the temporal-evolution of the interdependency values exhibit distinguishable patterns at different stages of seizure [30]. However, the information on the spatial changes among the channels is still missing. As we stated earlier, one of the primary objectives of this study is to determine the spatial-configurations and their temporal changes, at various stages in a seizure data. In this context therefore, clustering can be a useful tool to enable us to quantify groupings among channels and progressively track their changes.

We now describe step 2, with more details. The channel interdependencies obtained from SOM-SI, as indicated by κ_1 in (3.8) represent the spatio-temporal correlation indices obtained by computing pair wise similarity-index among 24 channels. In spectral clustering jargon, the k_1 matrix can also be interpreted as an affinity matrix representing the pair-wise distances between 24 nodes.

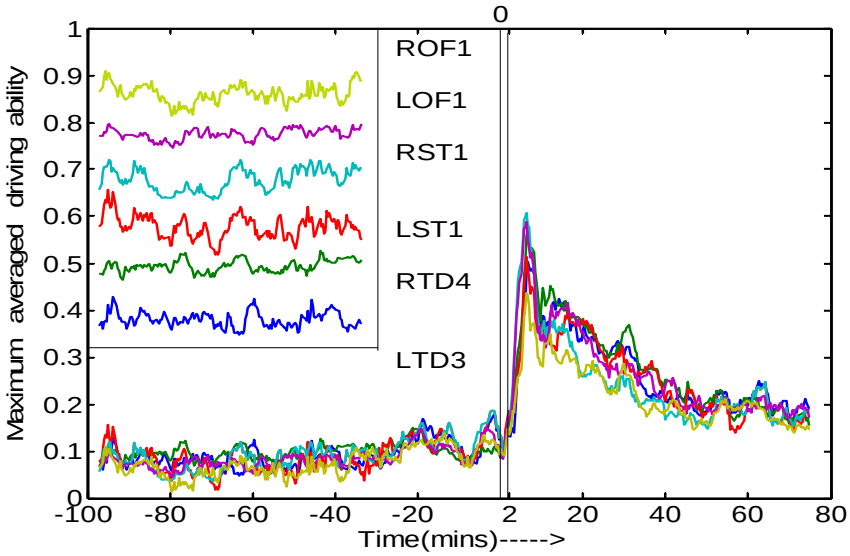

Figure 4-1. Maximum average driving ability of each of the six (6) channels, nearly 100 minutes before and 70 minutes after Seizure-1 in patient P092. (The thin vertical bar corresponds to the time when seizure occurred (0 to 2 on the x-axis). For clarity, the box inside the figure shows a small portion of the maximum average driving ability of each of the 6 channels, baseline-offset by different scales.) Drop in synchronization followed by an abrupt increase in phase synchronization at the onset of seizure is evident. Synchronization across channels during seizure is also clearly seen

However, notice that the affinity between nodes will not be symmetric, as is usually the case in spectral clustering. But the transpose transformation trick, mentioned in step 2, is applied to bring it to symmetric form. Since the weighting is normalized between 0 and 1, the diagonal elements representing the affinity of a channel with itself, are coded as 1. Consequently, after spectral-clustering, we have a set of labeled clusters

representing the membership of the channels [32]. Repeating this procedure on every 10-sec windows will yield a discrete-valued matrix κ_{spect} similar to (3.10).

Typically, the choice for the number of clusters n_1 in step 3 is conditioned on the significant eigen-values (say 90 %). In our analysis, the sum of first 3 eigen-values typically ranged from 60% to 80% of the total variance, due to changes in seizure states. Considering this variability between epochs and the fact that the number of clusters need to be the same for all epochs in order to be able to determine the overall grouping in channels (using cluster-similarity matrix P), we fixed the membership size to $n_1 = 3$.

The notion of pre-seizure state has widely been debated upon. A lot of studies argue against the notion of a 'pre-seizure' state transition. However, experimental studies using non linear dynamics have shown that the quantitative descriptors of EEG exhibit seizure pre-cursors in the form of inter-ictal to pre-ictal state transitions. The pre-ictal transition time is not exactly known, however literature suggests that it has a broad range of 5 minutes to 120 minutes before seizure. Therefore in step 5, as a tradeoff between state transition periods and time-resolution, we choose 30 minutes time window to characterize both the pre-ictal and the post-ictal periods.

4.3 Results

Following are the clustering results from applying the spatial-clustering procedure on different seizures.

Patient P093

This patient had a history of complex partial seizures, localized in the mesial structures of the temporal lobe. Surgery revealed a lesion in the right hippocampus (RTD electrodes) region.

The set of 24 channels are listed below,

Channels 1 to 4: {LTD3, LTD5, LTD7, LTD9}

Channels 5 to 8: {RTD4, RTD6, RTD8, RTD10}

Channels 9 to 12: {LST1, LST2, LST3, LST4}

Channels 13 to 16: {RST1, RST2, RST3, RST4}

Channels 17 to 20: {LOF1, LOF2, LOF3, LOF4}

Channels 21 to 24: {ROF1, ROF2, ROF3, ROF4}

Before data analysis, a validation test was performed to check whether application of different clustering algorithms on ***P*** would consistently result in same cluster memberships or not. For a given number of clusters n_2, it turned out that all the clustering algorithms including spectral clustering produced the same outputs. Therefore, we decided to choose the simple hierarchical clustering algorithm used in the Matlab 6.5 package owing to its graphical support.

Cluster-similarity matrices ***P*** indicating the probability that two channels share the same grouping in a 30-minute time segment are shown gray-scale coded in Fig. 4-2. Pre-seizure analysis on 30-minute windows is shown for up to 3 hours. Similarly, the post-seizure analysis is shown for the first 30 minutes. The ability of the left side channels to have a higher tendency to group together compared to the right hemisphere channels is quite noticeable from fig 4-2. In addition, the orbito frontal lobes seem like the only area on the brain to have a high probability of making a cross-hemisphere grouping. On the left hemisphere, the LST and the LTD channels are consistently seen to share the same clusters.

To confirm the observations from fig 4-2, the hierarchical clustering algorithm was applied on each of those ***P*** matrices. Fig. 4-3 graphically illustrates two instances of the clustering outputs through dendrograms. A dendrogram is strictly defined as a binary tree with a distinguished root that has all the data items at its leaves. Conventionally, all the leaves are shown at the same level of the drawing. The ordering of the leaves is arbitrary. The heights of the internal nodes are related to the metric information (***P*** here) used to form the clustering. Using a threshold of 0.4 and the average-linkage technique to determine fusion levels, clustering was performed on a pre-defined number of clusters (n_2). For determining apriori the number of clusters n_2, several dendrograms were visually analyzed. There seemed to be at least 3 to 4 strong groupings among channels in most of the dendrograms. For consistency, therefore, we chose to fix the number of clusters *n2* to 3 for all the analyses.

Both dendrograms in fig 4-3. clearly translate the spatial patterns observed in the corresponding ***P*** matrices of fig 4-2. The top dendrogram in fig 4-3. corresponds to the 2.5 hours to 3 hours time window (indicated by -5) in fig 4-2. It is easy to see that the dendrogram considers the RTD and the RST as isolated clusters due to their weak between-cluster fusion level. Since the number of clusters n2 is restricted to 3, all the remaining channels form a single large cluster. Similarly, the bottom dendrogram in fig 4-3. corresponds to the P matrix indicated by -1 in fig 4-2. In this case, the RST and the RTD channels group into one cluster; also well supported by a dark patch in fig 4-2. This enables the LST/LTD channels and the LOF/ROF channels to group together as separate clusters.

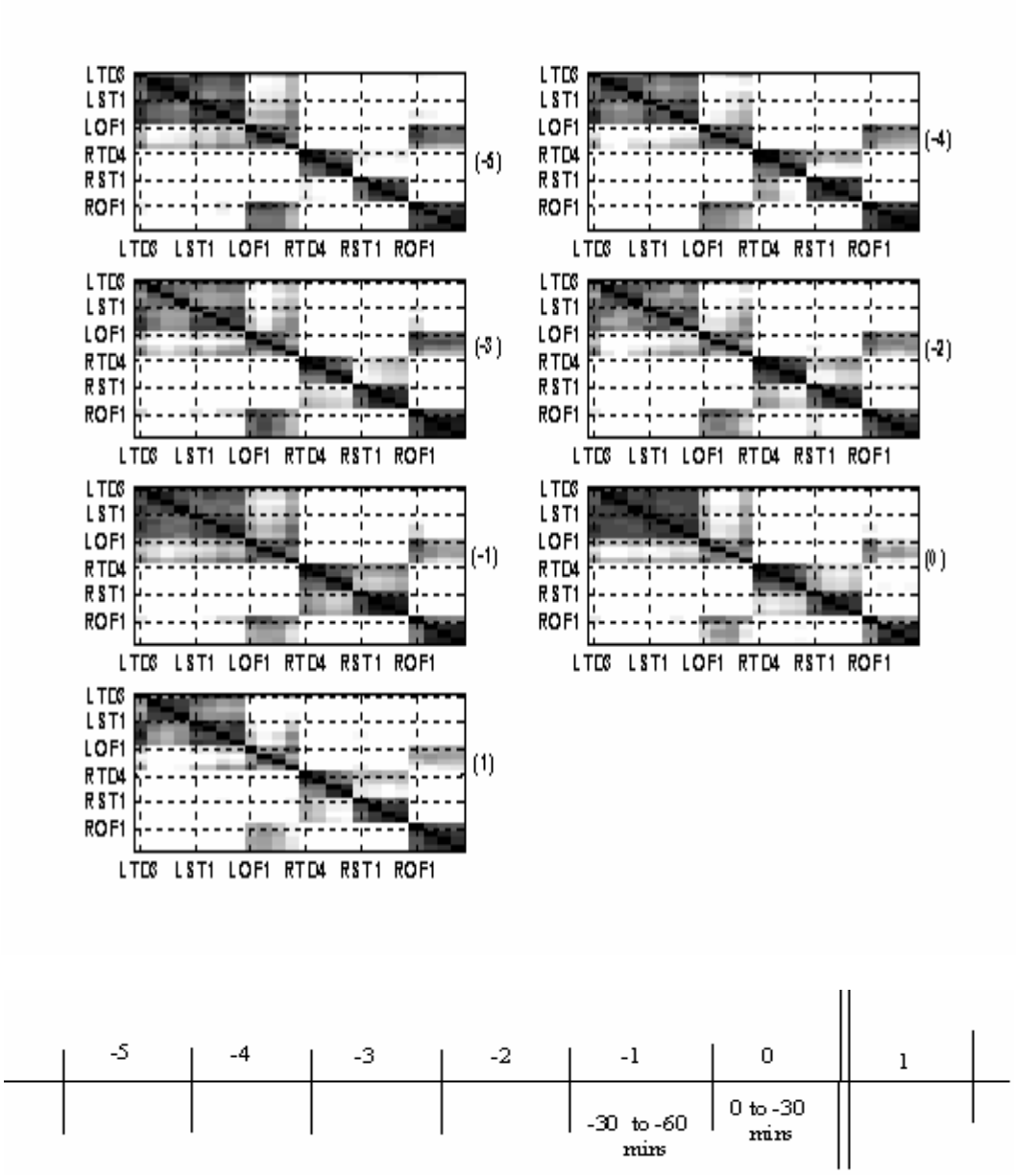

Figure 4-2. Seizure 11 of patient P093: Cluster-similarity matrices P indicating the probability that two channels share the same cluster label in a 30 minute time-interval.

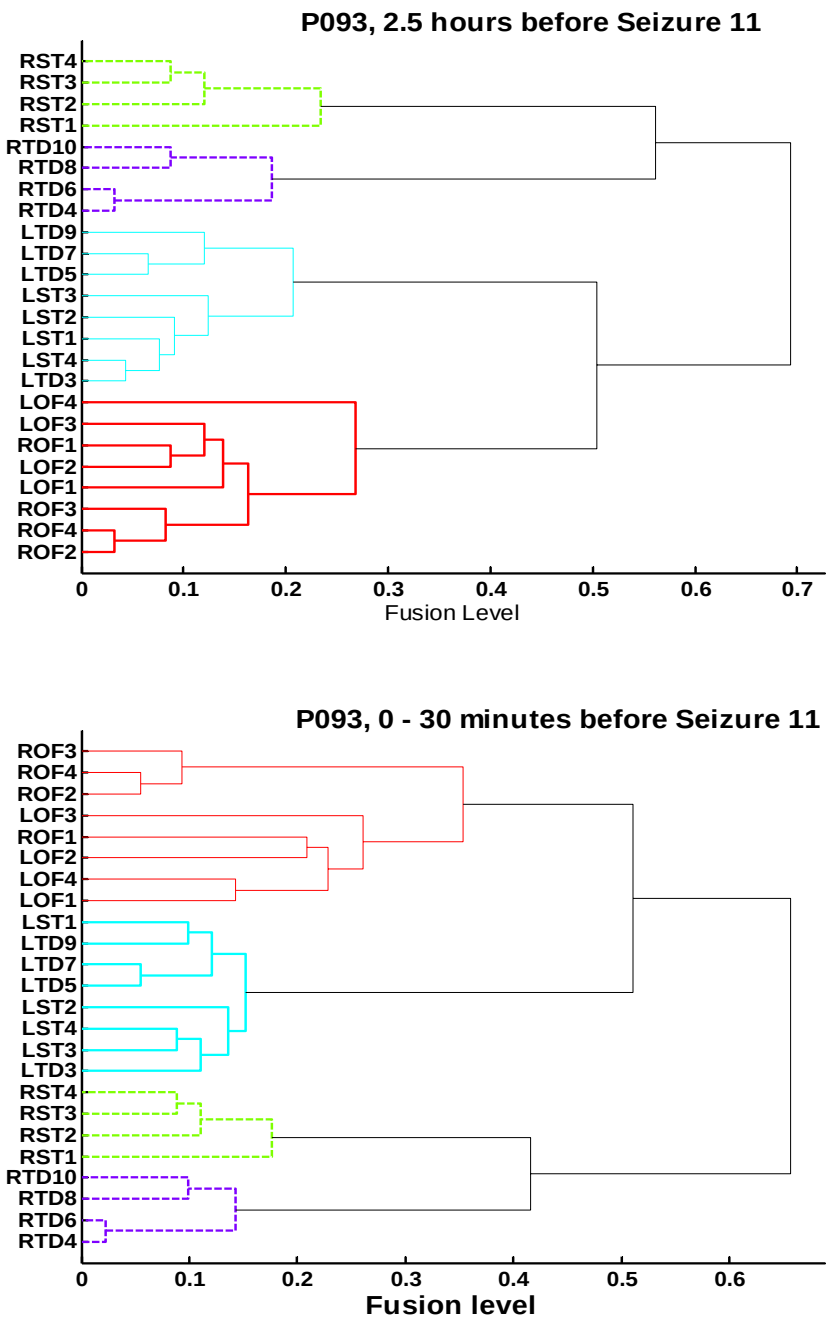

Figure 4-3. Dendrogram representation of the cluster results in Seizure 11, P093. TOP: Dendrogram corresponding to 2.5 hours before seizure. BOTTOM: Dendrogram corresponding to the 30 minute pre-seizure period.

The overall cluster configuration is listed in table 4-1.

Table 4-1. Spatio-temporal groupings as obtained for seizure 11 of patient P093

P093, Seizure 11	**C_1**	**C_2**	**C_3**
Pre seizure, (2.5 – 3 hrs)	RTD	RST	LTD, LST, LOF, ROF
Pre seizure, (2 – 2.5 hrs)	RTD, RST	LOF, ROF	LTD, LST
Pre seizure, (1.5 – 2 hrs)	RTD, RST	LOF, ROF	LTD, LST
Pre seizure, (1 – 1.5 hrs)	RTD, RST	LOF, ROF	LTD, LST
Pre seizure, (30mins – 1 hr)	RTD, RST	LOF, ROF	LTD, LST
Pre seizure, (0 - 30mins)	RTD, RST	LOF, ROF	LTD, LST
Post seizure, (30mins – 1hr)	RTD, RST	LOF, ROF	LTD, LST

We summarize the spatial patterns at different time-intervals of seizure 11 as follows:

1. The LST and the LTD channels in particular, exhibit a strong tendency to belong to the same group.

2. The LOF and the ROF channels form a strong bi-lateral homologous connection, as seen from all the matrices in fig 4-2.

3. Relatively strong similarity can be seen between RTD and the RST channels.

4. Common observation in all the matrices is the strong similarity between the left hemisphere channels as opposed to the right hemisphere channels. This is reflected in the ability of LOF channels to have a higher probability of sharing clusters with other left-hemisphere channels, as seen in Fig 4-2.

5. Interestingly, no temporal changes are seen in the spatial-patterns yet.

In Fig 4-3. even though the two dendrograms share certain common attributes, for instance, channel labels within a group, observe slight disparities in topologies and in the order of connections. Quantifying the difference between topologies may possibly serve to differentiate between dendrograms, obtained at different states of a seizure. Statistical

techniques, such as Double Permutation Statistics (DPS) and mantel statistics are widely [50, 51] known to be best suited to compare two dendrograms. However, the comparisons usually test the hypothesis that the two dendrograms under comparison are not more similar than the dendrograms randomly generated in terms of topology, leaf positions and fusion level positions. Such statistical comparisons are particularly useful when the goal is to detect whether the spatial-correlations have significantly changed over time or not. We address this particular issue of tracking the temporal changes in spatial connections in chapter 5. In the rest of this chapter, however, we analyze the spatial groupings for a larger set of seizures, from different patients.

4.4 Statistical Validation

The cluster configurations observed from analyzing 30 minute segments necessitates validation. Recall that, we partially validated our model (until the spectral clustering stage), using synthetically coupled multivariate time sequences (non linear and linear, both). Simulations involving creation of dynamic graphs involve multidimensional time series that continuously change cluster memberships over time. Determining the average spatio-temporal groupings from a collection of multi-variate time-series is relatively easier to demonstrate in linear coupling cases. However, non linear dynamic model constructions are extremely hard and mostly, non-trivial. We therefore decided to pursue a posterior verification of the time-averaged cluster groupings on the intracranial EEG data, using the quasi-surrogate analysis [40, 66-68, 73, 94-95], technique.

Recall that the cluster groupings obtained over 30 minute time-segments involve two steps. First step consists of applying spectral clustering technique on the SOM-similarity indices (computed on 10 second intracranial EEG data segments). Then similar grouping patterns among channels are extracted by using hierarchical clustering approach on the

cluster-similarity matrices ***P***. Specifically, 91 10-second windows (spanning 30 minutes, 3 windows per minute) are analyzed in each pass to obtain long-term groupings among channels.

In order to validate this 2-step approach, we define our hypothesis as follows

H_0: The average within-cluster channel interaction at each window (out of 91 10-second windows) is not significantly different from the corresponding between-cluster channel interactions.

We propose to test this hypothesis on all the 3 (n_2) clusters separately, for every 10-second window within the 30 minute period.

Within-cluster interaction is computed by averaging the pair-wise similarity indices for all the channels within a cluster. For between-cluster interaction, the pair-wise interactions between 3 channels, picked randomly from each of the 3 clusters are computed. A between-cluster interaction statistic is formed by computing the average interactions from random selection of 3 channels (one from each cluster), over a number of trials. We found that this statistic follows a quasi-normal distribution, implying that the within-cluster interaction value can now be compared with the mean and the variance sample estimates of the between-cluster statistic. Mathematically, we construct the z-score as follows

$$Z_t^i = \frac{\left| C_{w_t}^i - \left\langle C_{b_t} \right\rangle \right|}{\sigma(C_{b\,t})} \quad \text{t = 1, 2,.. ,90 \& i = 1, 2, 3.} \tag{4.2}$$

where C_{wt}^i is the within-cluster interaction at time '*t*', for cluster '*i*'. $\left\langle C_{b_t} \right\rangle$ is the mean and $\sigma(C_{b_t})$ is the standard-deviation of the between-cluster interaction at time '*t*'. Z_t^i reflects the z-score and is considered significant at the 95 percentile significance if $Z_t^i >$

1.96 (reject H_0). In table 4-2 the bolded value in each cell represents the number of windows (out of 91) having significant z-scores in the 30 minute period corresponding to fig 4-2 (P093, Seizure 11). It is easy to observe that the null-hypothesis H0 is rejected beyond doubt, validating the clustering results.

Table 4-2. P093, Seizure 11: Over each 30 minute (91 samples total) window, number of times the within-cluster interaction is greater than between-cluster interaction, at 95% significance level.

P093, Sz 11	**-5**	**-4**	**-3**	**-2**	**-1**	**0 (Sz)**	**1**
C1	1	1	0.91	0.95	0.99	1	0.93
C2	0.82	0.89	0.96	0.91	0.89	0.85	0.98
C3	0.95	0.55	0.80	0.70	0.46	0.46	0.97

Seizures 4, 5, 6 & 7:

Spatio-temporal clustering analyses, similar to the one described on seizure 11 were performed on several other seizures, of the same patient P093. The cluster-similarity matrices ***P*** obtained from time-intervals surrounding seizures 4 & 5 and 6 & 7 of patient P093 are shown in fig 4-5. & fig 4-6. respectively. Channel groupings for the same are listed in tables 4-3 & 4-4. All the 4 seizures present very consistent groupings.

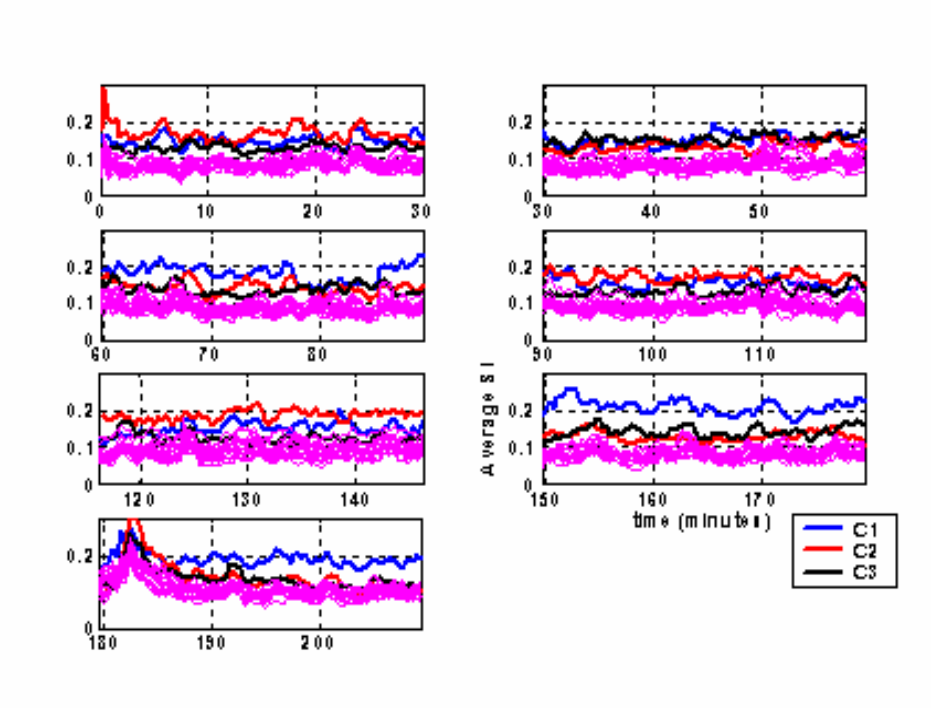

Figure 4-4. Statistical validation of the clustering results. In each panel, thick lines are used to represent the profiles of the three clusters in a 30 minute time interval. The thin lines are the surrogate profiles indicating between-cluster interactions. Cluster veracity can be visually verified by observing that amplitudes representing within-cluster interaction for cluster profiles are mostly higher that the amplitudes representing between-cluster interaction for surrogate profiles, at each time-instance.

1. Consistent to the observation in seizure 11, we observe the temporal depth and the sub-cortical regions of the left hemisphere are always bunched together.

2. Once again, the association of ROF-LOF areas into same cluster suggests a strong homologous connection between the orbito-frontal areas of the brain. This observation is also in agreement with those in seizure 11.

3. The dendrograms once again presented 4 unambiguous clusters in the form of RST, RTD, LST/LTD and LOF/ROF. The fusion levels, indicating the strength of connection between clusters, often turn out in favor of RTD and RST to be grouped separately. Owing to the fact that we have pre-defined the number of clusters to 3, the LST, LTD, LOF & ROF channels will consequently get grouped into one cluster.

4. Once again, temporal changes are not very evident in the spatial patterns. However, observing fig 4-5 & fig 4-6 and their corresponding dendrograms (not shown), the fusion levels and the topology of the connections change with time. These changes can only be quantified using statistical tests such as Mantel test statistics or the Double Permutation Statistics (DPS).

Patient P092

In this section, we present the summary results of the clustering analyses performed on patient P092 suffering from a lesion in the medial temporal lobe structures of the right hemisphere.

Channel configuration for the patient P092 is as follows

Channels 1 to 4: {LTD1, LTD3, LTD5, LTD7}

Channels 5 to 9: {RTD2, RTD4, RTD6, RTD8, RTD12}

Channels 10 to 13: {LST1, LST2, LST3, LST4}

Channels 14 to 17: {RST1, RST2, RST3, RST4}

Channels 18 to 21: {LOF1, LOF2, LOF3, LOF4}

Channels 22 to 24: {ROF1, ROF2, ROF3}

Note that a separate 2 dimensional 25x25 sized EEG-SOM grid was created to model the data dynamics of P092. Post spectral clustering analysis on 30 minutes data segments led to some interesting observations.

Fig 4-7. shows the dendrograms created for seizure segments 2 hours prior to seizure 1 and 30 minutes pre-seizure, respectively. As before, the number of clusters (n1) specified in the spectral-clustering step after SOM-SI block was fixed to 3. The fusion levels between most of the channel clusters is greater than 0.4, indicating a lack of strong connectivity between regions.

Table 4-3. Spatio-temporal groupings as obtained for seizures 4 and 5 of patient P093.

P093, Seizure 4 & 5	**C_1**	**C_2**	**C_3**
Pre seizure 4, (30 – 60 mins)	RTD, RST	LOF, ROF	LTD, LST
Pre seizure 4, (0 – 30 mins)	RTD, RST	LOF, ROF	LTD, LST
Post seizure 4, (0 – 30 mins)	RTD	LTD, LST, LOF, ROF	RST
Post seizure 4, (30 mins – 1 hr)	RTD	LOF, ROF	LTD, LST, RST
Pre seizure 5, (30mins – 1 hr)	RTD	LTD, LST, LOF, ROF	RST
Pre seizure 5, (0 - 30mins)	RTD	LTD, LST, LOF, ROF	RST
Post-Seizure 5, (30 – 1 hr)	RTD	LTD, LST, LOF, ROF	RST

Table 4-4. Spatio-temporal groupings as obtained for seizure 6 and 7 of patient P093.

P093, Seizure 6 & 7	**C_1**	**C_2**	**C_3**
Post seizure 6, (0 - 30 mins)	RTD, RST	LTD, LST	LOF, ROF
Pre seizure 7, (30 mins – 1 hr)	RTD, RST	LTD, LST	LOF, ROF
Pre seizure 7, (0 – 30 mins)	RTD	LTD, LST, LOF, ROF	RST
Post seizure 7, (0 – 30 mins)	RTD	LTD, LST, RST	LOF, ROF
Post seizure 7, (30mins – 1 hr)	RTD	LTD, LST, LOF, ROF	RST
Post seizure 7, (1 hr – 1.5 hrs)	RTD	LTD, LST, LOF, ROF	RST

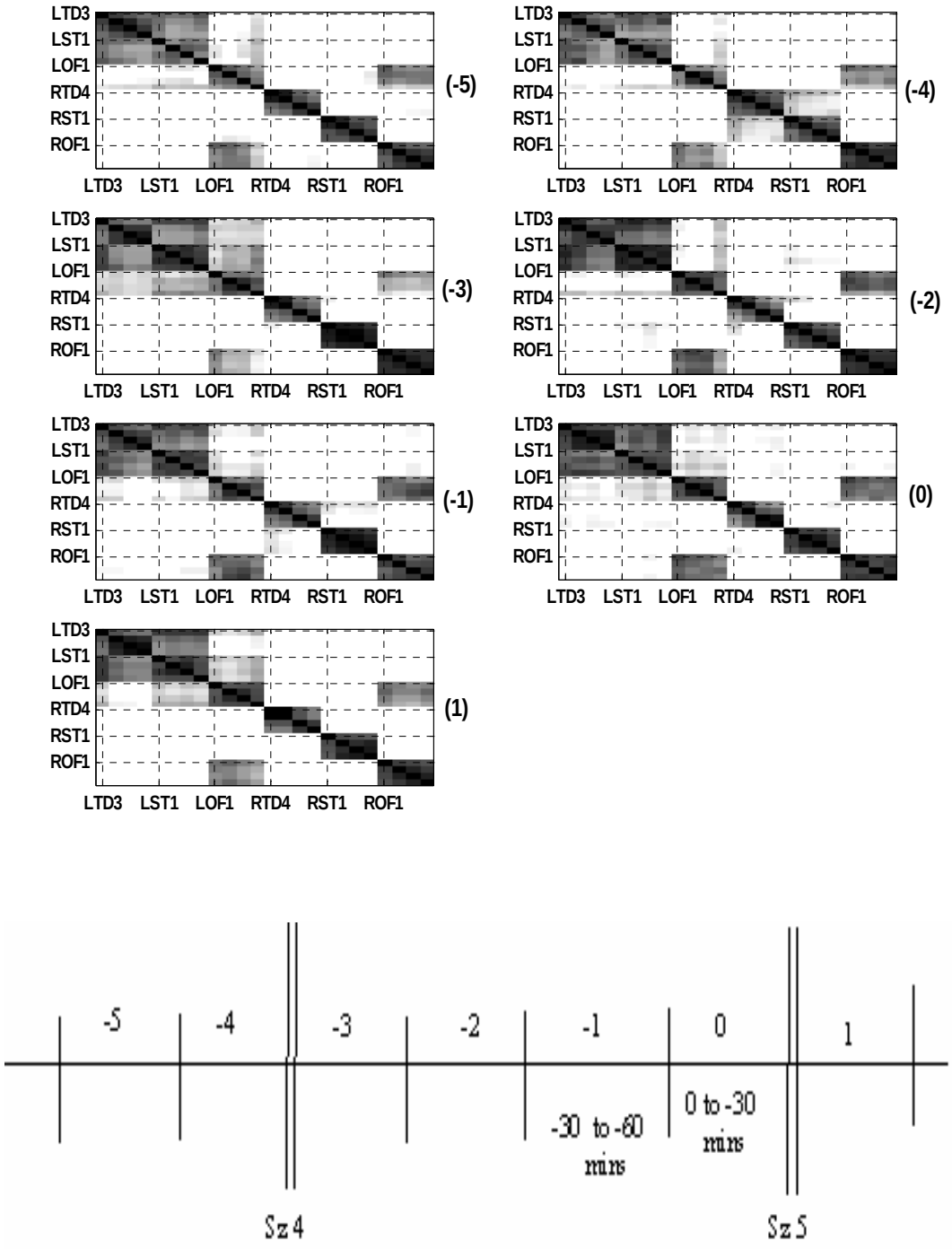

Figure 4-5. Seizures 4 and 5 of patient P093: Cluster-similarity matrices indicating the probability that two channels share the same cluster label in a 30 minute time-interval.

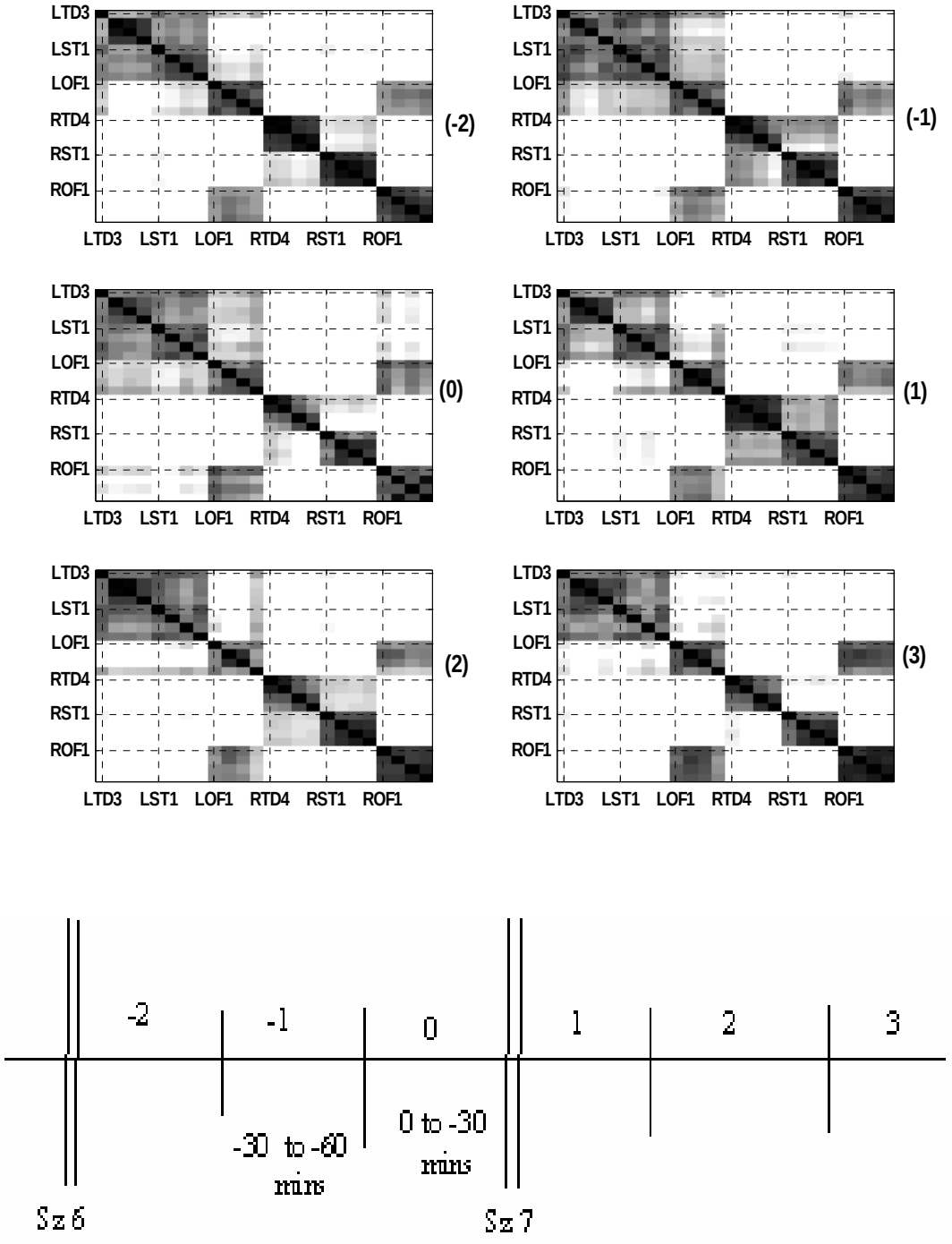

Figure 4-6. Seizures 6 and 7 of patient P093: Cluster-similarity matrices indicating the probability that two channels share the same cluster label in a 30 minute time-interval.

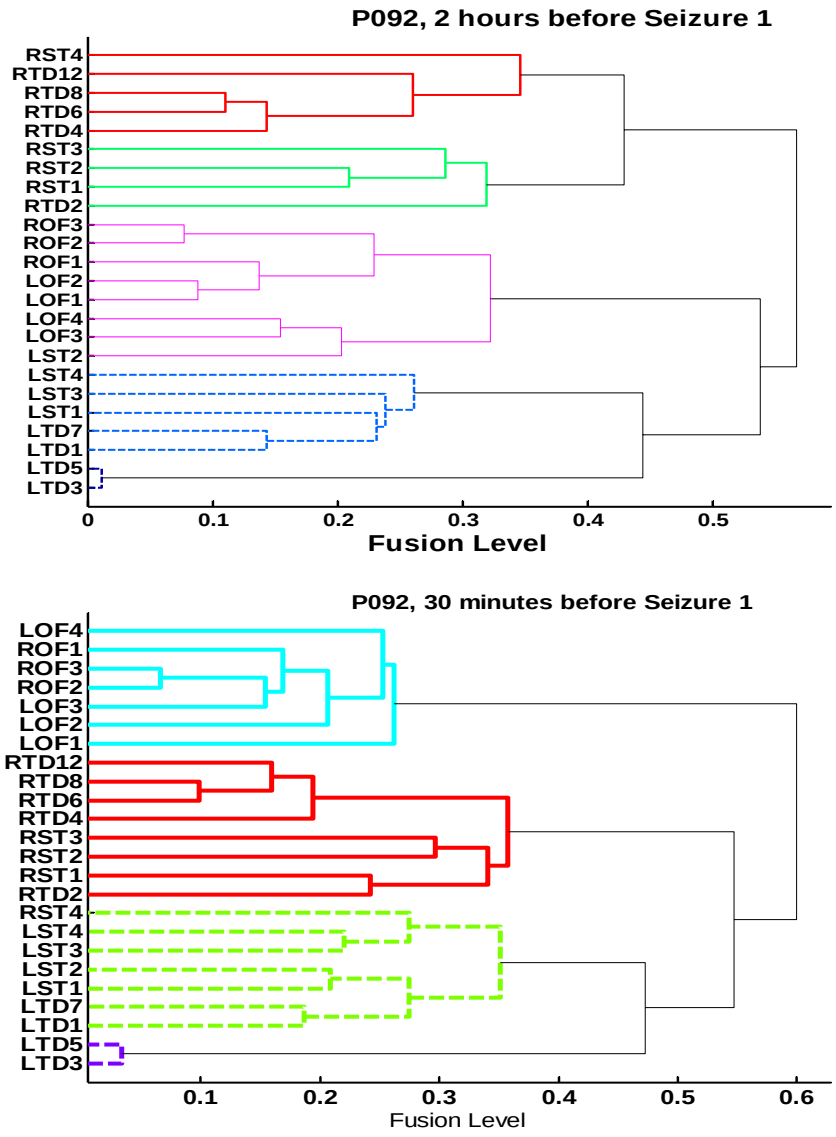

Figure 4-7. Dendrograms corresponding to P092, Seizure 1. Top: 2 hours before Seizure Bottom: 30 minutes pre-seizure.

For the second level of clustering, as before, let the number of clusters n2 be fixed at 3.

Cluster analysis on the 30 minutes segment 2 hours prior to seizure 1 (top dendrogram in Fig. 4-7) results in the following groups of channels:

Cluster #1: LTD & LST

Cluster #2: RTD & RST

Cluster #3: LOF & ROF

Observe the cluster formed from LTD & LST channels, in the dendrogram. It is made up of two sub-clusters, a large and a small cluster. The small cluster consists of only two channels, LTD (3 & 5) and fuses with the other sub-cluster at a very high fusion level (implying weak link). If n_2 was to be increased to 4, the clustering algorithm would classify this sub-cluster as an independent cluster. A detailed analysis on all seizures in P092 revealed a strong intra-channel correlation (or low fusion level) between channels LTD (3 & 5) and a weak inter-channel correlation with the rest of the channels. Surrogate analysis also confirmed the imbalance by having very few rejections for the cluster consisting of LTD (3 & 5) channels. It is obvious that the average interaction (within-cluster interaction) of the largest cluster would be pulled down if there are sub-clusters that have a strong within-sub-cluster interaction, but a weak between-sub-cluster interaction. Consequently, the within-cluster interaction of the largest cluster can be expected to be as weak as or marginally better than the between-cluster interactions, leading to fewer rejections of the null hypothesis H_0. This problem can possibly be overcome by increasing the number of clusters to 4 or more. However, for consistency, we let the number of clusters n_2 be fixed at 3 in the rest of the analyses.

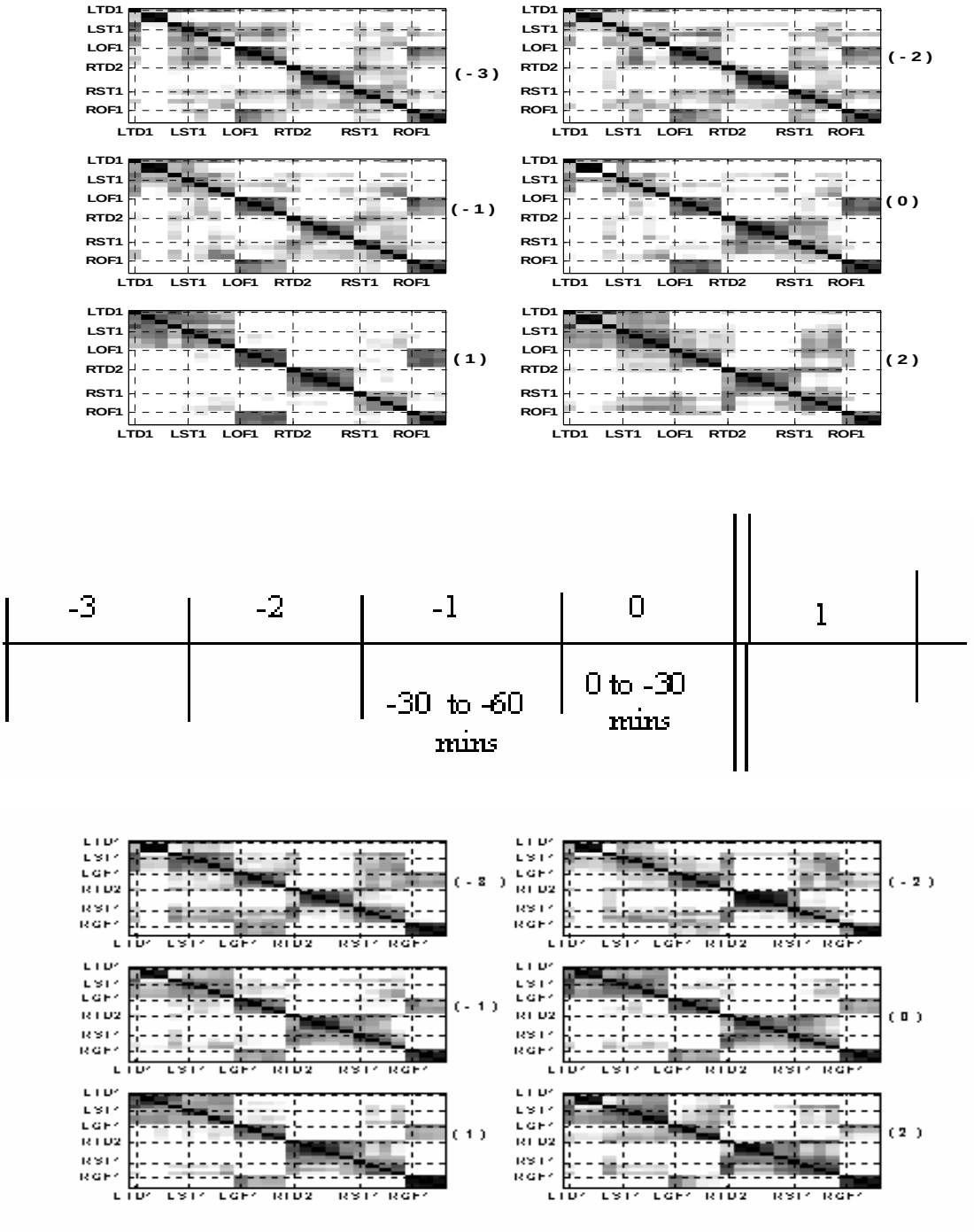

Figure 4-8. Cluster-similarity matrices indicating the probability that two channels share the same cluster label in a 30 minute time-interval. a) Seizure 1 of patient P092 b) Seizure 3 of patient P092.

Seizures 1, 3, 4, 5, 6 & 7:

The spatio-temporal clustering results for seizures 1, 3, 4, 5, 6 & 7 are summarized in tables 4-5 to 4-10.

Table 4-5. Spatio-temporal groupings as obtained for seizure 1 of Patient P092.

P092, Seizure 1	**C_1**	**C_2**	**C_3**
Pre seizure, (1.5 – 2 hrs)	RTD, RST	LTD, LST (1,3,4)	LOF, ROF, LST (2)
Pre seizure, (1 – 1.5 hrs)	RTD	LST, RST, LOF, ROF, LTD (1,7)	LTD (3,5)
Pre seizure, (30 mins – 1 hr)	RTD, RST	LTD, LST	LOF, ROF
Pre seizure, (0 - 30 mins)	RTD, RST	LTD, LST	LOF, ROF
Post-Seizure, (0 – 30 mins)	RTD, RST	LTD, LST	LOF, ROF
Post-Seizure, (30 – 1 hr)	RTD	LTD, LST, LOF, RST	ROF

Table 4-6. Spatio-temporal groupings as obtained for seizure 3 of Patient P092.

P092, Seizure 3	**C_1**	**C_2**	**C_3**
Pre seizure, (1.5 – 2 hrs)	RTD	LST, LTD, RST	LOF, ROF
Pre seizure, (1 – 1.5 hrs)	RTD	LST, LTD, RST	LOF, ROF
Pre seizure, (30mins – 1 hr)	RTD, RST	LST, LTD	LOF, ROF
Pre seizure, (0 - 30mins)	RTD, RST	LST, LTD	LOF, ROF
Post-Seizure, (0 – 30 mins)	RTD, RST	LST, LTD	LOF, ROF
Post-Seizure, (30 – 1 hr)	RTD, RST	LST, LTD	LOF, ROF

Table 4-7. Spatio-temporal groupings as obtained for seizure 4 of Patient P092.

P092, Seizure 4	**C_1**	**C_2**	**C_3**
Pre seizure, (1.5 – 2 hrs)	RTD, RST	LST, LTD	LOF, ROF
Pre seizure, (1 – 1.5 hrs)	RTD, RST	LST, LTD	LOF, ROF
Pre seizure, (30mins – 1 hr)	RTD	LST, LTD, RST	LOF, ROF
Pre seizure, (0 - 30mins)	RTD, RST	LST, LTD	LOF, ROF
Post-Seizure, (0 – 30 mins)	RTD, RST	LST, LTD	LOF, ROF
Post-Seizure, (30 – 1 hr)	RTD, RST	LST, LTD	LOF, ROF

Table 4-8. Spatio-temporal groupings as obtained for seizure 5 of Patient P092.

P092, Seizure 4	**C_1**	**C_2**	**C_3**
Pre seizure, (1.5 – 2 hrs)	RTD	LST, LTD, LOF, RST	ROF
Pre seizure, (1 – 1.5 hrs)	RTD	LST, LTD, LOF, RST	ROF
Pre seizure, (30mins – 1 hr)	LTD (3,5)	LST, LTD (1,7), RST, RTD	LOF, ROF
Pre seizure, (0 - 30mins)	LTD (3,5)	LST, LTD (1,7), RST, RTD, LOF	ROF
Post-Seizure, (0 – 30 mins)	RTD, RST	LST, LTD	LOF, ROF
Post-Seizure, (30 – 1 hr)	RTD, RST	LST, LTD	LOF, ROF

Table 4-9. Spatio-temporal groupings as obtained for seizure 6 of Patient P092.

P092, Seizure 4	**C_1**	**C_2**	**C_3**
Pre seizure, (1.5 – 2 hrs)	RTD, RST	LST, LTD	LOF, ROF
Pre seizure, (1 – 1.5 hrs)	RTD	LST, LTD, RST	LOF, ROF
Pre seizure, (30mins – 1 hr)	RTD	LST, LTD, RST	LOF, ROF
Pre seizure, (0 - 30mins)	LTD (3,5)	LST, LTD, RTD, RST	LOF, ROF
Post-Seizure, (0 – 30 mins)	RTD, RST	LST, LTD	LOF, ROF
Post-Seizure, (30 – 1 hr)	RTD, RST	LST, LTD, LOF	ROF

Table 4-10. Spatio-temporal groupings as obtained for seizure 7 of Patient P092.

P092, Seizure 4	**C_1**	**C_2**	**C_3**
Pre seizure, (1.5 – 2 hrs)	RTD, RST	LST, LTD	LOF, ROF
Pre seizure, (1 – 1.5 hrs)	RTD, RST	LST, LTD	LOF, ROF
Pre seizure, (30mins – 1 hr)	RTD	LST, LTD, RST	LOF, ROF
Pre seizure, (0 - 30mins)	RTD, RST	LST, LTD	LOF, ROF

From the P092 cluster results, we note the following:

1. The non-focal zone LTD has a strong coupling with the LST region. Correspondingly, strong affinity is observed between RTD and RST as well. These observations are consistent with the observations for P093. However, unlike in P093, we also see here that LTD connects and disconnects with several other channels, depending on the seizure state.

2. As in P093, we observe an exclusively strong connection between ROF-LOF regions at all stages surrounding a seizure. There are few instances where the ROF breaks into a separate group. We do not have any explanation for this drift in ROF, at this point in time.

3. Statistics from the surrogate analyses confirmed the veracity of the technique in most of the cases. As pointed out earlier, discrepancies occurred in a few instances for the clusters containing LTD (3, 5) channels.

Finally, we summarize the analysis on 2 patients and 11 complex partial seizures:

1. Contrary to the stand point that the seizure activity initiates in the focal zone followed by a gradual propagation to other regions, we observed that the spatial organization reflected by intracranial EEG activity exhibits either minimum or no progressive changes from the focal zone (RTD) to other zones (based on how it groups with other regions in the brain).

2. Evidence show stronger ipsilateral connection between the LTD and LST zones compared to the connection strength between RTD-RST. Statistical analysis to check if a significant difference in intra-hemisphere coupling strengths exists is needed.

3. We also found evidence to show a strong cross-hemispheric activity by observing consistent groupings of the right and left orbito-frontal lobes at all seizure states.

4. On how the overall spatial networks change every 30 minutes, patient P093 was seen to have qualitatively, lesser spatio-temporal changes in its P matrices than P092. It remains to be checked whether a significant change in the spatial organization before seizure is a pre-requisite to its subsequent occurrence. (See chapter 5 for further investigation).

4.4 Summary

From a clinical standpoint, one of the objectives of the above analysis, although qualitative, was two fold: 1) to have a better understanding of the spatial patterns in an epileptic brain and 2) to forge a link between the spatio-temporal organization and the evolution of seizure states. In cognitive terms, it would be particularly interesting to know if an epileptic brain exhibits certain predictable pattern differentials in its spatial configuration en-route to seizures. Such investigations would help us determine if it is possible to extract markers pointing to occurrence of seizures.

Although our first objective could be accomplished to a certain extent, analysis on 11 seizures from 2 patients failed to present any predictable and consistent changes, suggestive of a seizure marker. Qualitative comparisons between 30 minute pre-seizure

block with 30 minute post-seizure blocks are very inconclusive; therefore, we can only remark to the extent that the changes in spatial groupings surrounding seizures have no consistent and predictable patterns. Referring again to the consistent groupings among the brain sites regardless of the seizure states, we wonder if the grouping patterns are finger prints of an epileptic brain. In other words, are the results compelling enough to point to an abnormality in the brain? Similar clustering analyses on a normal brain and a subsequent comparison with analyses from an epileptic brain might be a worthwhile effort to make these hypothetical arguments complete

CHAPTER 5
STATISTICAL ASSESSMENT OF SPATIO-TEMPORAL DEPENDENCY CHANGES IN EPILEPTIC INTRACRANIAL EEG

5.1 Introduction

In the previous chapter, the proposed spatio-temporal clustering model was used to analyze the groupings among critical regions in an epileptic brain. Remarkably, certain regions in the brain displayed tendencies to strongly bind with each other, regardless of the clinical states. The model is useful as an indicator of the groupings in the brain; however, it does not quantify the exact changes in the overall associability patterns that are speculated to cause seizures.

In the next phase of this study therefore, we explore the possibility whether seizure events are coupled with changes in the functional relationships among certain groups of channels. The chapter is split into two independent parts. The first half discusses a statistical approach for analyzing the temporal changes in the overall spatial-patterns of an epileptic intracranial EEG. In particular, mantel statistics are used for comparing the similarities between affinity matrices, evaluated at different seizure states. Significant changes of mutual interactions in 2 hours windows prior to seizures are reported. The second half of the chapter determines the statistical differences in the synchronization levels between the focal and the non-focal hemispheres at pre-ictal and post-ictal states.

5.2 Spatio-temporal Changes

It is widely believed that the dynamics of the brain, understood as a multivariate biological system, can be characterized by analyzing its temporal state changes. Such

changes are known to eventually lead to certain clinical manifestations. Much of the previous studies [28, 35-40, 77, 82] in epilepsy have focused on analyzing the temporal changes associated with brain's non linear dynamics. Feature descriptors such as system's complexity or the short-term Lyapunov exponents [35-40] are derived individually on each of the systems dimensions. Temporal dynamical changes associated with such features, however, fail to explain a system's state associated changes in its overall spatial configuration. Rather than studying the temporal dynamics of each dimension individually, the emphasis should be on considering all the dimensions in unison in a multi-variate scheme of things. In other words, in spatially extended systems, dynamics change both in time and in space and therefore, approaches that track the temporal changes of the spatial networks can be much more effective and helpful in our efforts to characterize certain clinical events.

Earlier, we derived the SOM-SI measure to define mutual interactions among various nodes in a spatially coupled multi-dimensional system. The affinity matrix representation of the SOM-SI at every time window (of length 10 seconds) provides information on the interactions among all the possible pairs of nodes in a graph. For the epileptic brain, in particular, changes associated with the epileptic activity will therefore be reflected by changes in the overall spatial connectivities and we propose to quantify this by tracking the activity changes associated with the SOM-SI affinity matrices.

5.3 Mantel Test of Matrix Comparison

Mantel tests were first developed in 1967 to correlate temporal and spatial distributions of cancer incidences [58] and since then it has been widely used as a correlation tool in various biological [96] and ecological disciplines [18, 50-51]. It is a linear correlation estimate of the relationship between two square distance matrices based

on the degree of relationship of two sets of variables taken at the same sampling locations. In short, mantel test is essentially a statistical framework to test the consensus of two distance/proximity/affinity matrices.

In the mantel test, the hypothesis is that the distances (or similarities) in matrix A are independent of the distances, for the same set of objects, in another matrix B. In other words, we test the hypothesis that the two matrices under study are no more similar than they would be by chance assignment of the labels to the rows and corresponding columns. The normal procedure to test the hypothesis would be to compute a measure of resemblance between the values in the two upper (or lower) triangular parts of the square symmetric matrices under comparison and test against a random distribution. The random distribution is constructed by repeatedly permuting at random, the rows and corresponding columns of one of the matrices, and re-computing the statistic. Finally, the original value of the statistic is compared with the distribution obtained by randomly reallocating the order of the elements in one of the matrices.

The statistic used for the measure of correlation between the matrices is the classical Pearson correlation coefficient

$$r = \frac{1}{N-1}\sum_{i=1}^{N}\sum_{j=1}^{N}\left[\frac{A_{ij}-\overline{A}}{s_A}\right]\left[\frac{B_{ij}-\overline{B}}{s_B}\right] \tag{5.1}$$

where N is the number of elements in the lower or upper triangular part of the matrix, $\overline{A}$ is the mean for A elements and s_A is the standard deviation of A elements. If the two matrices are normalized, i.e.

$$a_{ij} = \frac{A_{ij}-\overline{A}}{s_A};\ b_{ij} = \frac{B_{ij}-\overline{B}}{s_B},$$

we have $\bar{a} = 0,\ s_A = 1,\ \bar{b} = 0,\ s_B = 1,$ and therefore (1) can be re-written as

$$r = \frac{1}{N-1} \sum_{i=1}^{N} \sum_{j=1}^{N} a_{ij} b_{ij} \tag{5.2}$$

Note that the coefficient measures the linear correlation coefficient; therefore if any non linear relationships exist, they will be lost. Finally, the testing procedure using the mantel test statistic is as follows.

Assume two square symmetric matrices A and B of size n x n. The rows and columns in both the matrices correspond to the same objects. The first step is to compute the Pearson correlation coefficient between the corresponding elements of the lower (or upper) triangular matrices.

1. Compute the original (or the non-permuted) statistic r_{AB} using (5-1)
2. Permute randomly the rows and the corresponding columns of one of the matrices (say B) to create a new matrix B'.
3. Recompute (5-1) using A and B' to obtain permuted statistic $r_{AB'}$
4. Repeat the steps (2) and (3) several times (> 500) to form a distribution of the permuted statistics. This distribution will be the reference distribution under the null hypothesis.
5. Assuming normal approximation on the reference distribution, compute the z-score by comparing the non-permuted statistic in step (1) with the mean and variance of the reference distribution. i.e, $z = \frac{r - \bar{r}'}{\sigma_{r'}}$

5.4 Application to Epileptic Intracranial EEG data

Recall from the 3rd chapter that the similarity indices on 10-second windows were evaluated over several hours of epileptic intracranial EEG recording. In this study, we propose to use the mantel-test on the SOM-SI affinity matrices, evaluated at different time periods. Particularly, the emphasis will be on tracking the temporal changes of the

spatial connections, in the intervals prior to seizure. Experimental design procedure is explained in the following steps.

1. Select 2 hours of intracranial EEG segments prior to a seizure.
2. Compute the SOM-SI affinity matrices on 10 second windows, for 2 hours pre-seizure (only the alternate 10 seconds are evaluated; therefore we get a total of 180 SOM-SI affinity matrices from 2 hours data).
3. Fluctuations between successive matrices are smoothened by temporal averaging. A window size of 3 (equal to 1 minute) was used.
4. Affinity matrix corresponding to the window 2 hours prior to seizure is individually compared with the affinity matrices at all other times leading to seizure. For comparison, every 3rd minute was used to ensure that the effects of correlation between matrices due to temporal averaging were eliminated. Note that the null-hypothesis distribution was formed from 700 randomly permuted statistics.
5. Hypothesis testing is done by checking the z-scores at the 95% significance level.

The mantel test statistic was tested on six seizures of the patient P092. Fig. 5-1 illustrates the temporal changes in the spatial-activity of the channels, in the interval 2 hours prior to seizure. z_α scores greater than $z_{crit,0.95} = 1.96$ indicates that the null hypothesis H_0 is rejected at the 95% significance level. Rejecting H_0 implies that the similarity statistic between the test-affinity matrix at time‘t’ and the reference affinity matrix (corresponding to 2 hours before seizure) is significantly different than the one obtained by randomly permuting the rows and columns of the test-affinity matrix. In Fig.1 the z_α scores in all seizures are almost always greater than z_{crit}. However, in a few instances, the z_α ‘s exhibit a tendency to decrease gradually as the seizures approach. In a few other seizures, z_α’s seem to have a negative bump that lasts for several minutes. Reduced z_α’s do not necessarily imply that the correlation estimates are small. However, verification of the original similarity statistic (r) indicated a reduced correlation estimate

at those points corresponding to reduced z_α's. This observation directly suggests that the spatial relationships in the intracranial EEG data at those points are indeed very different (less correlated) from the spatial relationships observed around 2 hours prior to seizures.

5.5 Statistical Approach

As stated earlier, even though the z_α's show a remarkable decrease they are still greater than the z_{crit}. Also, notice that the absolute values of z_α's vary across seizures. These non-uniformities will render any comments regarding spatio-temporal changes prior to seizures, purely qualitative. It is therefore absolutely necessary to quantify the temporal decrease observed in correlation estimates. We propose a simple approach to statistically verify the decrease in the mantel statistics, z_α's.

The approach consists of checking whether the decreases observed in the mantel test procedure are statistically significant or not. Let z_{ref} be the reference z_α score at a time instance close to 2 hours before seizure. If $z_{t\_diff} = z_{t,\alpha} - z_{ref,\alpha}$, the null hypothesis H_0 can be stated as follows

Null Hypothesis H_0: There is no difference in the z-scores, $z_{t,\alpha}$ and $z_{ref,\alpha}$.

The alternate hypothesis H_1: The z-scores $z_{t,\alpha}$ and $z_{ref,\alpha}$ are not equal.

Testing the hypothesis consists of following steps

1. Construct a distribution of z_α's from samples taken during inter-ictal states. Specifically, take any 2 hour segment from the background activity of the intracranial EEG data. Construct affinity matrices as before and evaluate mantel statistics to get z-scores. Repeat the above procedure on a number of such 2 hour segments (say 40) from background recording of the same patient and evaluate mantel test procedure for each one of them, to form an ensemble of z-scores, $z^i_{t,s}$ where t represents the time-index (hours), s represents the segment index (s = 1, 2, 3….., 40) and i is used to denote that these z-scores are computed on inter-ictal segments. For illustration, fig. 5-2 shows the smoothened z^i_α profiles

corresponding to the inter-ictal segments. The smoothened z_α profile corresponding to seizure 1 is also shown superimposed on the z_α^i profiles.

1. If $z_{t\_diff,s}^i = z_{ref,s}^i - z_{t,s}^i$ is the difference in the z-scores at time t relative to a reference time for the s_{th} segment, then $z_{t\_diff}^i$ forms a distribution that is constructed from all the 40 segments and is observed to be approximately Gaussian.

2. The idea is to check if the difference observed in the z-scores in the segment 2 hours before seizure (z_{t_diff}) is significantly different from the differences observed in the z-scores during inter-ictal states ($z_{t\_diff}^i$). We quantify this idea as follows

$$z_t = \frac{z_{t\_diff} - \bar{z}_{t\_diff}^i}{\sigma(z_{t\_diff}^i)} \qquad (5.3)$$

where $\bar{z}_{t\_diff}^i$ and $\sigma(z_{t\_diff}^i)$ are the mean and variances of, $z_{t\_diff}^i$ respectively. $Z_t >$ 1.96 indicates the difference is significant and so the null hypothesis can be rejected at a 95% significance level. Since the test is one-tailed, the null hypothesis cannot be rejected if $Z_t <$ -1.96. Even though it means that the differences are significant in those cases, a negative $z_{t\_diff} = z_{t,\alpha} - z_{ref,\alpha}$ implies an upward curve in fig 5-1. as the seizure is approached. Seizure 6 in fig. 5-1 can be one such instance.

Fig. 5-3 presents the Z_t scores as a function of time, for seizures 1 to 7 of the patient P092. Z_t scores were computed for three different reference times. In other words, the z-scores at 90 minutes, 100 minutes and 110 minutes prior to a seizure were used as $z_{ref,\alpha}$.

Fig 5-3. through to Figs 5-5 show profiles of Z_t scores for all the three reference times. Since we are particularly interested in Z_t scores > 1.96 (critical threshold), we make the following observations:

1. 6 out of the 7 seizures (the exemption being seizure 3) have clear time-instances where the Z_t scores are greater than the critical threshold.

2. The time-instances where critical thresholds are crossed vary from seizure to seizure.

3. The Z_t profiles corresponding to the three reference times (90, 100 & 110 minutes) are mostly consistent with respect to crossing the thresholds. Occasional discrepancies are seen, perhaps due to rapid fluctuations within the z-scores at reference times.

From the 1st observation above, we have clear evidence of spatial activity changes in the intracranial EEG data as the patient approaches seizure state (or a pre-seizure state!!). The 2nd observation tells us that the times at which the statistical changes are observed vary across seizures. This can lead us to conclude that the seizure markers in the form of spatio-temporal pattern changes perhaps are a function of the type of seizures and also the pathological state of the brain and many other variables, as well. There is also an ongoing debate on the notion of a pre-seizure state and the transition from inter-ictal state to pre-ictal state. The above analyses may be a step ahead in providing evidence to the existence of pre-seizure states and transition between states. Significant changes in the intracranial EEG's spatio-temporal patterns can possibly serve as one of the precursors for an impending seizure.

5.6 Inter-Hemisphere Synchronization Differences

In chapter 3, we addressed the problem of quantifying mutual interactions among various regions in the brain by proposing the nearest-neighbor based SOM-SI technique. The SOM-SI is fundamentally a state space approach that uses the recurrence in dynamical states of one signal to quantify the recurrence of dynamical states in another signal. The similarity indices, in fact, reflect the activity shared between the neuronal networks at the sub-cortical levels.

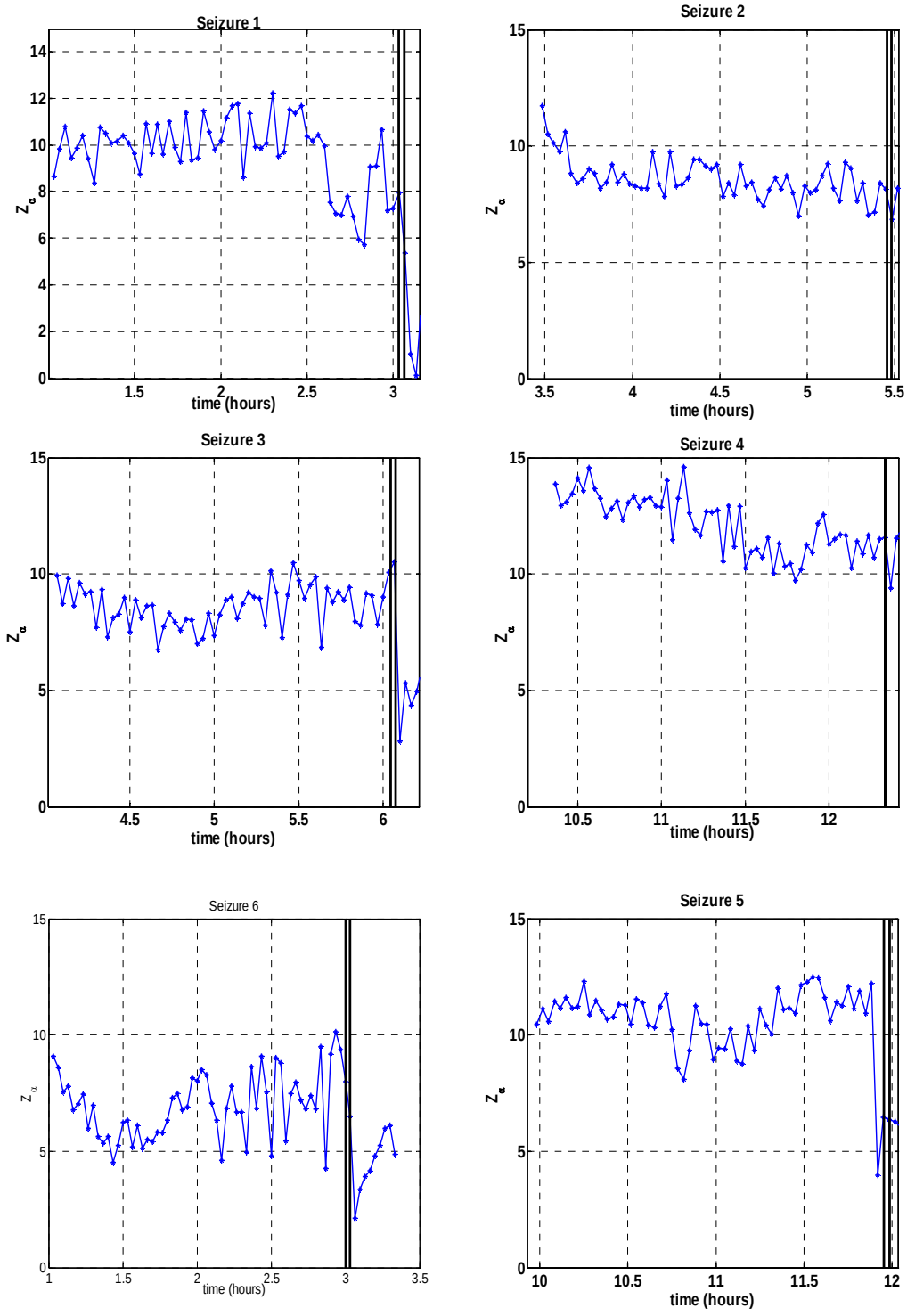

Figure 5-1. Quantifying the spatial changes along time using Mantel statistics. The vertical lines in the figure indicate seizure onset and termination periods. Notice that the statistical values show a slight decrease, approaching the seizures.

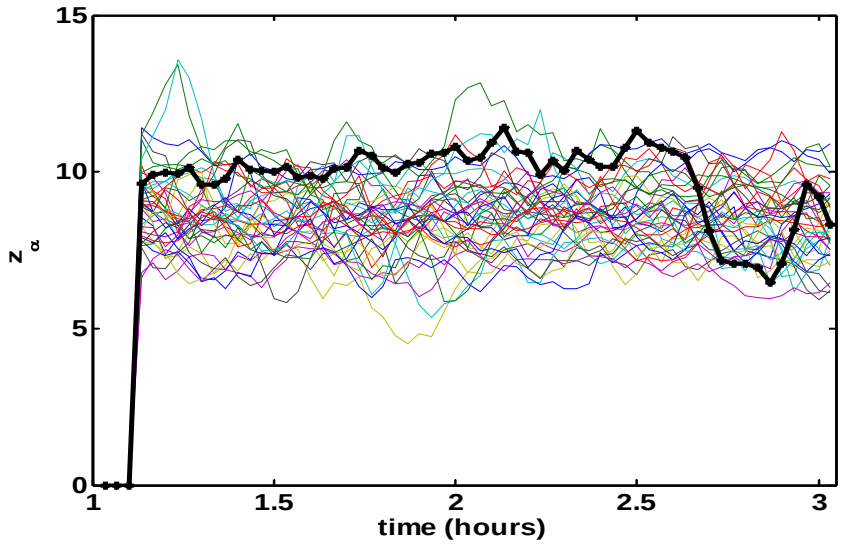

Figure 5-2. Time smoothened profiles of the Mantel statistics during inter-ictal states. The dark line shows the profile for seizure 1, P092.

The mesial lobe temporal lobe epilepsy is mainly characterized by partial seizures that are both complex and generalized in nature. While the generalized seizures are known to be widespread across both the hemispheres, the complex partial seizures are more localized. The complex partial seizures are known to be particularly active in the hippocampal networks that contain damaged lesions. Based on that, it is argued [46-47] that the neuronal networks corresponding to the focal zone have a higher synchronizing ability, compared to the networks in the non-focal zone. It has also raised speculations on whether the interaction levels over the entire focal-hemisphere are higher than the corresponding interaction levels in the non-focal hemisphere. A recent study by Kraskov et al. [46-47], showed that, in the inter-ictal period, the average synchronization in the focal hemisphere of the brain is indeed significantly higher than in the non-focal hemisphere.

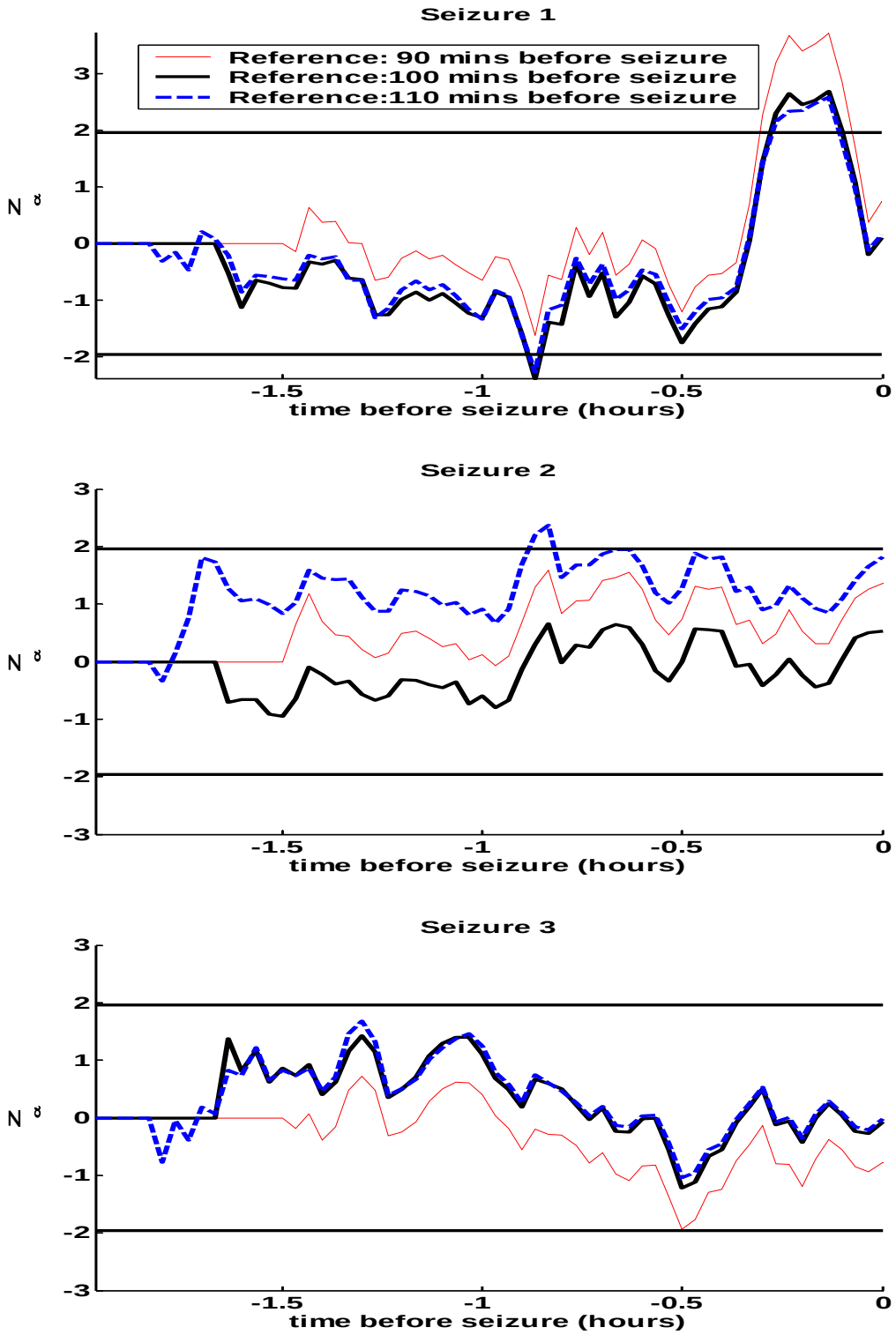

Figure 5-3. Illustrating the statistical difference between z-score at time‘t’ and z-score at a reference time, 90, 100 and 110 minutes before a seizure. Top to Bottom: profiles of z-score statistics for seizures 1 through 3 of patient P092.

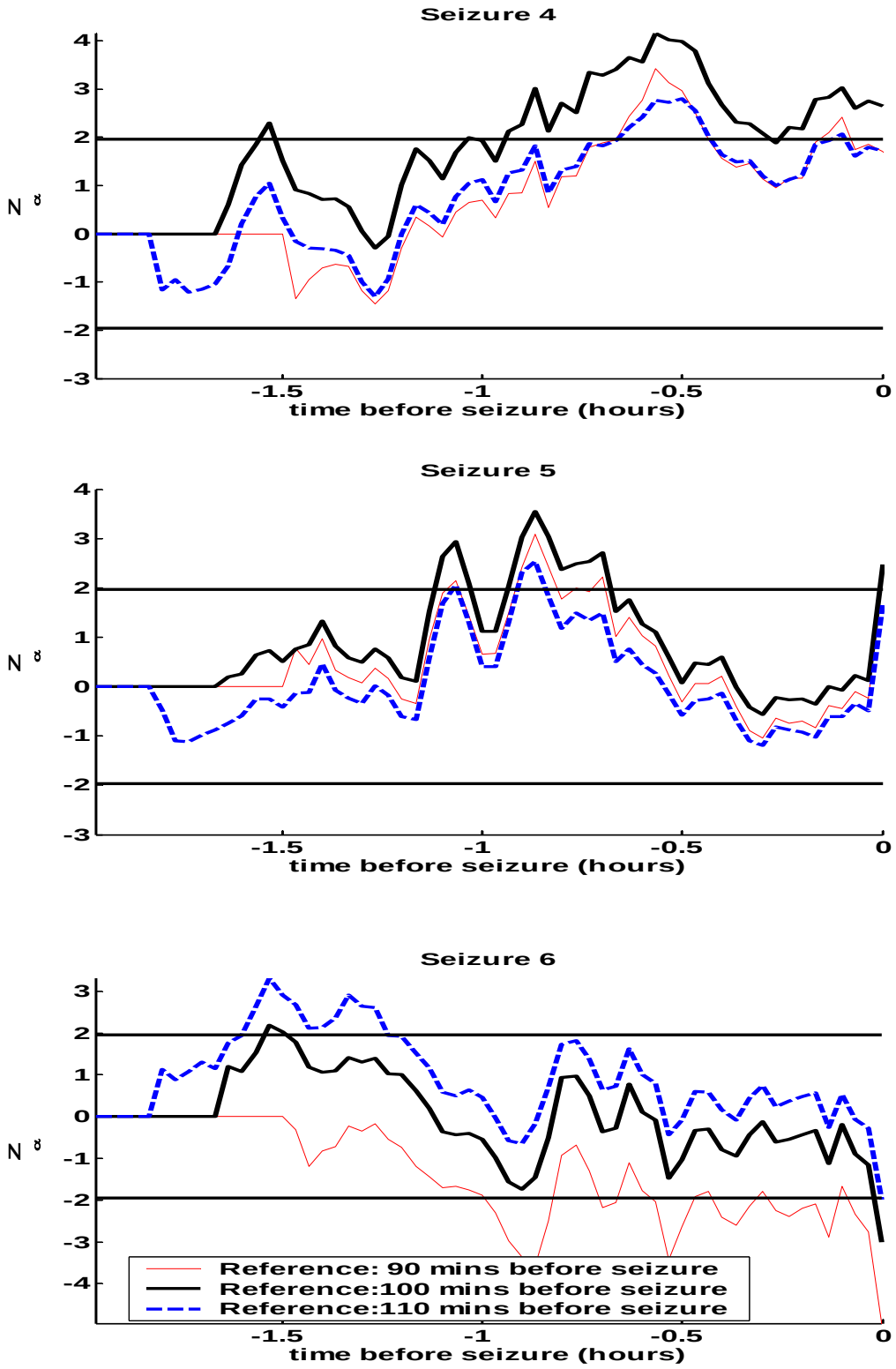

Figure 5-4. Illustrating the statistical difference between z-score at time‘t’ and z-score at a reference time, 90, 100 and 110 minutes before a seizure. Top to Bottom: profiles of z-score statistics for seizures 4 through 7 of patient P092.

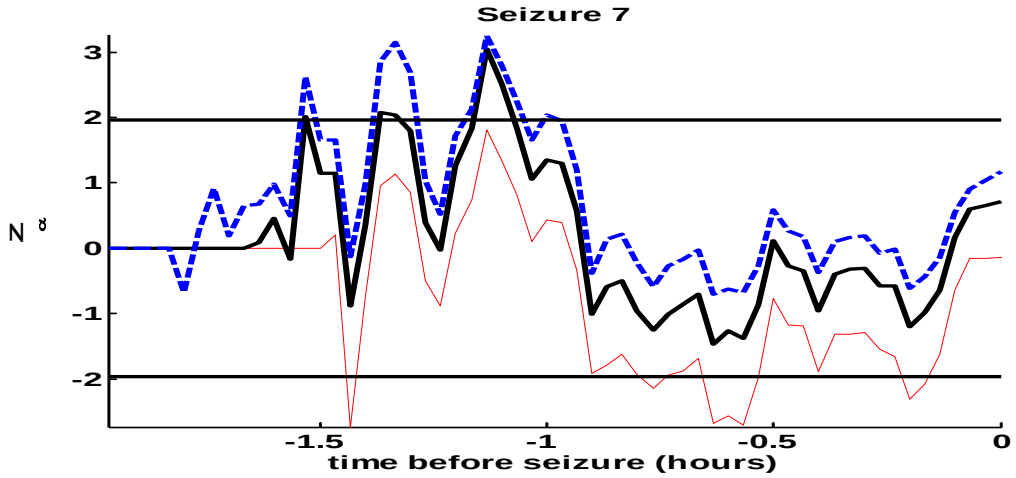

Figure 5-5. Illustrating the statistical difference between z-score at time‘t’ and z-score at a reference time, 90, 100 and 110 minutes before a seizure. Top to Bottom: profiles of z-score statistics for seizure 7 of patient P092.

In this study, we investigate on the differences in the synchronization levels between the focal and the non-focal hemispheres at pre-ictal and post-ictal states. Recall from the previous chapter that we observed that a sudden increase in synchronization levels was accompanied by a gradual decrease at post-seizure, in all the regions of an epileptic brain. Granted that the brain consistently observes an overall increase in synchronization post-seizure, it would be interesting to know whether the difference in synchronization levels between the two hemispheres continue or cease to exist. These questions bring us to the following hypothesis formulation:

Define the average interaction between the Right Temporal Depth (RTD) and all the other regions in the right hemisphere as R_{avg}.

Similarly, define the average interaction between the Left Temporal Depth (LTD) and all the other regions in the left hemisphere as L_{avg}.

H_0: Average synchronization difference between R_{avg} and L_{avg} is the same from pre-ictal to post-ictal state.

H_1: Average synchronization difference between R_{avg} and L_{avg} undergoes a change going from pre-ictal to post-ictal state.

5.7 Statistical Assessment

To test the hypothesis, the average synchronization index R_{avg} from the focal hemisphere is compared against the L_{avg}, from the non-focal hemisphere. As defined earlier, R_{avg} is obtained by averaging the mutual interaction between the right-temporal depth channels and the other channels (namely Right Orbito Frontal and the Right Sub-Temporal regions) in the right hemisphere. The same definition holds for L_{avg} obtained from the left hemisphere channels.

Comparisons consist of checking whether pairs of R_{avg} and L_{avg} synchronization indices, obtained from a group of successive windows, come from same distributions or not. Statistical significance is checked by using the Wilcoxon signed-rank test. It is a non-parametric procedure to check the null hypothesis that the two sets of variables come from same distribution or not. The test does not make any apriori assumptions about the distribution of the variables. However, it takes into account the magnitude of differences within pairs and gives more weight to pairs that show large differences than to pairs with small differences. The test statistic is based on the ranks of the absolute values of the differences between the two variables. An observed significance level is often called the p-value. This value is the basis for deciding whether or not to reject the null hypothesis. It is probability that a statistical result as extreme as the one observed would occur if the null hypothesis were true. If the observed significance level is small enough, usually less than 0.05 or 0.01, the null hypothesis is rejected.

5.8 Experimental Results

Intracranial EEG recordings consisting of 4 seizures from patient P093 and 6 seizures from patient P092 are analyzed, retrospectively. Both the patients had a history of temporal lobe epilepsy in the mesial structures. Following surgical resection, a lesion had been identified in the anterior RTD electrodes region. In the rest of the chapter, therefore, the right hemisphere would be called as the focal hemisphere and the RTD region as the epileptic zone. Correspondingly, the left hemisphere would be called as the non-focal hemisphere.

The definition of existence of a pre-seizure state is very subjective. Even more, the discussion on how long before seizures is a pre-seizure state differs very widely. Without getting into the intricacies of detecting inter-ictal to pre-ictal transitions, we just fix the window of analysis before seizures to 60 minutes. Due to the fact that the arguments on post-seizure durations also have no general consensus, we treat the entire 60 minutes of post-seizure as post-seizure state.

Synchronization analysis consisted of analyzing 60 minutes pre-seizure and 60 minutes post-seizure onset of intracranial EEG data, for each of the 10 seizures from 2 patients. For each non-overlapped 10-sec window (2000 samples, 200 samples/sec digitization rate), SOM-similarity index measure was applied to estimate the pair-wise synchronization index between the set of 24 channels. Note that, for computation reasons, only alternate 10-second windows were analyzed.

5.8.1 Experiment #1

The average synchronization indices R_{avg} and the L_{avg} are computed for every 10-second window, over the entire time range of 120 minutes (60 minutes pre and 60 minutes post-seizure interval). A 10 minute moving window is then used for statistical

validation of synchronization indices, using a paired signed rank test. Specifically, in each sliding window of 10 minutes, the test verifies whether the distribution formed from computing the paired difference between R_{avg} and L_{avg} indices have zero median or not. Null hypothesis is rejected if the test produces a score outside the critical score for 95% significance. For example, z > zcrit, 0.05 (1.96 according to the table), will reject the null hypothesis, implying that the R_{avg} and L_{avg} indices have different medians. Successive windows overlap; the amount of sliding being 20 seconds. Results of a signed-rank test on one of the seizures are presented in Fig 5-6. Consistent with our earlier observations in previous chapter, the average synchronization indices exhibit a seeming increase in synchronization post-seizure, lasting for several minutes. Results from the paired signed-rank test show significant pre-seizure synchronization differences. This seizure in particular, was a complex partial seizure implying that the seizure is more hemispheric or rather, localized. The pre-seizure statistical results provide convincing evidence on the nature of localization by pointing out to the differences in the interactions between the two hemispheres. The situation post-seizure, however, is different. The statistical results fail to reject the null-hypothesis, for a period lasting for about 30 minutes post-seizure. Between the 30 minutes and 60 minutes interval post-seizure, we again observe null-hypothesis rejections.

On a larger group of seizures (10 seizures from 2 patients), synchronization results were analyzed using the procedure described above. Define H to be the index of null-hypothesis evaluation. H = ‘1’ indicates a rejection of null-hypothesis and H = ‘0’ indicates insignificant evidence to do so. The average H from 10 seizures, corresponding to a 10 minute time-window are computed and plotted in fig 5-7. Clearly, the 60 minutes

interval prior to seizure onset seems to have high rejection percentage. It highlights the degree of difference in the way the focal zone (RTD) interacts with all other right-hemisphere channels and the way the non-focal zone (LTD) interacts with other left-hemisphere channels. Post-seizure results exhibit a sudden drop in H, from seizure onset to 6-8 minutes after seizure. The low rejection rate implies a higher degree of similarity between R_{avg} and L_{avg}. 20 minutes after seizure onset, we again observe a gradual transition from strong similarity between R_{avg} and L_{avg} to a strong difference between them. In summary, the statistics suggest that, in the first 20 minutes post-seizure, synchronization differences between R_{avg} and the L_{avg} cease to exist implying a global synchronization without any bias towards hemispheres.

5.8.2 Experiment #2

In the first experiment, analysis was primarily focused on testing the synchronization differences between R_{avg} and L_{avg} during the pre-ictal and post ictal states. While the test results clearly indicate that the RTD interactions with other right hemispheric channels are similar to the corresponding LTD interactions in the post-ictal state, it will be interesting to check whether the RTD interactions with channels in the left hemisphere also yield similar results. With this objective, we set up the hypothesis as follows:

Define the average interaction between the Right Temporal Depth (RTD) and all the other regions in the right hemisphere as R^{r}_{avg}.

Similarly, define the average interaction between the Right Temporal Depth (LTD) and all the other regions in the left hemisphere as R^{l}_{avg}

H_0: Average synchronization difference between R^r_{avg} and R^l_{avg} is the same from pre-ictal to post-ictal state.

H_1: Average synchronization difference between R^r_{avg} and R^l_{avg} undergoes a change going from pre-ictal to post-ictal state.

In tune with the design procedure of experiment #1, R^r_{avg} and R^l_{avg} synchronization profiles are computed from the SOM-SI indices, following which the wilcoxon signed rank test is applied to test the hypothesis. Defining H as before, the average H from 10 seizures is computed and plotted as a function of time in fig 5-8. As in experiment #1, the 60 minutes interval before seizure has a high null-hypothesis rejection percentage, suggesting the difference between the RTD interaction with right hemisphere channels and the corresponding left hemisphere channels. Interestingly, the interval post-seizure also exhibits a high rejection rate. It implies that significant synchronization differences continue to exist between R^r_{avg} and R^l_{avg}, as the brain transits between seizure states. Effectively, this may mean that the nature of the homologous interactions (or connectivities) of the focal zone are very different compared to its ipsilateral interactions (or connections), at all ictal states.

5-9 Summary

We addressed the question if the strength of connections between non-focal channels in the focal hemisphere (RST and ROF) and the channels in focal zone (RTD) differed significantly from the connections between non-focal channels in the non-focal hemisphere (LTD and LOF) and channels in non-focal zone (LTD). Hypothesis testing reported significant degree of differences in the pre-seizure states (1 hour before seizure). However fewer rejections of null-hypothesis in the time-intervals 20 minutes post-seizure

led us to concede that the non-focal interactions may be highly entrained (both in amplitude and phase) with that of the focal interactions following seizures. In a similar setup aimed at determining the functional differences between (RST and ROF) with focal zone RTD and the (LST and LOF) with RTD, we observed that with reference to the focal zone, the nature of cross-hemispheric connections always differed from the intra-hemispheric connections at all seizure states.

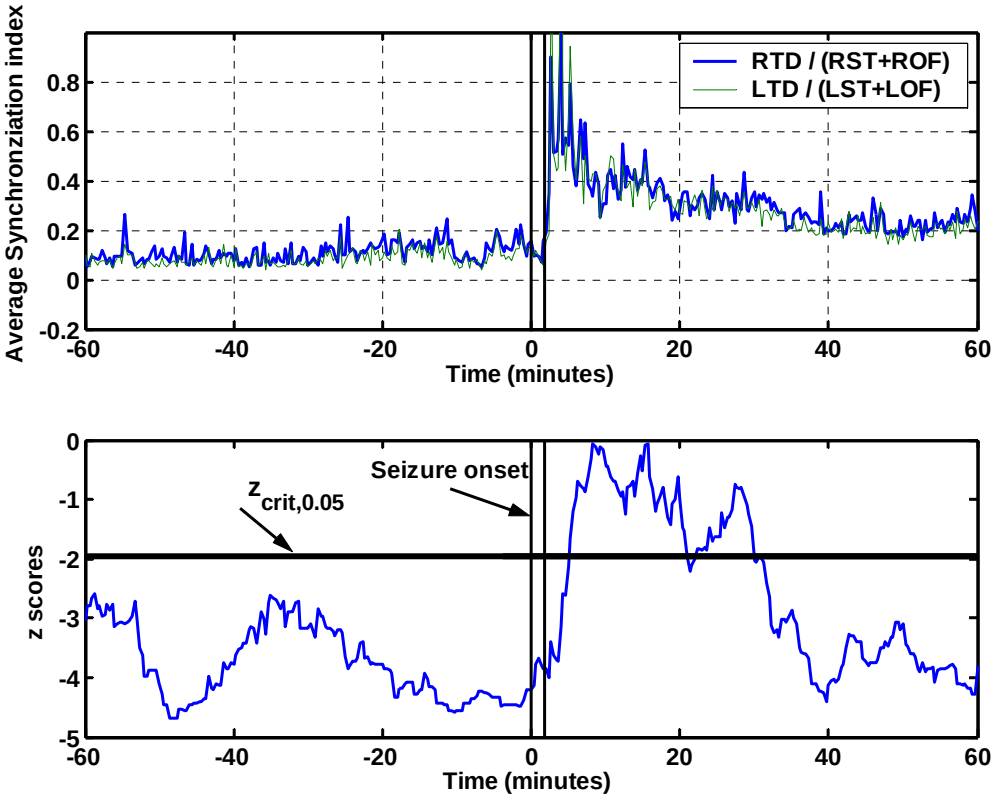

Figure 5-6. Results of synchronization analysis on seizure 1 of P092, to check the differences between the focal and non-focal hemispheric interactions, at pre and post-ictal states. Top: Average SOM-SI synchronization indices of the right (focal) and left (non-focal) hemispheres, 1 hour before and after seizure. Bottom: Results of Wilcoxon signed rank test show that the differences in hemispheric interactions cease immediately after seizure and lasts for several minutes post-seizure.

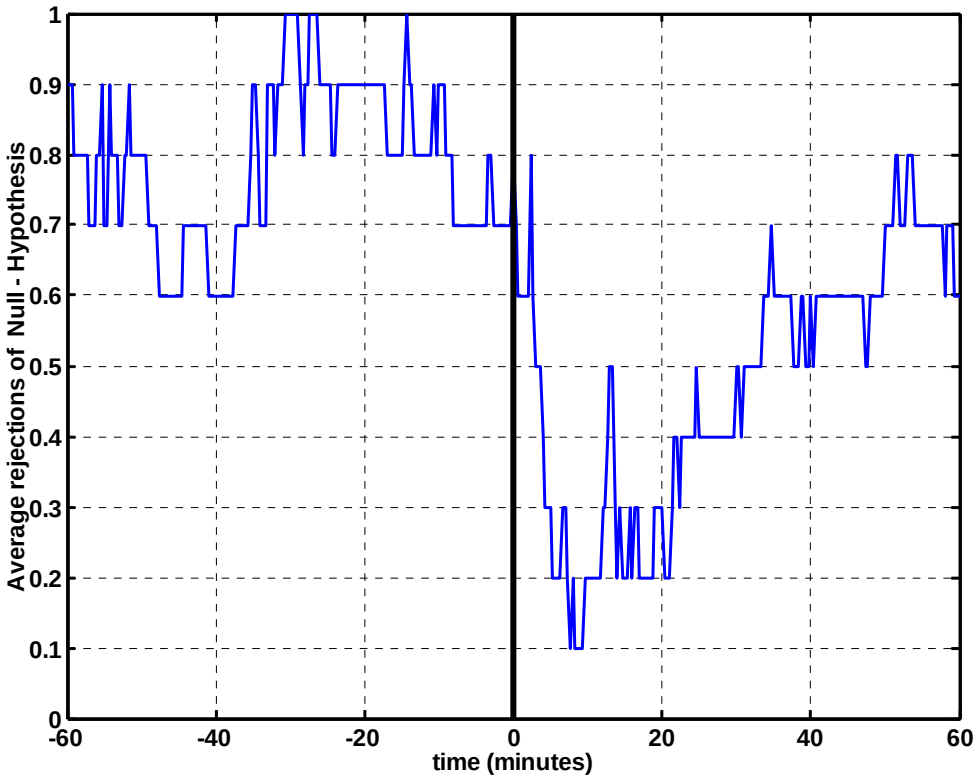

Figure 5-7. Null-hypothesis rejections rate averaged over 10 seizures for experiment 1 The vertical line at 0^{th} minute indicates seizure onset. 60 minutes interval prior to seizure onset seems to have considerable difference between the intra-hemispheric interactions. Post-seizure results suggest a very minimal difference between the intra-hemisphere interactions, approximately in the first 20 minutes. Later than 20 minutes seems to be a transition phase from strong similarity between hemispheres to a strong difference between them.

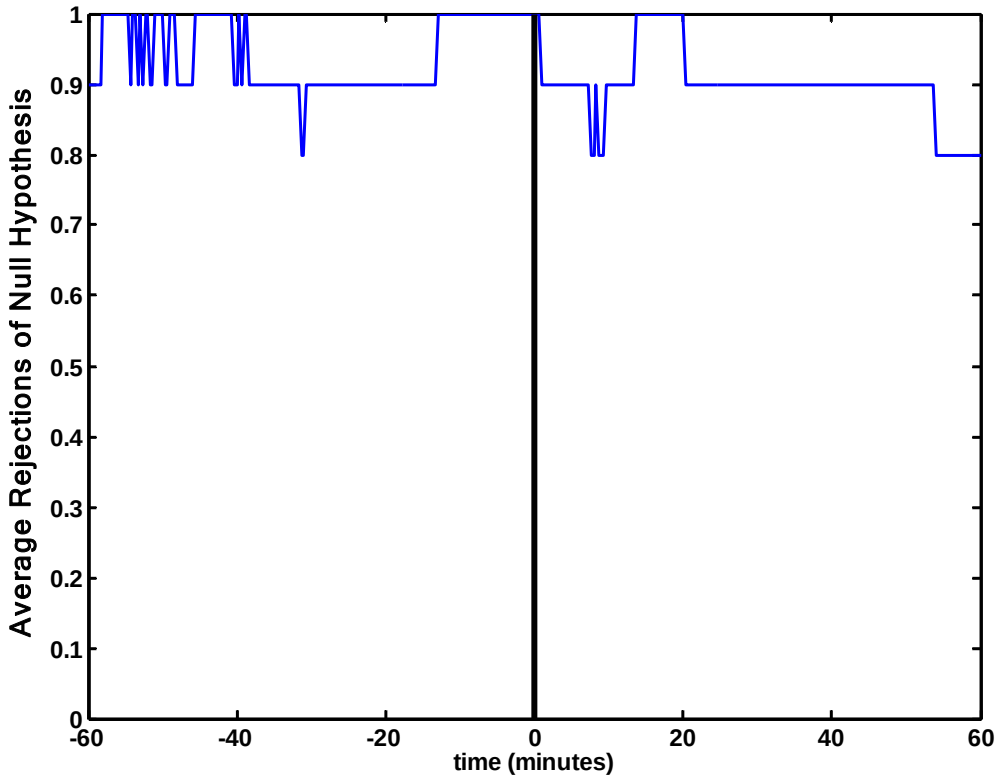

Figure 5-8. Null-hypothesis rejections rate averaged over 10 seizures for experiment 2. The vertical line at 0^{th} minute indicates seizure onset. 60 minutes interval prior to seizure onset seems to have considerable difference between the intra-hemispheric interactions. Post-seizure results suggest a very minimal difference between the intra-hemisphere interactions, approximately in the first 20 minutes. Later than 20 minutes seems to be a transition phase from strong similarity between hemispheres to a strong difference between them.

CHAPTER 6
CONCLUSIONS AND FUTURE DIRECTIONS

6-1 Conclusions

With the advent of sophisticated linear and non linear signal processing tools, application of engineering techniques to analyze epileptic data has taken a major step forward. A lot of advances are being seen in development of seizure detection and prevention systems. These advances have enhanced our basic understanding of neural dynamics associated with seizure generation.

There is sufficient evidence to believe that the brain as a functional model consists of highly complex non linear dynamics. Application of non linear dynamical measures such as short term Lyapunov exponents (STLmax) and correlation dimension on an epileptic brain has revealed that the complexity of the brain reduces significantly as seizure is approached. In other words, the temporal dynamics of the brain progresses from a 'severe chaotic' state to a much lesser or rather 'mildly chaotic' state.

Much of the analysis on temporal dynamics focuses on analyzing and characterizing the irregular behavior of the time-signal of either intracranial or scalp intracranial EEG. However, it is important to realize that the brain is a multi-dimensional system with a large set of neuronal oscillators that are physically coupled together. Obviously the neurons at different spatial locations communicate with each other through synaptic potentials resulting in spike discharges. In such an environment therefore, it would be natural to expect a spatio-temporal interaction at various patho-physiological states. Specifically, in the context of epilepsy, one can perceive that the seizure related

abnormal spike discharges and subsequently the seizure events are accompanied by different regions in the brain communicating in a structured fashion. Therefore, it is very essential to unravel the functional connectivity of the neural networks and analyze how the structures change during seizure events.

In this research, we proposed the SOM-based similarity index measure to analyze the mutual interactions among critical areas of an epileptic brain. We found that the interaction levels were very low at the inter-ictal and pre-ictal intervals. Post-seizure, where the intracranial EEG profiles are generally high frequency and low amplitude waveforms, the interactions exhibited a significant positive jump. Based on the functional relationships, we analyzed long term structural connectivity's related to various seizure states by proposing a spatio-temporal clustering model. On analyzing 12 complex partial seizures from 2 patients suffering from right temporal lobe epilepsy, we found that the orbito-frontal regions always exhibit a strong homologous connectivity while maintaining a low relationship with other regions. The left sub-temporal and the left-temporal depth regions (non-focal hemisphere) were identified to have a strong ipsilateral connection, regardless of seizure states. Finally, we found that the epileptic zone, namely the right hippocampus depth region maintained a relatively strong connection with the right sub-temporal region. Interestingly, the configuration of the groupings between different regions always remained the same, regardless of whether the patient was in an inter-ictal, pre-ictal or post-ictal state although the inter-region connectivity strengths seemed to vary slightly across states.

In a related study, we analyzed the differences between connectivity strengths from left-hemisphere regions and the right-hemisphere regions to the focal zone (right

temporal depth). Hypothesis testing reported significant degree of differences in the pre-seizure states (1 hour before seizure). However fewer rejections of null-hypothesis in the time-intervals 20 minutes post-seizure led us to concede that the non-focal interactions may be highly entrained (both in amplitude and phase) with that of the focal interactions following seizures.

Another aspect of this research was to analyze the temporal changes in the overall spatial-patterns of an epileptic intracranial EEG. Using Mantel statistics, we showed that as seizure is approached, the overall spatial connectivity can be significantly different in comparison to the connectivity 2 hours before seizure. The exact time where the spatial bindings change can vary from seizure to seizure.

6-2 Future Research Directions

In this dissertation, we explored the spatio-temporal structure in an epileptic brain from a signal processing perspective. Unlike in many other clustering approaches where dynamical features extracted from the data are used as basis to determine groupings, our proposed clustering approach uses the dependencies among the original data recordings to do the same. The SOM-based similarity index measure was proposed as a dependency metric to quantify couplings among different recordings and subsequently chosen to extract channel clusters. Comparisons of SOM-SI with other linear and non linear measures have already been articulated elsewhere [46]. However, in the context of clustering, it would be interesting to check if any other dependency measure would also produce same clusters as SOM-SI. Perhaps, the sensitivity of SOM-SI to non linear interactions can be confirmed by assessment of cluster groupings from linear measures.

So far, because of the data size, we were constrained to analyze only on 12 seizures from 2 patients. Future effort in this direction would be to apply the proposed approach

on a larger set of seizures and more patients. In addition, since we analyzed only on complex partial seizures, it would be worthwhile to check the cluster grouping in other types of seizures such as partial secondary generalized and sub-clinical seizures.

Recall from the results that certain channels were always grouped together regardless of the seizure states. This raises a question if this pattern is unique to an epileptic patient and therefore be considered as a blueprint of seizures. One plausible way to answer this speculation would be to apply the proposed clustering approach on normal subjects and then compare the differences in groupings with that of seizure patients

As we have mentioned a few times earlier, one of our main objectives in this research was to develop engineering tools to determine spatio-temporal groupings in a multivariate epileptic brain. We proposed a similarity-based clustering approach and used it to extract hidden structures from an epileptic brain. One of the obvious limitations with any clustering approach is determining the optimal number of clusters. Techniques to combat the cluster size problems have been researched upon, without much success. In eigen vector based methods such as spectral clustering, cluster size can possibly be approximated to be equal to the number of eigen vectors corresponding to significant eigen values. In multiple data sets however, the optimal cluster size need not have to be the same across different data sets rendering cluster comparisons weak. In our approach, we analyzed a large number of data sets and empirically, fixed the cluster size to 3. This may not be an efficient or a systematic approach to tackle the problem. Theoretic efforts are needed to develop mathematical criterion that allows us to determine a fixed cluster size, suitable to all groups of data. Besides, exploring tools better than clustering to unravel hidden patterns in multidimensional time-sequences would be very beneficial.

The Mantel statistics to track temporal changes in spatial patterns is a reasonably useful approach to distinguish pre-seizure patterns from those at inter-ictal stage of a seizure. So far, we have analyzed on a small set of seizures and the results have looked encouraging. Assuming distinct pre-seizure patterns exist; Mantel statistics analysis on a much larger set of seizures associated with different onset circumstances may help us in finding the general sensitivity of this technique.

LIST OF REFERENCES

1. J. Arnhold, P. Grassberger, K. Lehnertz, and C. E. Elger, "A Robust Method for Detecting Interdependencies: Application to Intracranially Recorded EEG," *Physica D*, vol. 134, pp. 419-430, 1999

2. L. A. Baccala, and K.Sameshima, "Overcoming the Limitations of Correlation Analysis for Many Simultaneously Processed Neural Structures," *Brain Research*, vol. 130, pp.33-47, 2001.

3. L. A. Baccala, and K. Sameshima, "Partial Directed Coherence: A New Concept in Neural Structure Determination," *Biological Cybernetics*, vol. 84, pp.463-474, 2001.

4. I. Baruchi, and E. Ben-Jacob, "Functional Holography of Recorded Neuronal Networks Activity," *Neuroinformatics*, vol. 2, pp. 333-351, 2004.

5. I. Baruchi, V. Towle, and E. Ben-Jacob, "Functional Holography of Complex Networks Activity – From Cultures to the Human Brain," *Complexity*, vol. 10 (3), pp. 38 -51, Wiley Periodicals, 2005.

6. J. S. Bendat, and A. G. Piersol, *Random Data: Analysis and Measurement Procedures,* 2nd Ed. New York, John Wiley, 1986.

7. J. Bhattacharya, H. Petsche, and E. Pereda, "Interdependencies in the Spontaneous EEG while Listening to Music," *International Journal of Psychophysiology*, vol. 42, pp. 287-301, 2001.

8. J. Bhattacharya, E. Pereda, and H. Petsche, "Effective Detection of Coupling in Short and Noisy Bivariate Data," *IEEE Transactions on Systems, Man and Cybernetics - Part B*, vol. 33 (1), pp. 85-95, 2003.

9. A. M. Bianchi, F. Panzica, F.Tinella, S. Franceschetti, S.Cerutti, and G. Baselli, "Analysis of Multichannel EEG Synchronization before and during Generalized Epileptic Seizures," *Proceedings of the 1st International IEEE EMBS Conference on Neural Engineering*, pp. 39-42, Capriland, 2003.

10. K. Blinowska, R. Kus, and M. Kaminski, "Granger Causality and Information flow in Multivariate processes," *Physical Review E*, vol. 70: 050902, pp: 01-04, 2004.

11. G. C. Carter, "Coherence and Time Delay Estimation," *Proceedings IEEE*, vol. 75(2), pp. 236-255, 1987.

12. T. M. Cover, and J. A.Thomas, *Elements of Information Theory*, New York, Wiley, 1991.

13. O. David, D. Cosmelli, and K. J.Friston, "Evaluation of Different Measures of Functional Connectivity Using a Neural Mass Model," *NeuroImage*, vol. 21, pp. 659-673, 2004.

14. O. David, D. Cosmelli, J. -P.Lachaux, S. Baillet, L. Garnero and J. Martinerie, "A Theoretical and Experimental Introduction to the Non-Invasive Study of the Large Scale Neural Phase Synchronization in Human Beings," *Invited Paper, International Journal of Computational Cognition*, vol. 1(4), pp. 53-77, December, 2003.

15. P. Dayan, and L. F. Abbot, *Theoretical Neuroscience*, MIT Press, Boston, MA, 2001.

16. R. B. Duckrow, and S. S. Spencer, "Regional Coherence and the Transfer of Ictal Activity During Seizure Onset in the Medial Temporal Lobe," *Electroenceph Clin Neurophysiol*, vol. 82, pp. 415-422, 1992.

17. J. P. Eckmann, and K. D. Ruelle, "Recurrence Plots of Dynamical Systems," Europhysics Letters, vol. 5, pp. 973-977, 1987.

18. M. -J. Fortin, M. R. T.Dale, and J, V. Hoef, "Spatial Analysis in Ecology," *Encyclopedia of Environmetrics*, Ed. By El-Shaarawi, A.H. and Piegorsch, W.W, vol. 4, pp. 2052-2058, 2002.

19. P. J. Franaszczuk, and G. K. Bergey, "Application of the Directed Transfer Function Method to Mesial and Lateral Onset Temporal Lobe Seizures," *Brain Topography*, vol. 11, pp. 13-21, 1998.

20. P. J. Franaszczuk, G. K. Bergey, and M. Kaminski, "Analysis of Mesial Temporal Seizure Onset and Propagation Using the Directed Transfer Function Method," *Electroenceph. clin. Neurophysiology*, vol. 91(6), pp. 413-427, 1994.

21. J. W. Freeman, "Characteristics of the Synchronization of Brain Activity Imposed by Finite Conduction Velocities of Axons," *International Journal of Bifurcation and Chaos*, vol. 10, pp. 2307-2322, 2000.

22. J. W. Freeman, and J. M. Barrie, "Analysis of Spatial Patterns of Phase in Neocortical Gamma EEGs in Rabbit," *Journal of Neurophysiology,* vol. 84, pp. 1266-1278, 2000.

23. J. K. Friston, "Brain Function, Non-Linear Coupling and Neural Transients," *The NeuroScientist*, vol. 7 (5), pp. 406-418, 2001.

24. J. Gao, and H. Cai, "On the Structures and Quantification of Recurrence Plots," *Physics Letters A*, vol. 270, pp. 75-87, 2000.

25. J. A. Garcia, J. Fdez-Valdivia, F. J. Cortijo, and R. Molina, "A Dynamic Approach for Clustering Data," *Signal Processing,* vol. 44(2), pp. 181-196, 1995.

26. J. Gotman, J. Ives, P. Gloor, A. Olivier, and L. F. Quesney, "Changes in Inter-Ictal EEG Spiking and Seizure Occurrence in Humans," *Epilepsia*, vol. 23, pp. 432-433, 1982.

27. C. W. J. Granger, "Investigating Causal Relations by Econometric Models and Cross-spectral Methods," *Econometrica*, vol. 37(3), pp. 424-438, 1969.

28. M. A. F. Harrison, I. Osorio, M. G. Frei, S. Asuri, and Y-C. Lai, Y-C. "Correlation Dimension and Integral do not Predict Epileptic Seizures," *Chaos,* vol. 15:033106, pp. 01-15, 2005.

29. A. Hegde, D. Erdogmus, Y. Rao, J. C.Principe, and J. B.Gao, "SOM-Based Similarity Index Measure: Quantifying Interactions between Multivariate Structures," *Proceedings of NNSP'03, pp. 819-828, Toulouse, France*, Sep 2003.

30. A. Hegde, D. Erdogmus and J. C. Principe, "Synchronization Analysis of Epileptic ECoG Data Using SOM-Based SI Measure," *Proceedings of EMBS 2004,* pp. 952-955, San Francisco, September 2004.

31. A. Hegde, D. Erdogmus, and J. C. Principe, "Quantifying Spatio-Temporal Dependencies in Epileptic ECOG," *IEEE Signal Processing Special Issue - Neural Co-ordination in the Brain*; A Signal Processing Perspective, vol. 85, pp. 2082-2100, 2005.

32. A. Hegde, D. Erdogmus, and J. C. Principe, "Spatio-Temporal Clustering in Epileptic ECOG," *Proceedings of EMBS,* Shanghai, September, 2005.

33. D. Hoyer, O. Hoyer, and U. Zweiner, "A New Method to Uncover Dynamic Phase Coordination and Synchronization," *IEEE Transactions on Biomedical Engineering,* vol. 47 (1), pp. 68-74, 2000.

34. N. E. Huang, Z. Shen, S. R. Long, M. L. Wu, H. H. Shih, Q. Zheng, N. C. Yen, C. C. Tung, and H. H. Liu, "The Empirical Mode Decomposition and Hilbert Transform for Non-Linear and Non-Stationary Time Series Analysis," *Proc. Roy. Soc. London A,* vol. 454, pp. 908-995, 1998.

35. L. D. Iasemidis, L. D. Olson, J. C. Sackellares, and R. Savit, "Time Dependencies in the Occurrence of Epileptic Seizures: a NonLinear Approach," *Epilepsy Research*, vol. 17, pp. 81-94, 1994.

36. L. D. Iasemidis, J. C. Principe, J. M. Czaplewski, R. L. Gilmore, S. N. Roper, and J. C. Sackellares, *Spatiotemporal Transition to Epileptic Seizures: a Nonlinear Dynamical Analysis of Scalp and Intracranial EEG Recordings*. In: Lopes da Silva F. H., Principe J. C., Almeida L. B., eds. S*patiotemporal models in biological and artificial systems.* Amsterdam: IOS Press, pp: 81- 89, 1997

37. L. D. Iasemidis, J. C. Sackellares, H. P. Zaveri, and W. J. Williams,“ Phase Space Topography and the Lyapunov Exponent of Electrocorticograms in Partial Seizures,” *Brain Topography*, vol. 2, pp. 187-201, 1990.

38. L. D. Iasemidis, K. E. Pappas, J. C. Principe, and J. C. Sackellares, “SpatioTemporal Dynamics of Human Epileptic Seizures,” *Proceedings of the 3rd Experimental Chaos Conference*, eds. R.G. Harrison *et al.*, World Scientific, Singapore, pp. 26-30, 1996.

39. L. D. Iasemidis, P. Pardalos, J. C. Sackellares, and D. S. Shiau, “Quadratic Binary Programming and Dynamical System Approach to Determine the Predictability of Epileptic Seizures,” *Journal of Combinatorial Optimization*, vol. 5, pp. 09-26, 2001.

40. L. D. Iasemidis, D. S. Shiau, W. Chaovalitwongse, J. C. Sackellares, P. M. Pardalos, J. C. Principe, P. R. Carney, A. Prasad, B. Veeramani, and K. Tsakalis, “Adaptive epileptic seizure prediction system,” *IEEE Transactions on Biomedical Engineering,* vol. 50 (5), pp. 616-627, 2003.

41. M. Kaminski, and K. J. Blinowska, “A New Method of the Description of the Information Flow in the Brain Structures,” *Biological Cybernetics*, vol. 65, pp. 203-210, 1991.

42. E. R. Kandel, J. H. Schaertz, and T. M. Jessell, *Principles of Neural Science*, New York, 4th Ed., McGraw-Hill, 2000.

43. H. Kantz, and T. Schreiber, *Nonlinear Time Series Analysis*, Cambridge University Press, Cambridge, England, 1997.

44. E. Keogh, J. Lin, and W. Truppel, “Clustering of Time Series Subsequences is Meaningless: Implications for Past and Future Research” *Proceedings of the 3rd IEEE International Conference on Data Mining* (ICDM 2003), pp.115-122, Melbourne, Florida, 2003.

45. M. A. Kramer, E. Edwards, M. Soltani, M. S. Berger, R. T. Knight, and A. J. Szeri, “Synchronization Measures of Bursting Data: Application to the Electrocorticogram of an Auditory Event Related Experiment,” *Physical Review E*, vol. 70:011914, pp. 01-10, 2004.

46. A. Kraskov, T. Kreuz, Q. Quiroga,P. Grassberger, F. Mormann, K. Lehnertz, and C. E. Elger, “Phase Synchronization Using Continuous Wavelet Transform of the EEG for Inter-Ictal Focus Localization in Mesial Temporal Lobe Epilepsy,” *Epilepsia,* 42(7):43, pp. 01-04, 2001.

47. A. Kraskov, T. Kreuz, Q. Quiroga, P. Grassberger, F. Mormann, K. Lehnertz, and C. E. Elger, “Comparison of Two Phase Synchronization Analysis Techniques for Inter-Ictal Focus Lateralization in Mesial Temporal Lobe Epilepsy,” *Epilepsia,* vol. 43(7):48, pp. 01-04, 2002.

48. J. P. Lachaux, E. Rodriguez, J. Martinerie, and F. Varela, "Measuring Phase Synchrony in Brain Signals," *Human Brain Mapping*, vol. 8, pp. 194-208, 1999.

49. A. Laird, J. Carew, and M. E. Meyerand, "Analysis of the Instantaneous Phase Signal of a FMRI Time-Series Via The Hilbert Phase Transform," *Conference Record of the Asilomar Conference on Signals, Systems and Computers*, v 2, pp. 1677-1681, 2001.

50. F. –J. Lapointe, and P. Legendre, "A Statistical Framework to Test the Consensus Among Additive Trees (Cladograms)," *Systematic Biology,* vol. 41 (2), pp. 158-171, 1992.

51. P. Legendre, F. -J. Lapointe, and P. Casgrain,"Modeling Brain Evolution from Behavior: A Permutational Regression Approach," *Evolution*, vol. 48 (5), pp. 1487-1499, 1994.

52. K. Lehnertz, R. G. Andrzejak, J. Arnhold, T. Kreuz F. Mormann, C. Rieke, G. Widman, and C. E. Elger, "Nonlinear EEG Analysis in Epilepsy: Its Possible Use for Interictal Focus Localization, Seizure Anticipation, and Prevention, " *Journal of Clinical Neurophysiology*, vol. 18 (3), pp. 209-222, 2001.

53. K. Lehnertz, F. Mormann, T. Kreuz, R. G. Andrzejak, J. Arnhold, C. Rieke, P. David, and C. E. Elger, "Seizure Prediction By Nonlinear EEG Analysis, " *IEEE Engineering in Medicine and Biology Magazine*, pp. 57-63, 2003.

54. K. Lehnertz, "Non-Linear Time Series Analysis of Intracranial EEG Recordings in Patients with Epilepsy - an Overview," *International Journal of Psychophysiology*, vol. 34, pp. 45-52, 1999.

55. M. Li, J. H. Badger, X. Chen, S. Kwong, P. Kearney, and H. Zhang, "An Information-Based Sequence Distance and its Application to Whole Mitochondrial Genome Phylogeny," *Bioinformatics*, vol. 17 (2), pp.149-154, 2001.

56. F. H. Lopes da Silva, W. Blanes, S. N. Kalitzin, J. Parra, P. Suffczynski, and D. N. Velis, "Dynamical Diseases of Brain Systems: Different Routes to Epileptic Seizures (Invited Paper)," *IEEE Transactions on BioMedical Engineering*, vol. 50, pp. 540-549, 2003.

57. J. Malik, S. Belongie, T. Leung, and J. Shi, "Contour and Texture Analysis for Image Segmentation," International Journal of Computer Vision, 43(1), pp. 7-27, 2001.

58. N. Mantel, "The Detection of Disease Clustering and a Generalized Regression Approach," Cancer Research, vol. 27, pp. 209-220, 1967.

59. N. Marwan, and J. Kurths, "Nonlinear Analysis of Bivariate Data with Cross Recurrence Plots," *Physics Letters A*, vol. 302, pp. 299-307, 2002.

60. F. Mormann, R. G. Andrzejak, T. Kreuz, C. Rieke, P. David, C. E. Elger, and K. Lehnertz, "Automated Detection of a Preseizure State Based on a Decrease in Synchronization in Intracranial Electroencephalogram Recordings from Epilepsy Patients," *Physical Review E*, vol. 67:02192, pp. 01-10, 2003.

61. F. Mormann, T. Kreuz, R. G. Andrzejak, P. David, K. Lehnertz and C. E. Elger, "Epileptic Seizures are Preceded by a Decrease in Synchronization," *Epilepsy Research*, vol. 53, pp. 173-185, 2003.

62. F. Mormann, T. Kreuz, C. Rieke, R. G. Andrzejak, A. Kraskov, P. David, C. E. Elger, and K. Lehnertz, "On the Predictability of Epileptic Seizures," *Clinical Neurophysiology*, vol. 116, pp. 569-587, 2005.

63. F. Mormann, F., K. Lehnertz, P. David, and C. E. Elger, "Mean Phase Coherence as a Measure for Phase Synchronization and its Application to the EEG of Epileptic Patients," *Physica D*, vol. 144, pp. 358-369, 2000.

64. A. Y. Ng, M. I. Jordan, and Y. Weiss, "On Spectral Clustering: Analysis and an Algorithm," *Advances in Neural Information Processing Systems*, 14, pp. 849-856, 2002.

65. A. Ossadtchi, S. Baillet, J. C. Mosher, and R. M. Leahy, "Using Mutual Information to Select Event Related Components in ICA," *Proceedings of International Conference on Biomagnetism*, Finland, 2000.

66. M. Palus, "Detecting Phase Synchronization in Noisy Systems," *Physics Letters A*, vol. 225, pp. 341-351, 1997.

67. M. Palus, "Kolmogorov Entropy from Time Series Using Information-Theoretic Functionals," *Neural Networks World*, vol. 3, pp. 269 - 292, 1997.

68. M. Palus, V. Komarek, T. Prochazka, Z. Hrncir, and K. Sterbova, "Synchronization and Information Flow in EEGs of Epileptic Patients," *IEEE Engineering in Medicine and Biology*, pp. 65-71, 2001.

69. L. M. Pecora, and T. L. Caroll, "Synchronization in Chaotic Systems," *Physics Review Letter*, vol. 64, pp. 821 - 830, 1990.

70. B. Pompe, "A Tool to Measure Dependencies in Data Sequences," *Advanced Mathematical Tools in Metrology II, World Scientific*, Singapore, pp. 81-99, 1996.

71. B. Pompe, "Measuring Statistical Dependencies in a Time Series," *Journal of Statistical Physics*, vol. 73, pp. 587-610, 1993.

72. B. Pompe, P. Blidh, D. Hoyer, and M. Eiselt, "Using Mutual Information to Measure Coupling in the Cardiorespiratory System," *Proceedings of the Engineering in Medicine and Biology Magazine, IEEE*, vol. 17 (6), pp. 32-39, 1998.

73. D. Prichard, and J. Theiler, "Generating Surrogate Data for Time Series with Several Simultaneously Measured Variables," *Physical Review Letters*, vol. 73 (7), pp. 951-954, 1994.

74. J. C. Principe, N. R. Euliano, and W. C. Lefebvre, *Neural and Adaptive Systems: Fundamentals through Simulations*, John Wiley & Sons, 2000.

75. J. G. Proakis, *Digital Communications*, 4th edition, McGraw Hill, 2000.

76. Q. R Quiroga, J. Arhnold, and P. Grassberger, "Learning Driver-Response Relationships from Synchronization Patterns," *Physical Review E*, vol. 61, pp. 5142-5148, 2000.

77. Q. R. Quiroga, J. Arnold, K. Lehnertz, and P. Grassberger, "Kulback-Leibler and Renormalized Entropies: Applications to Electroencephalograms of Epilepsy Patients," *Physical Review E*, vol. 62 (6), pp. 8380 – 8386, 2000.

78. Q. R Quiroga, A. Kraskov, and T. Kreuz, "Performance of different synchronization measures in real data: a case study on EEG signals" *Physica Review E* vol. 65:041903, pp. 01 – 14, 2002.

79. Q. R Quiroga, T. Kreuz, and P. Grassberger, "Event Synchronization: A Simple and Fast Method to Measure Synchronicity and Time Delay Patterns," *Physica Review E*, vol. 66:041904, pp: 01-06, 2002.

80. Q. R. Quiroga, O. W. Sackowitz, E. Basar, and M. Schurmann, "Wavelet Transform in the Analysis of the frequency Composition of Evoked Potentials," *Brain Research Protocols*, vol. 8, pp. 16-24, 2001.

81. M. L. V. Quyen, C. Adam, M. Baulac, J. Martinerie, and F.J. Varela, "Nonlinear Interdependencies of EEG Signals in Human Intracranially Recorded Temporal Lobe Seizures," *Brain Research*, vol. 792, pp. 24- 40, 1998.

82. M. L. V. Quyen, J. Martinerie, V. Navarro, P. Boon, M. D. Have, C. Adam, B. Renault, F. Varela, and M. Baulac, "Anticipation of Epileptic Seizures from Standard EEG Recordings," *The Lancet*, vol. 357, pp. 183-188, 2001.

83. M. L. V. Quyen, J. Foucher, J. Lachaux, E. Rodriguez, A. Lutz, M. Francisco,and J. Varela, "Comparison of Hilbert Transform and Wavelet Methods for Analysis of Neuronal Synchrony," *Journal of Neuroscience Methods*, vol. 111, pp. 83-98, 2001.

84. E. Rodriguez, N. George, J. –P. Lachaux, J. Martinerie, B. Renault, and F.J Varela, "Perception's Shadow: Long-Distance Synchronization of Human Brain Activity," *Nature*, vol. 397, pp. 430-437, 1999.

85. M. Rosenblum, A. Pikovsky, J. Kurths, C. Schaefer, and P. A. Tass, *Phase Synchronization: from Theory to Data Analysis.* In F. Moss and S. Gielen, editors, Handbook of Biological Physics, page 297, Elsevier Science Foundation, Amsterdam, 2001.

86. M. Rosenblum, A. Pikovsky, and J. Kurths, "Phase Synchronization of Chaotic Oscillators," *Physics Review Letter*, vol. 76, pp. 1804-807, 1996.

87. M. G. Rosenblum, A. S. Pikovsky, and J. Kurths "From Phase to Lag Synchronization in Coupled Chaotic Oscillators," *Physics Review Letter*, vol. 76, pp. 1804-1807, 1996.

88. N. F. Rulkov, M. M. Sushchik, L. S. Tsimring, and H. D. I. Abarbanel, " Generalized Synchronization of Chaos in Directionally Coupled Chaotic Systems", *Physics Review E*, vol. 51(2), pp. 980-994, 1995.

89. S. Haykin, *Neural Networks: A Comprehensive Foundation*, 2nd edition, Prentice Hall, 1999.

90. V. J. Samar, A. Bopardikar, R. Rao, and K. Swartz, "Wavelet Analysis of Neuroelectric Waveforms: A Conceptual Tutorial," *Brain and Language*, vol. 66, pp. 07-60, 1999.

91. K. Sameshima, and L. A. Baccala, "Using Partial Directed Coherence to Describe Neuronal Ensemble Interactions," *Journal of Neuroscience Methods*, vol. 94, pp. 93-103, 1999.

92. S. J. Schiff, P. So, T. Chang, R. E. Burke, and T. Sauer, "Detecting Dynamical Interdependence and Generalized Synchrony through Mutual Prediction in a Neural Ensemble," *Physics Review E*, vol. 54, pp. 6708, 1996.

93. A. Schmitz, "Measuring Statistical Dependence and Coupling of Subsystems," *Physical Review E*, vol. 62, pp: 7508-7514, 2000.

94. T. Schreiber, "Measuring Information Transfer," *Physics Review Letters*, vol. 85, pp. 461-470, 2000.

95. T. Schreiber, and A. Schmitz, "Improved Surrogate Data for Nonlinearity Tests," *Physical Review Letters*, vol.77 (4), pp. 635-638, 1996.

96. W. D. Shannon, M. A. Watson, A. Perry, and K. Rich, "Mantel Statistics to Correlate Gene Expression Levels from Microarrays with Clinical Covariates," *Genetic Epidemiology*, vol. 23, pp. 87-96, 2002.

97. C. J. Stam, M. Breakspear, A. M. C. Walsum, and B. W. Dijk, "Nonlinear Synchronization in EEG and Whole-head MEG recordings of Healthy Subjects," *Human Brain Mapping*, vol. 19 (2), pp. 63-78, 2003.

98. F. Takens, *Detecting Strange Attractors in Turbulence*. In: Rand DA, Young LS, eds. Dynamical systems and turbulence. Lecture notes on mathematics. vol. 898, Berlin: Springer, pp. 366-381, 1981.

99. P. Tass, M. G. Rosenblum, J. Weule, J. Kurths, A. Pikovsky, and J. Volkmann, "Detection of n:m Phase Locking from Noisy Data: Application to Magnetoencephalography," *Physics Review Letter*, vol. 81, pp. 3291-3294, 1998.

100. Y. Weiss, "Segmentation Using EigenVectors: A Unifying View," *International Conference on Computer Vision*, pp: 975-982, 1999.

101. C. S. Burrus, R. A. Gopinath, and H. Guo, *Introduction to Wavelets and Wavelets Transforms*, A Primer, Prentice-Hall International Editions, Engions, Clifs, NJ, 1998.

BIOGRAPHICAL SKETCH

Anant graduated from Mysore University, India, with a bachelors of Engineering degree in Electronics and Communication engineering (1998). For a brief period, he worked in the personal communications sector at the Bangalore design center in Motorola India Ltd., Later, during master's research, he worked on evoked potentials at the Bio-Signal Analysis Laboratory at the University of Houston. Currently, he is pursuing his doctorate degree in electrical engineering at the University of Florida. His research at the Computational Neuroengineering Laboratory involves investigating the functional connectivities between brain areas at various states of epileptic seizures. His research interests are in biomedical signal processing, broad band communication technologies and machine learning networks adapted from information theoretic learning principles.